Modeling Alzheimer's Disease Using Cellular Reprogramming Technologies

Lily Chau

Submitted in partial fulfillment of the requirements
for the degree of Doctor of Philosophy in the
Graduate School of Arts and Sciences

COLUMBIA UNIVERSITY

2012

ABSTRACT

Modeling Alzheimer's Disease Using Cellular Reprogramming Technologies

Lily Chau

Two cellular reprogramming technologies have emerged that demonstrate that cell-fate can be converted by ectopic expression of defined transcription factors: induced pluripotent stem (iPS) cell technology and induced neuronal (iN) cell technology. These recent advances in cell reprogramming strategies have great potential utility for patient-specific disease modeling and for applications in regenerative medicine. Current models of neurodegenerative diseases are limited in their representation of disease phenotypes and there is an essential need for human cellular models of neurodegenerative disorders. Induced pluripotent stem (iPS) cell technology offers a two-step approach to disease modeling, in which patient somatic cells are first reprogrammed to a pluripotent state and subsequently differentiated in neurons. In contrast, induced neuronal (iN) cell technology allows for the direct conversion of somatic cells to neurons. Here I demonstrate the modeling of Alzheimer's disease (AD) using both iPS and iN cellular reprogramming technologies. These bioengineered human cell-based models of AD provide unique and invaluable tools for elucidating the mechanism of AD pathogenesis.

Table of Contents

Figures

I. Chapter 1: Introduction

II. Chapter 2: Reprogramming AD patient fibroblasts to induced pluripotent stem (iPS) cells

III. Chapter 3: Chapter 3: Generating an iPS cell-based model of AD to understand cell-type specificity in AD

IV. Chapter 4: An in-vitro cell based model of AD using induced neuronal (iN) cell technology

Chapter 1. A. Clinical, genetic, and molecular characteristics of Alzheimer's disease (AD)

Clinical Phenotype and Pathology

AD is the most common cause of dementia in the elderly (>65 years), accounting for 60-70% of all dementia cases; an estimated 26 million people are affected worldwide and this number is predicted to quadruple by 2050 (Daffner, 2010). AD is a neurodegenerative disorder clinically characterized by progressive cognitive decline. During early stages of the disease, short-term (episodic) memory decline is prominent. Disease progression results in further impairment of cognitive functions, including spatial orientation, reasoning and judgment, language skills, and emotional affect (Alzheimer et al., 1995). The major risk factor for AD is age; risk doubles every five years after the age of 65 (Brookmeyer et al., 1998). The prognosis for AD is poor, as there is presently no cure for AD; current therapies are only symptomatic and do not treat the underlying disease process (Daffner, 2010). The median survival after initial diagnosis is between five and ten years (Walsh et al., 1990).

The definitive diagnosis of AD requires post-mortem detection of two hallmark protein aggregate lesions: extracellular amyloid plaques and intracellular neurofibrillary tangles (NFTs), found most prominently in cortical and subcortical areas of the medial temporal lobe, including the hippocampal formation and amygdala (Alzheimer et al., 1995). The major proteinaceous component of amyloid plaques is the amyloid-β (Aβ) peptide, derived from

proteolytic cleavage of the amyloid precursor protein (APP). The length of Aβ peptide can vary from 39-43 residues; the 40-amino acid variant (Aβ40) is most common whereas the 42 amino-acid variant (Aβ42) is the more neurotoxic species, due to its propensity to aggregate into oligomers and fibrils (Glenner and Wong, 1984; Masters et al., 1985). Two varieties of amyloid plaques exist; diffuse plaques are comprised mainly of Aβ42 and few dystrophic axons and dendrites whereas dense-cored neuritic plaques are comprised of a dense Aβ42 core, Aβ40 and other proteinaceous components such as ubiquitin and alpha-synuclein, all surrounded by dystrophic neurites. Dense-cored plaques are more prevalent in the AD brain (Glenner and Wong, 1984) (Figure 1A).

Neurofibrillary tangles (NFTs) are filamentous inclusions composed of hyperphosphorylated microtubule associated protein tau (MAPT) forming paired helical filaments, found in neuronal cell bodies and apical dendrites. Additionally, tau protein is found in distal dendrites as neuropil threads and in the dystrophic neurites associated with dense-cored neuritic plaques (Selkoe, 1991). Within the AD brain, neurofibrillary lesions develop in a predictable pattern, providing a basis for distinguishing six stages of disease progression. Braak stages I-II with transentorhinal lesions signify the clinically silent stage; Braak stages III-IV with limbic lesions indicate early stage AD; Braak stages V-VI with neocortical lesions signify late stage AD (Braak and Braak, 1991). NFTs are also seen in other neurodegenerative disorders, including frontal temporal dementia with Parkinsonism linked to chromosome 17 (FTDP-17), Pick's disease, progressive

supranuclear palsy (PSP), and corticobasal degeneration (CBD) (Grundke-Iqbal et al., 1986; Goedert et al., 1988).

In addition to extracellular amyloid plaques and intracellular neurofibrillary tangles, the AD brain is further characterized by neuronal cell loss, loss of synapses and dendritic spines. Additionally, there is depletion of the acetylcholine neurotransmitter system (Khachaturian, 1985; Selkoe, 2002).

Proposed Genetic Mechanism

PSEN1, PSEN2, and APP mutations underlie FAD

The etiology of AD is complex, involving an interplay between environmental and genetic factors. At the genetic level, there are two forms of AD, familial and sporadic, which nevertheless share the same clinical and histopathological features. Comprising less than 1% of AD cases, familial AD (FAD) exhibits a Mendelian inheritance pattern and typically shows early-onset of clinical symptoms (<65 years) (Goate et al., 1991). FAD is caused by autosomal dominant mutations in genes encoding amyloid precursor protein (APP), which account for about 2-3% of FAD cases (Goate et al., 1991), presenilin 1 (PSEN1), which account for about 70-80% of FAD cases (Sherrington et al., 1995; Cruts et al., 1998), and presenilin 2 (PSEN2) (Rogaev et al., 1995). The remaining cases of AD are idiopathic or sporadic (SAD) (Delacourte et al., 2002). The onset of symptoms in SAD is typically after 65 years of age. Although SAD is not caused by particular genetic mutations, a few susceptibility genes have been identified in SAD, including apolipoprotein E (*ApoE*) (Bertram and Tanzi, 2005), clusterin

(*CLU*), phosphatidylinositol-binding clathrin assembly protein (*PICALM*), and complement component (3b/4b) receptor 1 (*CR1*) (Lambert et al., 2009; Harold et al., 2009; Jun et al., 2010). Inheritance of the epsilon 4 allele of apolipoprotein E (ApoE4) increases the risk for SAD (Bertram et al., 2008).

Over twenty APP mutations have been linked to FAD including the Swedish mutation APP K670D/M671L (Mullan et al., 1992), London mutation APP V717I (Goate et al., 1991), Arctic mutation APP E693G (Nilsberth et al., 2001) and Indiana mutation APP V717F (Murrell et al., 1991). APP is a type-1 integral transmembrane protein consisting of 695-770 residues. The APP gene undergoes alternate splicing; APP695, APP751, and APP770 are the most prevalent isoforms. APP695 is mostly expressed in neurons and lack the Kunitz-type serine protease domain, which is found in APP751 and APP770. The APP holoprotein contains the Aβ domain, which spans the transmembrane region of the protein (Kang et al., 1987). The functional significance of the APP holoprotein remains to be determined as mouse models show only minor neurological impairments (Muller et al., 1994; Zheng et al., 1995). Rather than mutations in the APP gene itself, the majority of FAD cases are caused by missense mutations in the presenilin genes (Hardy et al., 1997; Van Broeckhoven et al., 1992; Levy-Lahad et al., 1995). To date, over 130 PSEN1 and PSEN2 mutations have been linked to FAD, including PSEN1 A246E and PSEN2 N141I (Sherrington et al., 1995; Levy-Lahad et al., 1995; Jayadev et al., 2010). The presenilins form the catalytic core of the enzyme complex γ-

secretase (Wolfe, 2006), which, together with β-secretase, generates Aβ via proteolytic cleavage of the APP holoprotein.

FAD mutations affect APP processing

APP is processed by one of two pathways; the non-amyloidogenic pathway involves sequential cleavage of APP by the membrane-associated metalloprotease α-secretase and γ-secretase whereas the amyloidogenic pathway involves sequential cleavage of APP by the β-site APP-cleaving enzyme (BACE1) and γ-secretase; the latter activity generates the Aβ40 and Aβ42 peptides. In the non-amyloidogenic pathway, cleavage of APP by α-secretase activity occurs within the Aβ domain, thereby precluding formation of Aβ peptide. Alpha-secretase activity releases a soluble extracellular N-terminal fragment, sAPPα, and a C-terminal fragment, C83. C83 can further be cleaved by γ-secretase, generating the P3 peptide (P3 can be found in diffuse amyloid plaques) and the APP intracellular domain (AICD). In the amyloidogenic pathway, APP cleavage by BACE1 β-secretase results in the release of a soluble extracellular N-terminal fragment, sAPPβ, and the C-terminal fragment, C99, which is further cleaved by γ-secretase to form the Aβ peptide and AICD. While β-secretase activity generates the amino terminus of Aβ, cleavage by γ-secretase dictates the length of the Aβ peptide, with Aβ40 being the most common species and Aβ42 being the less common but more amyloidogenic and neurotoxic species (Vassar et al., 1999; Edbauer et al., 2003; LaFerla et al., 2007) (Figure 1B).

The mutations in APP, PSEN1 and PSEN2 that underlie FAD all affect APP processing and Aβ production. FAD mutations cause either increased production of Aβ or the preferential increase of the more neurotoxic Aβ42 isoform. Some APP mutations, including the Swedish mutation, cluster around the β-secretase cleavage site and cause APP to be preferentially metabolized by β-secretase, leading to an overall increase in the production of Aβ fragments (Haass et al., 1995). Other APP mutations, such as the Arctic and London mutations, occur in key amino acids within the transmembrane domain or around the γ-secretase cleavage site, altering the specificity of γ-secretase and resulting in the production of a higher ratio of Aβ42 to Aβ40 fragments (Suzuki et al., 1994; Lichtenthaler et al., 1997). This preferential accumulation of Aβ42 peptides relative to the Aβ40 species is also a consequence of all presenilin mutations, which alter γ-secretase activity and directly affect APP processing to cause an increase in the production of Aβ42 over Aβ40 (Haass and Selkoe; 1998). Indeed an increased Aβ42:Aβ40 ratio is the key molecular feature of AD (Hardy, 1997; Hardy and Selkoe, 2002).

The amyloid cascade hypothesis – a prevailing theory for AD pathogenesis

First proposed by Hardy and Higgins in 1992, the amyloid cascade hypothesis postulates that Aβ is the initiator of AD pathogenesis and that all other pathological features of AD, including tau pathology and neuronal loss, are a downstream consequence of Aβ accumulation, and in particular, Aβ42 (Hardy and Selkoe, 2002). The pathogenic Aβ42 fragment is generated by the altered

cleavage of APP by β-secretase and γ-secretase. Under this hypothesis, the same pathophysiological mechanism manifests in both FAD and SAD. Consistent with this hypothesis, all known FAD mutations cause an increase in Aβ accumulation, and in most cases, preferential accumulation of the Aβ42 isoform relative to the Aβ40 isoform. However, it is important to note that the amyloid hypothesis is not universally accepted; opponents of this hypothesis propose that Aβ accumulation may be an epiphenomenon while the initiating pathophysiological culprit lies upstream.

Mouse Models of Alzheimer's Disease

APP and PSEN Mouse Models

Recapitulation of amyloid plaque pathology

The first mouse models shown to recapitulate amyloid plaque pathology were generated by transgenic overexpression of human APP mutations. These mouse models developed amyloid pathology in an age-dependent manner. In 1995, Games et al. reported the PDAPP mouse model, generated by overexpression of the Indiana mutation APP V717F (Games et al., 1995). In these mice, the APP V717F mutation caused a selective increase in Aβ42 production and robust amyloid plaque pathology developed by six to nine months of age, with most plaques being diffuse. Plaque pathology was accompanied by age-dependent synaptic loss (Games et al., 1995). Subsequently, in 1996, Hsiao et al., reported the Tg2576 mouse model, which overexpressed the cDNA of human APP carrying the Swedish mutation K670M/N671L (APPswe) (Hsiao et

al., 1996). The APPswe mutation increased the production of both Aβ40 and Aβ42, and amyloid plaque pathology developed in an age-dependent manner. Most of the plaques were dense-cored plaques and few were diffuse. Additionally, these mice were shown to have memory deficits. PDAPP and Tg2576 mice demonstrated that altered Aβ42 to Aβ40 ratio affects the location plaque deposition and the particular type of plaque that is preferentially produced (dense-cored vs. diffuse). Beyond PDAPP and Tg2576 mice, various other mouse models that express mutant human APP have been generated that also develop amyloid pathology and cognitive deficits (Chishti et al., 2001; Janus et al., 2001; Mucke et al., 2000).

Despite accounting for the overwhelming majority of FAD cases, PSEN mutant mice failed to exhibit overt plaque pathology. Mice carrying mutations in PSEN1 M146V or PSEN1 M146L showed selective elevation of Aβ42. However, crossing PSEN1 mutant mice with APP mutant mice resulted in enhanced amyloid pathology. The increase in Aβ42 production mediated by PSEN1 mutations resulted in acceleration of amyloid deposition (Duff et al., 1996; Borchelt et al., 1997; Holcomb et al., 1998). APP and PSAPP transgenic mice exhibited amyloid plaques, including both diffuse and dense-cored plaques, that are structurally and biochemically similar to those found in the AD brain (Games et al., 1995; Hsiao et al., 1996; Borchelt et al., 1997; Holcomb et al., 1998).

Memory decline and soluble Aβ

Despite showing no significant neuronal loss, multiple lines of APP and PSAPP transgenic mice have been shown to exhibit cognitive deficits in various

behavioral tests, including the Morris water maze test (Hsiao et al., 1996; Westerman et al., 2002; Chen et al., 2000; Janus et al., 2000; Morgan et al., 2000), strongly suggesting that cognitive decline in AD may not be due solely to neuronal loss. Indeed, Morris water maze studies in PDAPP, PSAPP and TgCRND8 (which express both APP Swedish and Indiana mutations) mouse models have shown that spatial reference memory deficits correlates with levels of insoluble Aβ aggregates (Chen et al., 2000; Janus et al., 2000; Morgan et al., 2000; Gordon et al., 2001). Furthermore, analysis of age-dependent memory loss in Tg2576 suggests that the real correlate to memory deficits may be a soluble Aβ species. In initial studies, Westerman et al., showed that spatial reference memory deficits developed progressively from 6 months of age and this decline corresponded with the development of detergent-insoluble Aβ aggregates. (Westerman et al., 2002). However, while this correlation was seen within stratified age groups, it was not observed in a combined group of old and young mice. Theses results were interpreted to indicate that insoluble Aβ is a surrogate marker for small soluble assemblies of Aβ that are intermediaries in the formation of insoluble Aβ (Westerman et al., 2002).

This correlation between soluble Aβ and memory decline was further examined in anti-Aβ immunization studies in APP and PSAPP mouse models. These studies demonstrated that active or passive immunotherapy resulted in the reversal of memory deficits in APP and PSAPP mice, despite little effect on clearing pre-existing plaque pathology (Janus et al., 2000; Morgan et al., 2000; Kotilinek et al., 2002; Dodart et al., 2002).

Synaptic degeneration and amyloid plaques

Multiple APP and PSAPP mice have demonstrated synaptic degeneration and dysfunction that occurs after significant amyloid plaque deposition (Irizarry et al., 1997; Takeuchi et al., 2000). In addition to plaque-dependent synaptic loss reported in Tg2576 and PSAPP mice (Spires et al., 2005; Tsai et al., 2004), there is also evidence for plaque-independent synaptotoxicity. Mucke et al. have demonstrated that the density of pre-synaptic terminals inversely correlates with levels of Aβ but not APP or amyloid plaque load (Mucke et al., 2000). Furthermore, Buttini et al. have shown that active or passive Aβ immunotherapy hinders progression of age-dependent synaptic deficits in PDAPP mice (Games et al., 1995; Buttini et al., 2005). This study demonstrated that the loss of synapses is also linked to a toxic Aβ species.

Limitations of APP and PSEN models

Despite their high Aβ levels and robust recapitulation of amyloid plaque pathology, APP and PSAPP mouse models suffer from substantial limitations. Neither APP nor PSAPP mouse models develop substantial neuronal loss (although APP23 mice, which express APPswe under control of the Thy1 promoter do show limited neuronal loss in the CA1 region of the hippocampus (Sturchler-Pierrat et al., 1997; Calhoun et al., 1998; Calhoun et al., 1999)) (Irizarry et al., 1997a; Irizarry et al., 1997b). Moreover, NFT pathology, one of the two hallmark lesions of AD, is absent in these mice.

MAPT Mouse Models

Despite NFTs being a hallmark lesion in the AD brain, mutations in *MAPT* have not been linked to FAD. However, mutations in *MAPT* are found in patients with frontotemporal dementia with parkinsonism linked to chromosome 17 (FTDP-17) (Hutton et al., 1998; Poorkaj et al., 1998), demonstrating that tau dysfunction can lead to neurodegeneration and dementia.

Recapitulation of neurofibrillary tangle pathology

The transgenic mouse model rTg4510, which expresses mutant human MAPT P301L, a mutation that is linked to FTDP-1 (Hutton et al., 1998; Poorkaj et al., 1998) develop robust neurofibrillary pathology and exhibit significant neuronal loss in AD-related cortical and limbic structures (Ramsden et al., 2005). Furthermore, NFT pathology and neuronal loss correlates with spatial reference memory deficits. These mice, however, do not develop amyloid pathology. Nonetheless, this and other MAPT transgenic models demonstrate that neurofibrillary pathology and neurodegeneration are closely related, consistent with the correlation between NFT pathology and disease progression (Braak and Braak, 1991).

Neurodegeneration, memory loss and soluble Tau species

In the inducible rTg4510 mouse model, the onset of memory decline preceded significant NFT accumulation and neuronal loss. Suppression of the inducible transgene with doxycycline treatment after NFT formation has occurred

did not affect the progression of NFT formation. However, transgene suppression inhibited neuronal loss and allowed for partial recovery of spatial reference memory (Ramsden et al., 2005). These findings suggest that NFT formation may not be directly responsible for neuronal loss and memory decline. Rather, an intermediate Tau species may be the mediator of toxicity. These findings parallel the findings in APP mice that a soluble Aβ species rather than insoluble Aβ underlies memory loss (Ramsden et al., 2005).

Interaction between Aβ and Tau

Extensive AD pathology has been modeled in a triple-transgenic mouse model (3xTg-AD) that harbors three mutant transgenes: PSEN1 M146V, APPswe and MAPT P301L (Oddo et al., 2003). These mice show an accumulation of intraneuronal Aβ and develop amyloid plaques, neurofibrillary tangles, synaptic dysfunction and memory deficits in an age-dependent manner. Synaptic dysfunction and memory deficits were shown to correlate with the accumulation of intraneuronal Aβ. Interestingly, the memory deficits in these mice correlate with intraneuronal Aβ rather than plaque load, as seen in studies using Tg2576 mice (Billings et al., 2005).

The 3xTg-AD mouse model, and other models combining APP and MAPT mutations (Gotz et al., 2001; Lewis et al., 2001) demonstrate that Aβ and tau interaction is important in the pathogenesis of AD. Mouse models show that Aβ can promote tau pathology. Furthermore, an interplay between APP, presenilin and tau may underlie the disease process of AD.

Mouse Models are Insufficient for Modeling AD

While transgenic models of AD have been invaluable tools for understanding the pathophysiological mechanism underlying AD, they fail to fully recapitulate the disease phenotype. Although FAD is linked to mutations in APP and PSEN, mutant mice harboring FAD mutations show limited representation of the disease profile. APP mice exhibit only several features of AD, including amyloid plaque formation, synaptic degeneration and memory decline. Additionally, despite accounting for the overwhelming majority of FAD cases, PSEN mutant mice exhibit only the accumulation of Aβ42. While the 3xTg-AD mouse model recapitulates many aspects of AD, including NFT pathology, amyloid plaque formation, synaptic deficits and memory decline, MAPT mutations are not linked to FAD. Furthermore, that this aggressive genetic approach was necessary to recapitulate salient features of AD speaks to the complexity of modeling AD in mice and more importantly, the limitation of the mouse system for modeling this human disease (that involves higher cognitive function and occurs late in life).

Moreover, while FAD mutations have provided a genetic signature to model AD, it remains that FAD represents less than 1% of all AD cases. The majority of AD cases are sporadic, with no known genetic links, although studies have identified susceptibility genes, including *ApoE.* As such, further strategies are needed for modeling AD.

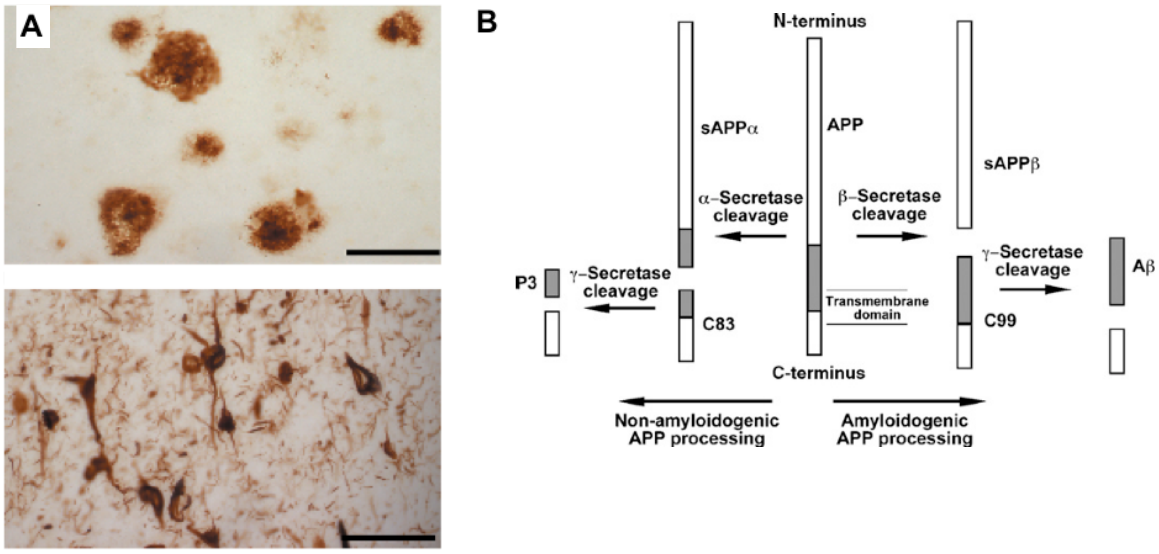

Figure 1. (A) Amyloid beta (Aβ) Plaques and Neurofibrillary Tangles in the AD brain. (top panel) A representative micrograph of amyloid plaques in the AD brain. Plaques were visualized by immunostaining with an antibody specific to Aβ42. (bottom panel) A representative micrograph of neurofibrillary tangles. Tangles were visualized by immunostainig with an antibody specific to paired helical filament. (adapted from LaFerla and Oddo, 2005)
(B) APP Processing. Non-amyloidogenic APP processing: α-secretase mediated processing cleaves APP within the Aβ domain to produce secreted sAPPα and the non-amyloidogenic C-terminal fragment C83. C83 can undergo further processing mediated by Ƴ-secretase cleavage at the C-terminal end of the Aβ domain to yield non-amyloidogenic P3. Amyloidogenic APP processing: β-secretase cleaves at the N-terminal end of the Aβ domain to produce secreted sAPPβ and the amyloidogenic C99 fragment. Subsquent Ƴ-secretase cleavage of C99 at the N-terminal end of the Aβ domain gives rise to amylodogenic Aβ. (adapted from Crouch et al., 2008) .

Chapter1. B. Reprogramming technologies and cell-based modeling of diseases

Somatic cell nuclear transfer (SCNT) and embryonic stem (ES) cell fusion

Nuclear reprogramming involves epigenetic changes

Cellular differentiation is the process whereby pluripotent cells acquire a mature identity. The molecular mechanism for this cell-type specification involves epigenetic changes to the cellular genome that dictate specific gene expression patterns and provide a signature for cell identity and function (Bernstein et al., 2007; Meissner et al., 2008). These epigenetic changes include DNA methylation and histone modifications. DNA methylation is important in the regulation of gene expression and silencing of repetitive elements in the genome (Wolffe et al., 1999; Jaenisch et al., 2003). Histone modifications include acetylation, methylation, and phosphorylation. Typically, histone acetylation results in gene activation and histone deacetylation results in gene repression (Hebbes et al., 1988; Schultz et al., 1999).

It was previously thought that epigenetic modifications during cellular differentiation were irreversible and that once a cell acquires a mature identity, no further change in cell fate would be possible. However nuclear reprogramming strategies, including somatic cell nuclear transfer (SCNT) and ES cell fusion experiments have proven that epigenetic modifications to the genome during cellular differentiation can be erased and that somatic cells can be reprogrammed to a pluripotent state. The process of reprogramming the nucleus

of a somatic cell into an embryonic state requires removal of epigenetic changes in the genome acquired during the course of cell differentiation so that a new set of epigenetic marks for pluripotency can be established. This involves inactivation of the somatic cell's gene expression pattern and activation of the gene expression pattern for pluripotent cells (Reik et al., 2001; Rideout et al., 2001).

Somatic Cell Nuclear Transfer (SCNT) and ES cell fusion experiments

Nuclear reprogramming by SCNT involves the transfer of a somatic cell nucleus into an enucleated oocyte, resulting in an embryo with the same genetic information as the donor nucleus (except for mitochondrial genes, which are maternally inherited) (Hochedlinger and Jaenisch, 2006; Pickering et al., 2005). The first successful nuclear transfer experiments were demonstrated in amphibians. In 1952, Briggs and King generated normal swimming tadpoles by transplanting nuclei from blastula cells into enucleated *Rana pipiens* (frog) eggs. Thereafter, Gurdon et al. generated normal and fertile adult frogs by transferring tadpole intestinal epithelial cell nuclei into enucleated *Xenopus laevis* eggs (Gurdon et al., 1966; reviewed in Gurdon and Byrne 2003). These results led to the conclusion that the process of cell differentiation does not involve irreversible changes in genetic content but only epigenetic changes that dictate gene expression patterns. As cells undergo progressive loss of developmental potential during cell-fate specification, their genomic content remains the same

(with lymphocytes being an exception) and the process of specification can be entirely reversed so that cells regain pluripotency.

The next major advance in SCNT was in the cloning of mammalian species, including Dolly the Sheep (Wilmut et al., 1997; Wakayama et al., 1998; Kato et al., 1998; Baguisi et al., 1999). A normal adult sheep was produced by transplanting mammary gland cells of an adult sheep into enucleated sheep eggs (Wilmut et al., 1997). This critical experiment demonstrated that cell differentiation was also reversible in mammalian cells. More recently, SCNT has been confirmed in non-human primates. Rhesus macaque embryonic stem (ES) cells were generated from adult nuclei by reprogramming via SCNT; nuclei from adult skin fibroblast cells were transplanted into enucleated oocytes and cells from the inner cell mass of the resulting blastocyst were cultured to generate ES cells (Byrne et al., 2007). These ES cells contained the same genetic information as donor cells, with the exception of mitochondrial DNA originating from oocytes. These ES cells exhibited typical ES cell morphology, expressed stem cell markers, OCT4, SSEA-4, TRA1-60 and TRA1-81, and differentiated into cells of the three embryonic germ layers (Byrne et al., 2007).

Despite progress in non-human primates, the reprogramming of adult human somatic cells has been wrought with difficulty and successful SCNT in the human system remains elusive. However, a few breakthroughs in the reprogramming of human somatic cells have occurred in recent years. First, reprogramming of human cells has been achieved by fusion of human somatic cells with human ES cells to form tetraploid hybrids. This ES cell fusion process

reprograms the somatic cell nucleus to a pluripotent state (Cowan et al., 2005; Yu et al., 2006). Second, while the feasibility of human SCNT remains to be seen, Noggle et al. have demonstrated that human oocytes have the capacity to reprogram human somatic cells to pluripotency (Noggle et al., 2011). The transplantation of human somatic cell nuclei into enucleated human oocytes resulted in developmental arrest at late cleavage stages. However, when a somatic cell genome was transplanted into an oocyte with its genome intact, the oocytes developed to the blastocyst stage. Human stem cells derived from these blastocysts were triploid, containing the haploid oocyte genome and the diploid donor somatic cell genome that has been reprogrammed to a pluripotent state (Noggle et al., 2011).

The results from these reprogramming experiments in mammalian species demonstrate that, as in earlier amphibian experiments, the genomic content of pluripotent cells remains the same as they undergo cell-fate specification. The molecular changes that occur during cellular differentiation are epigenetic modifications and given the right context, these epigenetic modifications in somatic cells can be reversed so that the cells return to a pluripotent state.

Despite advances in SCNT, the specific nature of the trans-acting factors present in oocytes and ES cells that mediate reprogramming remain unknown. However, a novel nuclear reprogramming strategy has emerged in recent years that offers insight into this question. Pioneered by Dr. Shinya Yamanaka, this technology, termed induced pluripotent stem (iPS) cell technology, utilizes ectopic expression of defined transcription factors, Oct4, Sox2, Klf4 and c-Myc,

to reprogram somatic cells to a pluripotent state. Somatic cells reprogrammed in this way are termed iPS cells.

Nuclear reprogramming by defined factors - induced pluripotent stem (iPS) cell technology

Reprogramming strategies for mouse and human iPS cells

Induced pluripotent stem (iPS) cell technology is a nuclear reprogramming strategy that allows for reprogramming of somatic cells to a pluripotent state using defined transcription factors. The resulting iPS cells are similar to ES cells derived from blastocysts in both form and function.

The reprogramming of somatic cells through cellular fusion with ES cells had indicated that factors exist within ES cells that can induce pluripotency. Takahashi and Yamanaka hypothesized that factors that induce pluripotency may also play a role in maintaining pluripotency, and furthermore, that ectopic expression of these factors may be able to reprogram somatic cells to pluripotency. This reasoning led to their finding in 2006 that retroviral transduction of four transcription factors, Oct4, Sox2, Klf4, c-Myc, and selection for the expression of Fbx15*,* a transcription target of pluripotency factors Oct4 and Sox2, enabled the reprogramming of mouse embryonic and adult fibroblast cells to a pluripotent state (Takahashi and Yamanaka, 2006). These four transcription factors all play a role in pluripotency. The reprogrammed iPS cells possessed many features of embryonic stem (ES) cells including morphology, proliferation and the ability to differentiate into cells from all three germ layers.

They also expressed characteristic ES cell markers, including alkaline phosphatase, Nanog and mouse ES cell-specific surface marker, SSEA-1. However, these Fbx15-selected iPS cells differed significantly from mouse ES cells in their gene expression profiles and DNA methylation patterns. Moreover, chimeras from Fbx15-selected iPS cells were embryonic lethals. Subsequently, isolation of germline-competent iPS cells was achieved via selection for Nanog or Oct4 (Okita et al., 2007; Maherali et al., 2007; Wernig et al., 2007). The discrepancy between these two selection systems stems from Fbx15 being dispensable for pluripotency whereas Nanog and Oct4 being critical for the maintenance of pluripotency (Tokuzawa et al., 2003). The capacity for germline-transmission is critical because it is the most definitive criteria for pluripotency.

Nanog-selected and Oct4-selected mouse iPS cells were epigenetically and functionally virtually identical to mouse ES cells. Their the global gene expression profile, DNA methylation pattern and histone modification pattern were similar to that of mouse ES cells (Okita et al., 2007; Maherali et al., 2007; Wernig et al., 2007). These iPS showed typical ES cell gene expression, including Nanog, Eras, Esg1, Cripto and Rex1. Bisulphite genomic sequencing analyses showed that promoter regions of *Nanog* and *Oct4* were vastly unmethylated, like that of ES cells. In female Nanog-selected iPS cells, silenced X chromosomes were reactivated and furthermore, underwent random X-inactivation when subjected to differentiation (Maherali et al., 2007). Beyond the molecular level, mouse iPS cells recapitulated two functional criteria that define stemness: the ability for self-renewal and the capacity to differentiate into cells of

all three embryonic germ layers. Mouse iPS cells have been shown to differentiate into cells of the ectoderm, endoderm and mesoderm in both in vitro differentiation and in vivo teratoma formation when injected into immunodeficient mice (Okita et al., 2007; Maherali et al., 2007; Wernig et al., 2007). Adult chimeras generated from mouse iPS cells show germline transmission (Okita et al., 2007; Boland et al., 2009) and can give rise to viable mice through tetraploid complementation (Zhao et al., 2009; Kang et al., 2009).

Following the generation of mouse iPS cells, human orthologs of Oct4, Sox2, Klf4, and c-Myc have been shown to successfully reprogram human somatic cells to iPS cells (Takahashi et al., 2007). Additionally, an alternative set of transcription factors, Oct4, Sox2, Nanog and Lin28 have also been shown to induce pluripotency in human somatic cells (Yu et al., 2007). Subsequently, human iPS cells have been successfully generated from embryonic, neonatal and adult fibroblasts using both sets of transcription factors and combinations of the two (Takahashi et al., 2007; Yu et al., 2007; Park et al., 2008b; Lowry et al., 2008). Like their mouse iPS cell counterparts, human iPS cells are similar to human ES cells, meeting epigenetic and functional criteria for pluripotency. Human iPS cells are similar to human ES cells in morphology, cell-growth rates, global gene expression profile and DNA methylation status. They express ES cell markers, including alkaline phosphatase, Nanog, and human ES cell-specific surface markers SSEA-3, SSEA-4, Tra-1-60 and Tra-1-80. Bisulphite genomic sequencing analyses showed that promoter regions of *Nanog, Oct4,* and *Rex1* were vastly unmethylated, like that of human ES cells. Additionally, human iPS

cells can differentiate into cells of three germ layers in vitro and form teratomas when injected into immunodeficient mice (Takahashi et al., 2007; Yu et al., 2007; Park et al., 2008b; Lowry et al., 2008). Beyond fibroblasts, various sources of somatic tissue have been reprogrammed to pluripotency, including B lymphocytes (Hanna et al., 2008), hepatocytes (Aoi et al., 2008), keratinocytes (Aasen et al., 2008), adipose tissue (Sun et al., 2009), and hematopoietic cells (Loh et al., 2009).

The maintenance of pluripotency in mouse and human iPS cells does not depend on continual viral transgene expression. Studies using doxycycline-inducible lentiviral expression vectors for delivery of reprogramming factors have demonstrated that viral transgene expression for about two weeks is sufficient for establishment of stable pluripotency (Wernig et al., 2008; Stadtfeld et al., 2008a). This period of viral transgene expression is thought to initiate a reprogramming process involving stochastic events that lead to induction of pluripotency. The reprogramming process causes changes in the epigenetic state of somatic cells that becomes indistinguishable from ES cells derived from the inner cell mass of blastocysts. Critically, Dnmt3a and Dnmt3b methyltransferases become activated and silence gene expression from the reprogramming viruses. Endogenous pluripotency genes become reactivated (Jaenisch and Young 2008; Brambrink et al., 2008). It is remarkable that the same four factors for pluripotency in mice were also able to induce pluripotency in human cells, even without selection for a pluripotency marker. This may indicate that a canonical gene network governing pluripotency exists in mammalian species.

Making iPS cells suitable for clinical applications: modifications to initial reprogramming strategies

One of the greatest utility for nuclear reprogramming is in the generation of patient-specific cell replacement therapies. The advent of iPS cell technology has made this goal more feasible than ever before. However, concerns regarding the use of viral vectors and reactivation of potent oncogenes c-MYC and Klf4 need to addressed before this end can be achieved. Indeed, much research has focused on eliminating these concerns and generating iPS cells that are suitable for clinical purposes.

Transduction of somatic cells with retroviruses and lentiviruses result in random integration of viruses into the host genome. These integrations can result in potential oncogenesis due to insertional mutagenesis; proviruses integrated into the host genome can affect expression of nearby genes, leading to oncogenesis, as seen in preclinical and clinical gene therapy trials (Li et al., 2002; Hacein-Bey-Albina et al., 2003; Howe et al., 2008). Furthermore, while integrated proviruses are silenced during iPS cell generation, viral transgenes have the potential to be reactivated. Indeed, reactivation of retroviral c-Myc has been found to cause tumors in mouse chimeras generated from iPS cells (Takahashi and Yamanaka 2006; Okita et al., 2008). To address this concern, several groups have shown that reprogramming can be achieved in mouse and human cells without the use of c-MYC. Chimeric mice generated with mouse iPS cells were tumor-free (Wernig et al., 2008; Nakagawa et al., 2008). The

drawback of removing c-MYC from the pool of reprogramming factors is that reprogramming efficiency, typically ranging from 0.01% - 0.05%, becomes very low, up to one order of magnitude lower and the reprogramming kinetics is slower (time to iPS cell colony formation is increased).

Given the concerns of genomic integration of viral vectors, methods for reprogramming without viral integration have been developed. Non-integrating adenoviruses that allow for transient expression of the reprogramming factors have been shown to reprogram murine and human somatic cells but with low efficiency (Stadtfeld et al., 2008b; Zhou and Freed, 2009). Additionally, the Cre/LoxP recombination system has been utilized so that integrated viral transgenes can be excised after generation of stable iPS cell lines (Kaji et al., 2009; Sommer et al., 2010). However, the Cre/LoxP system is not optimal since residual vector sequences remain after removal of transgenes. Clean excision of viral transgenes has been shown using the piggyBac transposon system in both mouse and human somatic cells. After induction of pluripotency, randomly integrated reprogramming factors can be removed without leaving behind any sequences or changes to the genome (Woltjen et al., 2009). Furthermore, polycistronic lentiviral vectors that contain the original four reprogramming factors, Oct4, Sox2, Klf4 and c-Myc, in a single lentiviral construct have been shown to successfully reprogram human fibroblasts to pluripotency with only single vector integrations (Sommer et al., 2009; Carey et al., 2009). The combination of the piggyBac transposon system with polycistronic lentiviral vectors may be an optimal system to achieve transgene-free iPS cells.

Completely viral-free methods have also been successfully employed to generate iPS cells, including plasmid transfection (Okita et al., 2008) and whole protein delivery of reprogramming factors (Zhou et al., 2009, Kim et al., 2009). The plasmid approach involves repeated transfection of two expression plasmids, one encoding Oct4, Sox2 and Klf4 cDNAs and the other encoding c-Myc cDNA. In the protein approach, reprogramming has been achieved by either using reprogramming factors along with pharmacological induction of cell permeability or reprogramming factors tagged to polyarginine for cell permeation (Zhou et al., 2009). Viral-free iPS reprogramming strategies result in even lower reprogramming efficiencies than the non-viral integration strategies.

Concerns regarding low reprogramming efficiency have been addressed with the use of small molecules involved in chromatin modification, which can increase reprogramming efficiency. The DNA methyltransferase inhibitor 5'-azacytidine has been shown to increase reprogramming efficiency about tenfold. Histone deacetylase inhibitors including, suberoylanilide hydroxamic acid, trichostatin A, and valproic acid also increase reprogramming efficiency, with valproic acid being most efficacious, increasing reprogramming efficiency more than 100-fold (Huangfu et al., 2008a). Valproic acid has also been shown to substitute for c-MYC and Klf4 factors, allowing for reprogramming of human fibroblasts to pluripotency with just Oct4 and Sox2 (Huangfu et al., 2008b; Shi et al., 2008).

Another means to increase reprogramming efficiency is by inhibiting the tumor suppressor gene p53, which has been shown to inhibit the reprogramming process. Transient siRNA-mediated knockdown of p53 or overexpression of MDM-2 to increase p53 degradation results in the increase of reprogramming efficiency by one to two orders of magnitude (Banito et al., 2009; Hong et al., 2009; Li et al., 2009; Marion et al., 2009; Kawamura et al., 2009). These advances in reprogramming strategy are paving the way towards clinical application of iPS cells.

The generation of patient-specific iPS cells

While much excitement surrounds the use of iPS cells for patient-specific cell replacement therapies, another critical utility of iPS cells is the generation of disease-specific cell-based models for the study of human diseases. These human cell-based models are crucial for diseases that cannot be fully recapitulated through in vitro or animal models. A proof-of-concept experiment has shown that human iPS cell lines can be generated from fibroblasts obtained from patients with a variety of diseases ranging from genetic diseases with Mendelian inheritance to complex multi-factorial diseases, including adenosine deaminase deficiency-related severe combined immunodeficiency (ADA-SCID), Gaucher's disease (GD) type III, Duchenne's muscular dystrophy (DMD), Huntington's disease (HD), Parkinson's disease (PD), juvenile-onset, type 1 diabetes milletus (JDM), and Down's syndrome (DS) (Park et al., 2008a). Patient-specific iPS cell lines display characteristic ES cell morphology, express

markers of pluripotency, and form cells of the three primary germ layers in vitro differentiation and in vivo formation of teratomas in immunodeficient mice.

Furthermore, another proof-of-concept experiment has shown that iPS cells can be derived from fibroblasts cells of elderly patients. Fibroblasts cells isolated from patients with amyotrophic lateral sclerosis in their eighth decade of life was successfully reprogrammed to pluripotency (Dimos et al., 2008). This experiment confirmed that iPS cells can be generated from elderly patients with progressive neurodegenerative disease, a group that is most likely to benefit from cell replacement therapies. The ability to generate patient-specific iPS cells offers an unparalleled opportunity to recapitulate human disease pathology in vitro. These human cell-based disease-specific models may provide tremendous aid in the elucidation of disease pathophysiologies and facilitate drug-screens for therapeutic advances (see Chapter 1, Section C).

Direct lineage reprogramming by defined factors - induced neuronal (iN) cell technology

While nuclear reprogramming results in the resetting of somatic cells to a pluripotent state, somatic cells can also be induced to express traits of other cell types via ectopic expression of lineage-specific transcription factors, a process classically referred to as trans-differentiation. Various experiments have demonstrated this conversion between closely related cell lineages arising from the same germ layer. Ectopic expression of MyoD, a muscle cell-specific transcription factor, converts fibroblasts to myoblast-like cells (Davis et al., 1987;

Weintraub et al., 1989). Lineage-committed B and T cells can be reprogrammed to macrophage-like cells via ectopic expression of myeloid transcription factor C/EBPalpha (Xie et al., 2004; Laiosa et al., 2006). Fibroblasts can also be converted to macrophage-like cells via ectopic expression of PU.1 and C/EBPalpha/beta (Feng et al., 2008). Additionally, lymphoid progenitor cells can be converted to myeloid cells by ectopic expression of IL2 and GM-CSF receptors (Kondo et al., 2000). Furthermore, pancreatic exocrine cells can be reprogrammed in vivo to endocrine insulin-producing beta cells via forced expression of Ngn3, Pdx1 and MafA, three transcription factors required for beta-cell differentiation, (Zhou et al., 2008).

More remarkably, a recent advance in reprogramming technology has demonstrated that this direct lineage conversion can occur between cells from vastly different cell lineages, arising from different germ layers. In 2010, Vierbuchen et al. demonstrated that lentiviral expression of a set of transcription factors involved in neuronal development, Brn2, Ascl1, and Myt1l, Olig2 and Zic1, directly reprogrammed mouse fibroblasts to induced neuronal (iN) cells. Further investigation revealed that expression of only Brn2, Ascl1, and Myt1l, were sufficient for this conversion. Induced neuronal cells showed typical neuronal morphology, expressed mature neuronal markers, including Tuj1, NeuN, MAP2, and synapsin and exhibited functional neuronal properties, including the ability to generate action potentials and functional synapses. The majority of iN cells were glutamatergic, expressing marker vGLUT1 and a

minority expressed markers of gabaergic neurons, GABA (Vierbuchen et al., 2010).

Unlike reprogramming to pluripotency, where the same set of transcription factors is effective for reprogramming both mouse and human somatic cells, direct reprogramming of human fibroblasts to neurons was shown to require an additional transcriptional factor, NeuroD1 (this phenomenon speaks to the fact that different regulatory networks govern human and rodent neuronal development). Forced expression of Brn2, Ascl1, Myt1l, and NeuroD1 converted primary human fetal and postnatal fibroblasts into functional iN cells (Pang et al., 2011). The efficiency of conversion ranged from 2%-4%. These human iN cells displayed typical neuronal morphology and expressed neuronal markers, Tuj1, NeuN, PSA-NCAM, and MAP2. Single-cell gene-expression profiling revealed co-expression of pan-neuronal and synaptic markers, including β-III-tubulin, DCX, MAP2, NCAM, and synapsin. The majority of neurons seemed to be glutamatergic, expressing vGLUT1 and vGLUT2 mRNAs. In electrophysiological analyses, hiN cells generated action potentials and demonstrated voltage-dependent Na^+ channel activity. Human iN cells also formed functional synapses. These cells showed GABA and glutamate receptor activity. Additionally, after co-culture with primary mouse cortical neurons, whole-cell recordings of human iN cells showed spontaneous postsynaptic currents, including both inhibitory postsynaptic currents (IPSCs) and excitatory postsynaptic currents (EPSCs).

After initial reports of direct reprogramming to neuronal cells, additional studies have shown that fibroblasts can be directly reprogrammed to various other cell types including cardiomyocytes (Ieda et al., 2010), blood progenitors (Szabo et al., 2010) and hepatocytes (Huang et al., 2011; Sekiya and Suzuki, 2011). Additionally, hepatocytes have been directly converted to functional neurons (Marro et al., 2011). These direct cell-fate conversions were mediated by ectopic expression of lineage-specific transcription factors.

Like iPS cell technology, iN cell technology has the utility for modeling neurological diseases and in particular, for neurodegenerative diseases (see Chapter1, Section C).

Chapter 1. C. Cell-based modeling of neurodegenerative diseases using iPS vs. iN cell reprogramming technology

Modeling neurodegenerative diseases using cellular reprogramming technologies

Two cellular reprogramming technologies have emerged that demonstrate that cell fate can be converted by ectopic expression of defined transcription factors: induced pluripotent stem (iPS) cell technology and induced neuronal (iN) cell technology. While both iPS cell technology and iN cell technologies can be utilized to generate human cellular models of neurodegenerative diseases, these molecular tools allows for the achievement of that end through direct and indirect means, respectively. Disease modeling via iPS cell technology is a two-step process that requires first the generation of iPS cells from patient somatic cells (usually skin fibroblasts) and subsequent directed differentiation of patient-specific iPS cells into specific neuron subtypes. In contrast, iN cell technology enables generation of patient-specific neuronal cells in one direct reprogramming step.

While much work is necessary to further develop these technologies, as a whole, patient-specific models have been able to recapitulate molecular and cellular pathologies of various neurodegenerative diseases. These patient-specific models can enable us to understand diseases in a human cellular context. Furthermore, nuclear reprogramming technologies have made possible

the modeling of sporadic forms of neurodegenerative diseases, which when present, comprise the most prevalent forms.

The utility of bioengineered human cellular models for studying neurodegenerative diseases

There is an essential need for human cellular models of neurodegenerative disorders because current cellular and animal models are inadequate. In particular, cell reprogramming-based models can provide a powerful means for elucidating the molecular mechanisms for selective loss of specific neuron cell types, a defining feature of neurodegenerative disorders. Patient-specific disease models offer the unprecedented opportunity for examining disease pathophysiology within the human neuronal context, and furthermore, within the genetic backgrounds of patients. Because primary human neurons are inaccessible, previous cellular models for neurodegenerative diseases have been based on available tissue, such as human cancer cell lines and patient fibroblast cell lines, but these models cannot recapitulate the unique neuronal environment in which disease pathology occurs. In this regard, primary neuronal cultures from animal models have been used in studies but this approach also has its limitations since these models do not fully recapitulate clinical disease phenotypes and are therefore limited in their representation of disease pathophysiology. Indeed, drugs found to be effective in mouse models have generally not been therapeutic in human clinical trials. Furthermore, for many neurodegenerative diseases, only about 5%-10% of cases are familial,

attributable to specific genetic mutations, while the majority of cases are sporadic, involving a complex interplay between genetic factors and environmental insults. Cell reprogramming technologies uniquely enable the modeling of sporadic forms of neurodegenerative diseases, as it is impossible to generate sporadic animal models.

Patient-specific disease models are also particularly useful in the context of neurodegenerative diseases for examining the ontogenesis of neuronal cell death. Most neurodegenerative disorders are late onset while iPS cell-derived neurons or iN cells are newly derived neurons and it would be surprising to see neuronal loss phenotypes in cellular models of late onset disorders. However, these young neurons may be representative of pre-disease stage neurons. Modeling of this pre-disease state permits development of assays for identifying exogenous factors that instigate or promote cellular phenotypes and neuronal cell death. Indeed, for all neurodegenerative diseases with mid to late onset that have been modeled from cellular reprogramming technologies thus far, including amyotrophic lateral sclerosis (ALS) (Dimos et al., 2008), Alzheimer's disease (AD) (Yagi et al., 2011), Parkinson's disease (PD) (Hargus et al., 2010; Nguyen et al., 2011; Seibler et al., 2011), and Huntington's disease (HD) (Zhang et al., 2010), there has been no report of neuronal death phenotypes. Conversely, cell reprogramming-based models that do exhibit neuronal death phenotypes are useful in screening for drugs that can slow progression of neuronal loss. For example, in the case of spinal muscular atrophy (SMA) type 1, where the age of onset is before six months, a SMA type 1 patient-specific cell model potentially

recapitulates the phenotype of motor neuron cell death (Ebert et al., 2009). If so, this model would be particularly useful in screening for drugs that hinder neuronal cell death in SMA type 1.

Various groups have modeled neurodegenerative diseases using both iPS and iN cell reprogramming strategies. Patient-specific iPS cell-derived neurons have been generated from somatic cells of sporadic and genetic forms of neurodegenerative diseases. In the case of genetic disease, iPS cells and subsequent iPS cell-derived neurons have been shown to maintain the genetic mutation found in the starting somatic cells. On the iN cell-based modeling front, cortical glutamatergic neurons, motor neurons, and dopaminergic neurons have been directly reprogrammed from fibroblasts, allowing for the potential modeling of diseases such as AD, ALS, SMA and PD.

Advantages and limitations of iPS and iN cell technologies for disease modeling

IPS and iN cell technology each has its own advantages and limitations for disease modeling. Indeed, these two approaches to cellular reprogramming are being explored vigorously for cell-based modeling of neurodegenerative diseases. What are the pros and cons of these two novel molecular tools and which should be utilized to create patient-specific disease models?

With regards to ease of reprogramming and efficiency, iN cell technology is at an advantage. Relative to iN cell reprogramming, iPS cell reprogramming is labor intensive, time consuming, and inefficient. The neuronal yield from iN cell

reprogramming ranges from 2%-9% (Vierbuchen et al., 2010; Pang et al., 2011) whereas the efficiency in iPS cell reprogramming is typically about 0.01% -0.05% (Okita et al., 2007; Takahashi et al., 2007; Yu et al., 2007). Furthermore, there is variability in differentiation efficiency both across iPS cell lines and within iPS cell lines, from one differentiation experiment to the next. Moreover, the iPS cell approach is tremendously labor intensive and time consuming. The derivation of one iPS line, from the time of fibroblast infection to establishing a stable line, takes at least one to two months and subsequent differentiation of iPS cells into a specific desired neuron type takes at least four to six weeks. In contrast, iN cell reprogramming generates neurons in about three weeks and cultures are relatively easy to maintain.

However, with respect to generating specific neuronal cell types, iPS cell technology may be at an advantage. Thus far, only a handful of neuronal subtypes have been generated via iN cell technology, including cortical glutamatergic neurons, motor neurons, and dopaminergic neurons (Pang et al., 2011; Son et al., 2011; Kim et al., 2011). Furthermore, these human induced neuronal cells appear to be less mature in their functional properties (e.g., the ability to form functional synapses) relative to iPS-cell derived neurons or primary neurons (Yang et al., 2011). In addition, if other neuronal subtypes are desired (for example medium spiny neurons for the modeling of Huntington's disease), the transcription factors would have to be newly determined. Moreover, it is uncertain whether all neuronal cell types (relevant for neurodegenerative disease modeling) can be generated by direct reprogramming (although current progress

in the field seems to suggest this is possible). In consequence, iPS cells may be more useful for cell-based disease modeling; in theory, they have the potential to generate all types of neurons and indeed various neuronal differentiation protocols exists and neuronal cell types with mature functional properties have been differentiated from ES cells and iPS cells.

Lastly, the utility of iPS vs. iN cell reprogramming technologies for modeling neurodegenerative diseases ultimately depends on feasibility for meaningful experiments. Direct cell reprogramming technology is advantageous for large-scale studies as it is relatively easy to generate iN cells from a large sample of patients. In contrast, it would be very labor, time, and cost intensive to generate and differentiate a large panel of patient-specific iPS cell lines. However, iPS cell technology would be useful for studying intermediate cell types such as neuronal precursors, which would be impossible using iN cell technology since direct reprogramming precludes intermediate developmental cell stages.

iPS-cell based models of neurodegenerative diseases

Amyotrophic lateral sclerosis (ALS)

The modeling of ALS using iPS cell technology was the first proof-of-concept experiment that demonstrated that iPS cells can be derived from fibroblasts cells of elderly patients. Fibroblast cells isolated from patients with ALS in their eighth decade of life was successfully reprogrammed to pluripotency (Dimos et al., 2008).

ALS is characterized by a progressive loss of motor neurons in the spinal cord and motor cortex. Disease progression results in weakening and wasting of muscles, leading to paralysis and death, typically within 1-5 years of initial diagnosis (Pasinelli et al., 2006). Using retroviral transduction of Oct4, Sox2, Klf4, and c-Myc (Takahashi et al., 2007), iPS cells were generated from the skin cells of a 82-year-old patient harboring a mutation in the *SOD1* gene. These ALS patient-specific iPS cells were subsequently differentiated into two cell types thought to be involved in the pathophysiology of ALS: motor neurons and glia. The patient-specific motor neurons express motor neuron markers, HB9 and Islet1/2. Glial cells expressed glial markers, GFAP and S100. Further characterization of these cells is necessary for examining molecular and cellular phenotypes (Dimos et al., 2008).

Spinal muscular atrophy (SMA)

The modeling of SMA using iPS cell technology was the first proof-of-concept experiment that demonstrated the utility of iPS cell-based models in drug screens. iPS cells derived from SMA patients were able to differentiate into motor neurons that responded to compounds known to increase SMN protein levels, a key pathological feature in SMA (Ebert et al., 2009).

SMA is a neurodegenerative disorder caused by autosomal recessive mutation in the survival motor neuron 1 gene (*SMN1),* resulting in the selective loss of lower motor neurons. At the molecular level, SMA is characterized by reduced *SMN* gene transcripts and SMN protein expression (Lefebvre et al.,

1995; Coovert et al., 1997). SMA patient-specific iPS (SMA-iPS) cells have been generated from SMA type 1 patient fibroblasts via lentiviral transduction of Oct4, Sox2, Nanog and Lin28 (Yu et al., 2007). SMA-iPS cells show reduced levels of full-length *SMN* gene transcripts. Extended culturing of SMA-iPS cell motor neuron differentiation cultures resulted in significantly fewer motor neurons with reduced size, relative to control iPS cell differentiation cultures. As such, the disease phenotype may selectively impede the generation of motor neurons and/or promote the degeneration of motor neurons. SMA-iPS cell-derived motor neurons responded to SMN-inducing compounds, valproic acid and tobramycin, resulting in a significant increase in SMN protein levels.

Alzheimer's disease (AD)

Like iPS cell-based model for SMA type 1, the iPS cell-based model for AD provide an important proof-of-principal for using iPS cell-based models in drug screens (Yagi et al., 2011). iPS cells derived from AD patients were able to differentiate into neurons that responded to compounds that modulated Aβ levels, the putative mediators of AD pathophysiology.

AD is the most common neurodegenerative disorder and most common cause of dementia in the elderly. Neuronal degeneration in AD occurs in the forebrain and hippocampal regions. The hallmark pathological features of AD include extracellular amyloid beta (Aβ) plaques and intracellular neurofibrillary tangles (Alzheimer et al., 1995). Retroviral transduction of Oct4, Sox2, Klf4, Lin28 and Nanog has been used to generate iPS cells from familial AD (FAD)

patient fibroblasts containing mutations in the *PSEN1* and *PSEN2* genes. Neurons derived from FAD patient-specific iPS (FAD-iPS) cells show increased Aβ42:Aβ40 ratio, a molecular feature of FAD. FAD-iPS cell-derived neurons also responded to γ-secretase inhibitors and modulators, drugs known to affect Aβ levels; neurons show dose-dependent reduction in Aβ42 and Aβ40 levels when exposed to compound E, a strong γ-secretase inhibitor and reduction in Aβ42:Aβ40 ratio when exposed to compound W, a selective Aβ42 lowering agent (Yagi et al., 2011).

Parkinson's disease (PD)

A few patient-specific iPS cell-based models of PD have been generated that demonstrate both the utility of iPS cell technology for in vitro disease modeling and in regenerative medicine. PD, the second most prevalent neurodegenerative disorder, is characterized by progressive loss of midbrain dopaminergic neurons in the substantia nigra while sparing dopaminergic neurons in the ventral tegmentum. Clinical features include both motor and cognitive symptoms.

iPS-cell based models of genetic forms of PD have been generated from patients with mutations in LRRK2 or PINK1 (Nguyen el at., 2011; Seibler et al., 2011). The iPS cell-based LRRK2 PD model was generated using fibroblasts from a PD patient who carries the LRRK2 G2019S mutation. Retroviral transduction of Oct4, Sox2, and Klf4 reprogrammed patient fibroblasts to iPS cells. Dopaminergic neurons derived from LRRK2 PD patient-derived iPS (PD-

iPS) cells expressed dopaminergic marker TH, and other midbrain neuronal markers, including NURR1, PITX3, and FOX2A. LRRK2 PD-iPS cell-derived DA neurons exhibited key features of PD pathology, including increased levels of α-synuclein protein and oxidative stress genes (Nguyen el at., 2011). The iPS-cell based PINK1 PD model was generated using fibroblasts from PD patients with mutations in the *PINK1* gene. Fibroblasts were reprogrammed to pluripotency using retroviral transduction of Oct4, Sox2, Klf4 and c-Myc along with valproic acid treatment, a histone deacetylase inhibitor that has been found to increase the efficiency of pluripotency induction. Dopaminergic neurons derived from PINK1 PD-iPS cells displayed a previously described phenotype, in which Parkin (another protein implicated in the pathogenesis of PD) recruitment to the mitochondria is impaired. This phenotype was rescued with overexpression of wild type PINK1 (Seibler et al., 2011).

An iPS-cell based model of sporadic PD was derived from sporadic PD patient fibroblasts using doxycycline (DOX)-inducible lentiviral vectors that encode either Oct4, Sox2, Klf4, and c-Myc (4F) or 4F minus c-Myc (3F). PD-iPS cells derived from 3F and 4F were both able to differentiate into dopaminergic neurons, expressing dopaminergic neuron marker TH. Transgene free PD-iPS cells were further generated using DOX-inducible vectors that were excisable with cre-recombinase. These cells also gave rise to dopaminergic neurons when subjected to directed differentiation (Soldner et al., 2009). When transplanted into the striatum of adult rodent brain, transgene-free PD-iPS cell-derived dopaminergic (DA) neurons survived for up to 16 weeks. Furthermore,

transplantation of PD-iPS cell-derived DA neurons into the striatum 6-OHDA-lesioned rats, a behavioral model of PD, resulted in partial functional recovery; lesioned rats that received cell transplantations showed reduction in amphetamine- and apomorphine-induced rotations (Hargus et al., 2010).

Huntington's disease (HD)

HD is an autosomal dominant neurodegenerative disease caused by expanded and unstable CAG repeats in the huntingtin gene (Duyao et al., 1993; The Huntington's Disease Collaborative Research Group, 1993). HD is characterized by degeneration of striatal medium spiny neurons (MSNs) and to a lesser extent, cortical neurons. Clinical features include progressive worsening chorea and cognitive decline leading to dementia. Retroviral transduction of Oct4, Sox2, Klf4 and c-Myc was used to reprogram fibroblasts from a HD patient with 72 CAG repeats in the huntingtin gene (Park et. al., 2008a). These iPS cells derived from HD patients (HD-iPS cells) were subsequently differentiated into neural stem cells (NSCs) and mature medium spiny neurons (MSNs) that expressed markers, calbindin and DARPP-32 (Zhang et al., 2010). The phenotype for HD-iPS cell-derived MSNs was not examined due to a low yield. However, in response to serum withdrawal, HD-iPS cell-derived NSCs showed elevation of caspase-3/7 activity, a known pathological feature of HD. Although focused on HD patient-specific NSCs and not MSNs, this study nevertheless shows promise for iPS-cell based modeling of HD (Zhang et al., 2010).

iN cell-based models of neurodegenerative diseases

Parkinson's disease

A number of studies have used different combinations of midbrain dopaminergic neuron-specific transcription factors to generate induced dopaminergic neuronal (iDA) cells, to varying degrees of success. One study used a combination Lmx1a and Fox2a along with Brn2, Ascl1, and Myt1l (Vierbuchen et al., 2010) to reprogram fibroblasts (Pfisterer et al., 2011). The resulting neurons expressed dopaminergic neuron markers TH, AADC and Nurr1 but these cells were unable to release dopamine, the critical functional activity of dopaminergic neurons (Pfisterer et al., 2011). Another group, using transcription factors Asc1, Nurr1 and Lmx1, were able to reprogram PD patient fibroblasts to neurons that expressed a panel of dopaminergic neuron markers, including TH, VMAT2, DAT, ALDH1A1 and calbindin. These neurons were capable of dopamine release, displaying the critical functional activity of dopaminergic neurons (Caiazzo et al., 2011). Lastly, a third group, using a combination of transcription factors Ascl1, PitX3, Nurr1, Lmx1a, Fox2a and En1, were able to generate eGFP positive cells from PitX3:eGFP fibroblasts. These cells expressed dopaminergic neuron markers TH, DAT, AADC and VMAT2 and were capable of dopamine release. Transplantation of iDA neurons into the 6-OHDA PD model resulted in reduction of amphetamine-induced rotation. This study illustrates the potential for iDA neurons for disease modeling (Kim et al., 2011). While these studies are promising as initial attempts for modeling PD, it is

important to note that iDA cells generated thus far have not displayed midbrain phenotype. In future studies, it would be imperative to generate midbrain iDA (and from somatic cells of PD patients) in order to properly model PD using iN technology.

Amyotrophic lateral sclerosis (ALS)

Mouse fibroblasts have been reprogrammed to induced motor neurons (iMN) by retroviral transduction of Lhx3, HB9, Isl1, and Ngn2 along with Brn2, Ascl1, and Myt1l. Induced motor neurons expressed HB9 and displayed functional neuronal properties, including the ability to form functional synaptic connections with myotubes. When these iMN cells were co-cultured with glia that carried the SOD1 G93A mutation, a mutation found in familial form of ALS, iMN cell loss was detected. While it remains to be seen whether iMN cells can be generated from ALS patient fibroblasts for modeling human disease, this study nevertheless shows the utility of iMN for elucidating molecular mechanisms of ALS (Son et al., 2011).

Chapter 2: Reprogramming AD patient fibroblasts to induced pluripotent stem (iPS) cells

Introduction

Recent advances in cellular reprogramming technologies have fueled excitement for the generation of human cell-based models of neurological diseases and patient-specific cellular replacement strategies in regenerative medicine. Our aim was to utilize induced pluripotent stem (iPS) cell technology to generate a patient-specific iPS cell-based model of Alzheimer's disease (AD). Our general strategy was to reprogram AD patient fibroblasts to pluripotency and subsequently differentiate these AD patient-specific iPS (AD-iPS) cells into cortical glutamatergic neurons. For the purpose of content organization, the generation of AD-iPS cells and their subsequent differentiation into neurons are discussed in separate chapters but it would be useful to keep this greater context in mind when reading this chapter.

Reprogramming experiments were conducted using familial AD (FAD) and sporadic AD (SAD) patient fibroblasts obtained from Coriell Cell Repository. We conducted two rounds of experiments to generate AD patient-specific iPS (AD-iPS) cell lines. In the initial round of experiments, the reprogramming efficiency was low and the resulting iPS cell lines expressed few pluripotency markers. In the second round of experiments, after modifying our protocol to increase efficiency of reprogramming and improve our method of screening for iPS cell colonies, we were able to isolate and expand a group of partially reprogrammed

FAD-, SAD- and control-iPS cell lines. These partially reprogrammed iPS cells lines expressed some pluripotent markers, including Oct4, Nanog and Tert.

Results

Generation of AD patient-specific iPS cell lines: initial round of experiments

In an initial attempt to generate AD patient-specific iPS (AD-iPS) cell lines, we used the viPS vector kit from Open Biosystems for lentiviral infection of FAD fibroblasts. This vector kit consisted of six separate lentiviral expression vectors containing the cDNAs of human Oct4, Sox2, Klf4, c-Myc, Nanog and Lin28 genes under control of the constitutive human elongation factor-1 alpha (EF1α) promoter. Previous studies had shown that human somatic cells can be reprogrammed to pluripotent stem cells via ectopic expression of a combination of either (1) Oct4, Sox2, Klf4, and c-Myc (Takahashi et al., 2007) or (2) Oct4, Sox2, Nanog and Lin28 (Yu et al., 2007). We chose to use the original Yamanaka factors, Oct4, Sox2, Klf4, and c-Myc for reprogramming.

Four individual viruses were generated and combined to make a stock virus for infecting FAD and control fibroblasts. At 2-3 weeks after lentiviral transduction, cell colonies appeared. The reprogramming efficiency was low, at about 0.01%. Efficiency was determined by the formula, ((# colonies formed)/ (number of fibroblasts infected)) x (100). We manually picked and clonally expanded cell colonies. After the fourth passage, colonies were maintained by enzymatic passaging using TrypLE (Invitrogen).

Characterization of pluripotency in first set of iPS cell lines

We selected two AD-iPS cell lines, B2-iPS and C8-iPS, and one control iPS cell line, Z1-iPS, for characterization. B2-iPS was generated from Coriell fibroblast line AG09908, which carries the PSEN2N141I mutation; C8-iPS was generated from Coriell fibroblast line AG06840, which carries the PSEN1246E mutation. iPS cells were positive for pluripotent stem cell markers alkaline phosphatase (AP) and Oct4. However, Nanog levels were low, and surface markers SSEA-4, Tra-1-60 and Tra-1-81 could not be detected. The morphology of these iPS cell colonies differed from that of human ES cell colonies, typically large, flat, and round colonies with well-defined borders. In contrast, our iPS cell colonies were small and irregularly shaped, with ill-defined boundaries (Figure 1). Furthermore, upon cortical neuron differentiation, iPS cell lines were unable to generate cortical neurons (see Chapter 3).

Generation of AD patient-specific iPS cell lines: second round of experiments

Because the first set of iPS cell lines did not possess traits of pluripotency at both the molecular level and functional level, we performed a second round of reprogramming experiments to generate iPS cell lines. In this second set of experiments, we modified our protocol to increase the likelihood of obtaining true iPS cells.

One of the parameters we sought to improve was the efficiency of reprogramming, the rationale being that with more colonies available for

screening, there would be a greater chance to obtain genuine iPS colonies. To increase the efficiency of reprogramming, we used a polycistronic lentiviral expression vector encoding the cDNAs of human Oct4, Sox2, Klf4, and c-Myc under control of the constitutive human elongation factor-1 alpha (EF1α) promoter (Sommer et al., 2010) (Figure 2). Previous studies had shown reprogramming efficiency using this polycistronic vector (estimated at 0.05%) to be 10-fold higher than that observed for reprogramming achieved via multiple individual viral vectors (approximately 0.01%-0.05%) (Sommer et al., 2009; Sommer et al., 2010).

Another parameter we modified was the morphological criteria used when screening plates for cell colonies, since having good morphology is critical for identifying potential iPS cell colonies. We increased our stringency in evaluating morphology when selecting colonies for isolation, only picking colonies with excellent morphology: these colonies were sufficiently large, flat and round, with well defined borders and contained small cells with a high nucleus-to-cytoplasm ratio.

Additionally, in this second round of experiments, we also altered the method of viral infection, using repeated innoculations of unconcentrated viral supernatant rather than one innoculation of concentrated virus (Figure 3). In discussions with colleagues also conducting iPS cell reprogramming experiments, infection of cells using unconcentrated virus seemed to produce more consistent reprogramming results. Additionally, using viral supernatant was more labor-efficient than using concentrated virus.

A total of ten FAD-iPS lines, twenty-two SAD-iPS lines and sixteen control-iPS lines were initially picked and clonally expanded. Of these iPS cell lines, a total of eighteen lines survived initial manual expansion and gave rise to stable cell lines. Five of these iPS cell lines were derived from FAD patient fibroblasts: three, 9908-1, 9908-5, and 9908-6, from the Coriell fibroblast line AG09908 (containing the PSEN2N141I mutation) and two, 6840-3 and 6840-4, from the Coriell fibroblast line AG06840 (containing the PSEN1246E mutation). Seven of these iPS lines were derived from SAD patient fibroblasts, Coriell lines AG04401, AG04402, AG06262, AG06263, AG06264. Finally, six of these iPS lines were derived from control fibroblasts, Coriell lines AG10788, AG07573, AG07871, and AG11368 (Figure 4).

The efficiency of reprogramming for the second round of experiments was greater than the first round of experiments, at approximately 0.02-0.2%. The colonies that were selected for expansion satisfied our stringent morphological criteria. These iPS cell lines were all passaged manually at least five times after initial isolation, after which the colonies were maintained by enzymatic passage using dispase (Invitrogen).

Characterization of pluripotency in second set of iPS cell lines

We focused on the group of iPS cell lines derived from FAD patients and control iPS cell lines for initial characterization by immunostaining for pluripotent stem cell markers, Oct4 and Nanog. AD-iPS cells stained positive for Oct4 and Nanog (Figure 5A). We then focused on two AD-iPS cell lines, 9908-5 and 6840-

4, containing mutations in the PSEN2 and PSEN1 genes, respectively, for further characterization.

We first examined their level of expression of pluripotent surface markers. Rather than immunostaining to achieve this end, as we had done with the first set of iPS cell lines, we used fluorescence activated cell sorting (FACS) analysis, which has higher sensitivity and specificity for immunodetection. FACS analysis experiments were performed by the commercial FACS facility at the New York Stem Cell Foundation (NYSCF).

Using FACS analysis, we examined the expression of pluripotent surface markers, SSEA-3, SSEA-4 and Tra-1-60 in AD-iPS cell lines 9908-5 and 6840-4. The human ES cell line Hues HB9:GFP was used for positive control and both fibroblasts and unstained iPS lines were used for negative controls. AD-iPS lines showed low expression levels of all three surface markers. The mean fluorescence intensity for SSEA-3, SSEA-4 and Tra-1-60 in both AD-iPS cell lines were about two orders of magnitude lower than that for Hues HB9:GFP (10^2 vs. 10^4). Additionally, only 0.01% of 9908-5 cells were triple positive, and 0% of 6840-4 cells were triple positive. In comparison, about 7.5% of Hues HB9:GFP cells were triple positive. Thus, the level of expression of pluripotent surface markers in AD-iPS cell lines were low and the percentage of cells that expressed these markers were also low, relative to the Hues HB9:GFP line (Figure 5B).

To further characterize AD-iPS lines 9908-5 and 6840-4, we used quantitative RT-PCR analysis to examine mRNA expression levels of pluripotency genes, FoxD3, Tert, Nanog and Cripto. All mRNA expression levels

in AD-iPS cells were normalized to that in Hues HB9:GFP cells. We found that AD-iPS cell lines expressed low levels of pluripotency genes FoxD3, Nanog and Cripto. Nanog and Cripto mRNA levels were negligible; FoxD3 mRNA levels were about 60%-75% lower than that in Hues HB9:GFP cells. However, Tert mRNA levels were comparable to that in Hues HB9:GFP cells (Figure 5C, top panel).

We also used quantitative RT-PCR analysis to examine the total mRNA expression levels (viral levels plus endogenous levels) and viral mRNA expression levels of the four reprogramming factors, Oct4, Sox2, Klf4 and c-Myc. The total mRNA levels of Oct4 and Sox2 were negligible. However, the total mRNA levels of Klf4 and c-Myc were about one- to two-fold higher than that in Hues HB9:GFP. Viral mRNA levels of Oct4 and Sox2 were undetectable, whereas the viral mRNA levels of Klf4 and c-Myc were substantially higher than that in Hues HB9:GFP. The results of viral mRNA levels are consistent with the results of total mRNA levels of the 4 reprogramming factors; for Oct4 and Sox2 both total and viral mRNA levels are negligible whereas for Klf4 and c-Myc, both viral and total mRNA levels are high. As such, the mRNA levels of Klf4 and c-Myc is attributable to high gene expression from viral vectors rather than an endogenous locus (Figure 5C, bottom panel; Figure 5D).

Taken as a whole, these experiments show that our second set of iPS cells expressed some but not all pluripotency markers. AD-iPS and control-iPS cell lines stain positive for Oct4 and Nanog protein (Figure 5A). Focusing on two AD-iPS cell lines, 9908-5 and 6840-4, for further characterization, we found that

the expression level of surface pluripotency markers SSEA-3, SSEA-4 and Tra-1-60 were low in these lines. Furthermore, while a small percentage of cells in AD-iPS cell line 9908-5 were positive for all three pluripotent surface markers, no cells in AD-iPS cell line 6840-4 were triple positive (Figure 5B). Examining mRNA expression levels of pluripotency markers, we found that Tert mRNA expression levels in these lines were comparable to that in human ES cell line, Hues HB9:GFP. However, FoxD3, Cripto, Nanog Oct4 and Sox2 mRNA expression levels were low (Figure 5C and 5D). While the expression levels of Klf4 and c-Myc were high, this is attributable to transcription of integrated lentiviral vectors rather than gene expression from an endogenous locus. As such, we have partially reprogrammed iPS cells that express some pluripotency markers, namely Oct4, Nanog and Tert.

Discussion

In conducting reprogramming experiments on a large panel of human fibroblast cell lines (approximately 20 lines in total), we observed variables that consistently affected the efficiency of reprogramming. One such factor was the use of a single polycistronic lentiviral expression vector vs. multiple monocistronic expression vectors for the delivery of reprogramming factors. Similar to previous reports (Sommer et al., 2009; Sommer et al., 2010; Carey et al., 2009), we found that reprogramming efficiency was increased when we used a single polycistronic viral vector compared to multiple individual viral vectors. The reprogramming efficiency in our first set of experiments using multiple viral

vectors was about 0.01%, whereas the reprogramming efficiency in our second set of experiments using a polycistronic vector was about typically about 0.1%.

Additionally, we found that the growth rate and passage number of individual fibroblast cell lines affected their reprogramming efficiency. Fibroblasts lines that had a slower population doubling time generally exhibited lower reprogramming efficiency. Indeed, studies have shown that cell division is necessary for reprogramming to occur. Furthermore, fibroblast cell lines that had a higher passage number also exhibited lower reprogramming efficiency. It is possible that sustained maintenance of fibroblasts in tissue culture results in the accumulation of subtle changes at the molecular level that affect their capacity to be reprogrammed. This notion is slightly reminiscent of studies that have shown that the differentiation status of cells influences their ease for reprogramming. For example, hematopoietic stem cells can be more efficiently reprogrammed than terminally-differentiated B and T lymphocytes (Eminli et al., 2009).

When we first set out to generate a patient-specific iPS cell-based model of AD, the reprogramming of human somatic cells using iPS cell technology was still very much in its infancy. As such, there was much trouble-shooting involved in our first set of fibroblast reprogramming experiments. That we were not able to generate true iPS cells in this first set of experiments is not surprising. However, in our second set of experiments, despite our efforts to improve our protocol by using a polycistronic vector to increase reprogramming efficiency and exercising precision in screening for iPS cell colonies, we nevertheless were unable to generate iPS cells that expressed the panel of pluripotency markers

necessary for the validation of stemness. Instead, our iPS cells appear to be partially reprogrammed, expressing only some pluripotency markers, namely, Oct4, Nanog and Tert. The most probable explanation for our failure to generate fully reprogrammed iPS cells is likely to be the stochastic nature of the reprogramming process. During the course of reprogramming, somatic cells become randomly trapped at various stages of de-differentiation, resulting in iPS cells that are incompletely reprogrammed (Hanna et al., 2009).

Studies on the molecular mechanism of reprogramming in mouse somatic cells have shown that the de-differentiation of fibroblasts to iPS cells is a stochastic process during which cells progress through a series of sequential stages to reach pluripotency. In early reprogramming stages, AP is activated, followed by SSEA-1. Reactivation of endogenous Nanog and Oct4 occurs late in the reprogramming process. Exogenous viral reprogramming factors need to be expressed for about 10-12 days before cells reach a stable pluripotent state (Brambrink et al., 2008; Stadtfeld et al., 2008a).

In the reprogramming of human somatic cells, Chan et al. have found that the use of colony morphology to identify potential iPS cells is inadequate (Chan et al., 2009). Many colonies with excellent morphology turned out to be partially reprogrammed; one such type of colony expressed neither SSEA-4 nor Tra-1-60 and another type expressed SSEA-4 but not Tra-1-60. Curiously, these incompletely reprogrammed iPS cells were nevertheless capable of self-renewal (Chan et al., 2009). This capacity for self-renewal is most likely due to expression of viral c-Myc. This oncogene can induce arbitrary self-renewal in

many cell types. Indeed, exclusion of c-Myc from the cocktail of reprogramming factors decreases the number of partially reprogrammed colonies (Nakagawa et al., 2008; Judson et al., 2009).

While our AD-iPS cell lines had excellent morphology, they expressed only low levels of Oct4, Nanog and Tert and little to no levels of surface markers, SSEA-3, SSEA-4 and Tra-1-60. As such, our iPS cell lines are partially reprogrammed, not fully de-differentiated to pluripotent stem cells, but rather, suspended in an incompletely de-differentiated state. The capacity for self-renewal in these cells may be attributable to their high levels of viral c-Myc transcripts.

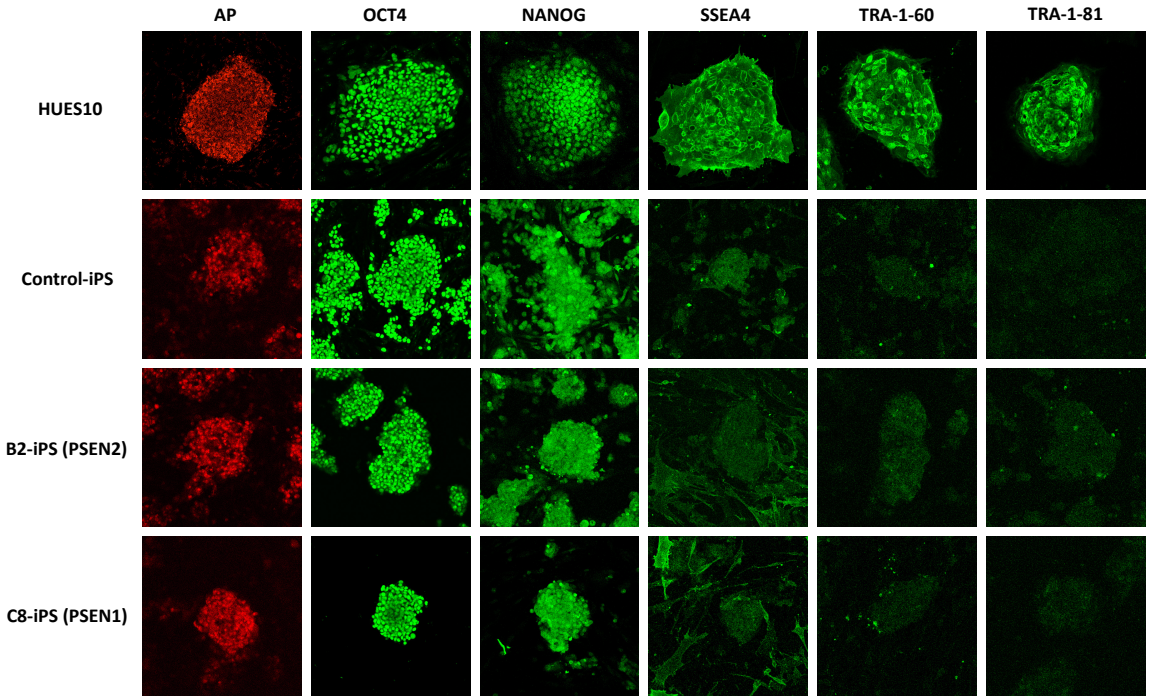

Figure 1. AD patient-specific iPS (AD-iPS) cells generated using the viPS vector kit (Open Biosystems) display only some markers of pluripotency
Pluripotency marker analysis of AD-iPS cells (B2-iPS and C8-iPS) and control-iPS cells. iPS cells were immunostained with antibodies specific to OCT4, NANOG, SSEA4, TRA-1-60 and TRA-1-81. Alkaline phosphatase (AP) activity was detected using an alkaline phosphatase substrate kit (Vector). AP and OCT4 protein levels are comparable to that of human ES cells (HuES10) (Cowan et al, 2004). NANOG levels are low relative to HuES10. SSEA4, TRA-1-60 and TRA-1-81 expression was not detected. The morphology of “iPS cell” colonies differed from that of human ES cell colonies; “iPS cell” colonies were small, irregularly shaped, and had ill-defined boundaries.

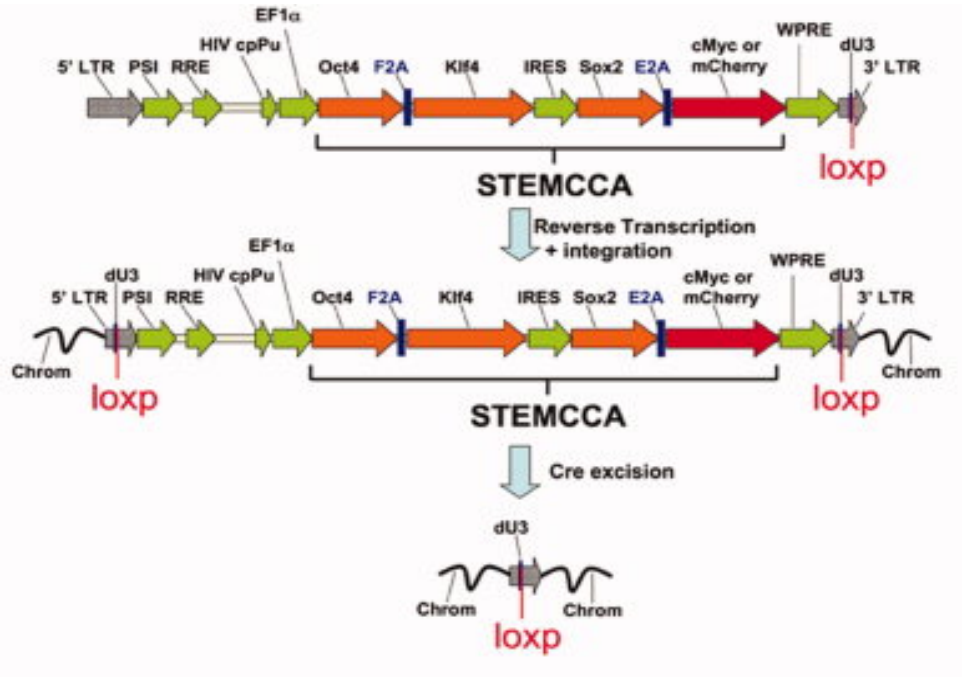

(Sommer et al., 2010)

Figure 2. Schematic of the polycistronic lentiviral vector used to derive second set of AD patient-specific iPS cell lines (courtesy of Dr. Rudolph Jaenisch)

The vector contains a cassette consisting of the cDNAs of human Oct4, Klf4, Sox2 and cMyc under the control of a constitutive EF1α promoter. An IRES element separates two fusion cistrons: (1) Oct4 and Klf4 cDNA fused via self-cleaving F2A peptide and (2) Sox2 and cMYC cDNA fused via self-cleaving peptide E2A.

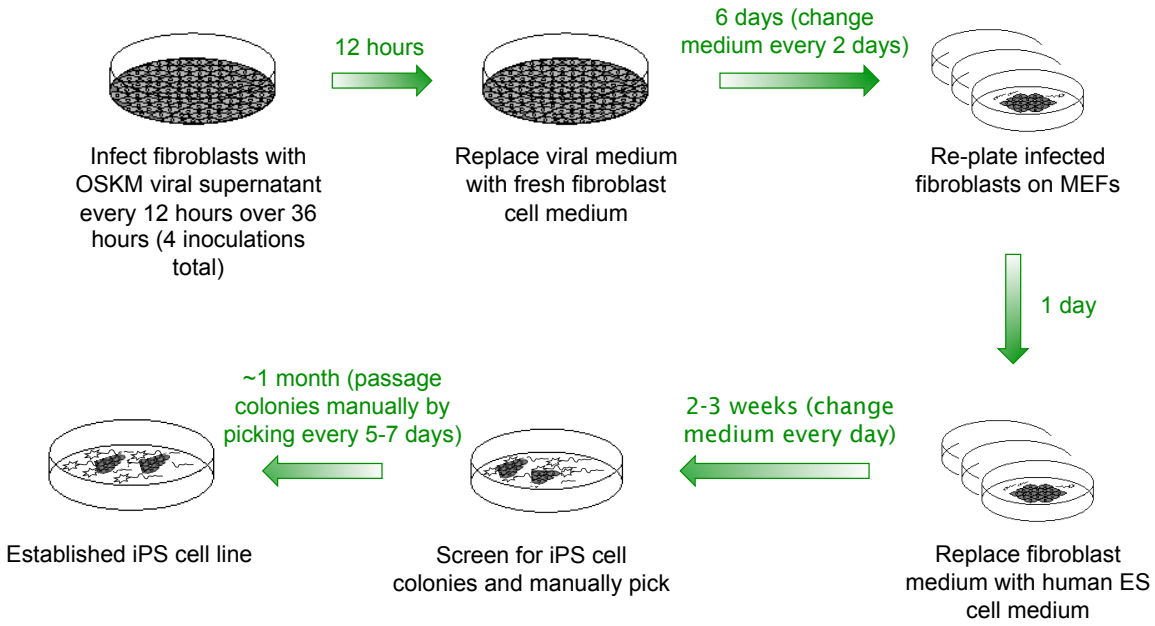

Figure 3. Schematic outlining the protocol for reprogramming second set of AD patient-specific iPS cell lines

OSKM, lentiviral vector encoding reprogramming factors Oct4, Sox2, Klf4, and cMyc; fibroblast cell medium, DMEM supplemented with 10% FBS; human ES cell medium, DMEM/F12 with GlutaMAX supplemented with 20% knockout serum replacement, 1% nonessential amino acids, 55μM b-mercaptoethanol and 20 ng/ml bFGF.

A

Genetic (FAD) iPS lines (5 total)	Control iPS lines (6 total)	Sporadic (SAD) iPS lines (7 total)
9908 – 1, 5, 6 (PSEN2 N141I)	10788 – D	4401 – 1
6840 – 3, 4 (PSEN1 A246E)	7573 – 10	4402 – 1, 2
	7871 – 2, 4	6262 – 1, 2
	11368 – 1, 3	6263 – 1
		6364 – 8

B

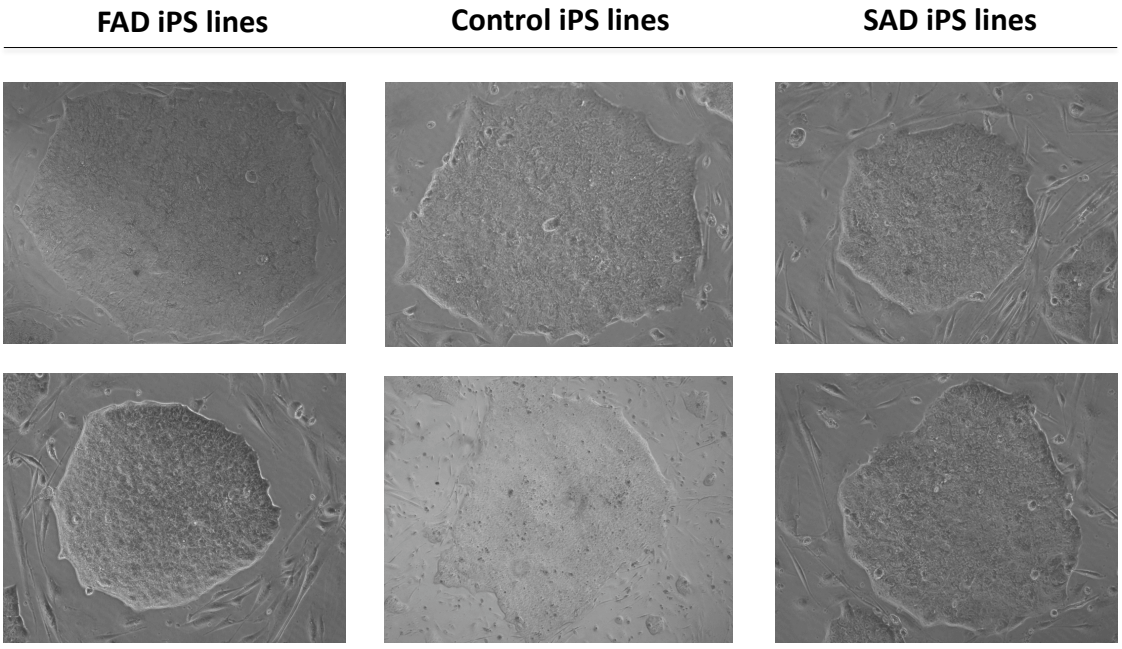

Figure 4. Second set of AD patient-specific iPS cell lines display characteristic human ES cell morphology

(A) iPS cell lines were generated from familial AD (FAD) and sporadic AD (SAD) patient skin fibroblasts obtained from Coriell Insititute. Familial patient fibroblasts contain either presenilin 1 (PSEN1) or presenilin 2 (PSEN2) mutations.

(B) Representative phase contrast images of iPS cell colonies. Colonies are flat and round, with clearly-defined borders.

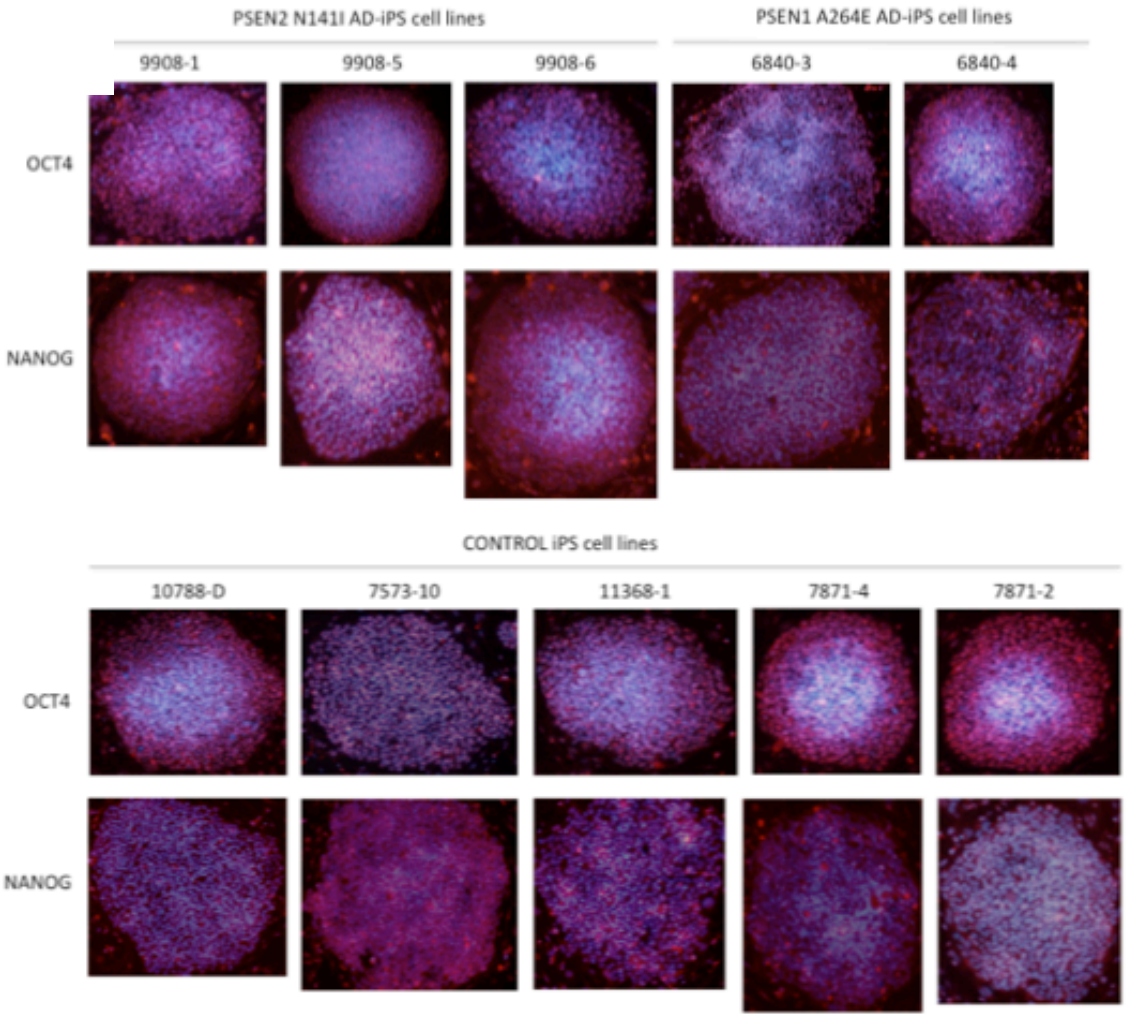

Figure 5A. Second set of AD patient-specific iPS (AD-iPS) cell lines display OCT4 and NANOG activity

Control and AD-iPS cell lines were immunostained for antibodies specific for pluripotency markers, OCT4 and NANOG. iPS cells showed positive immunostaining OCT4 and NANOG, shown in red. DNA is in blue.

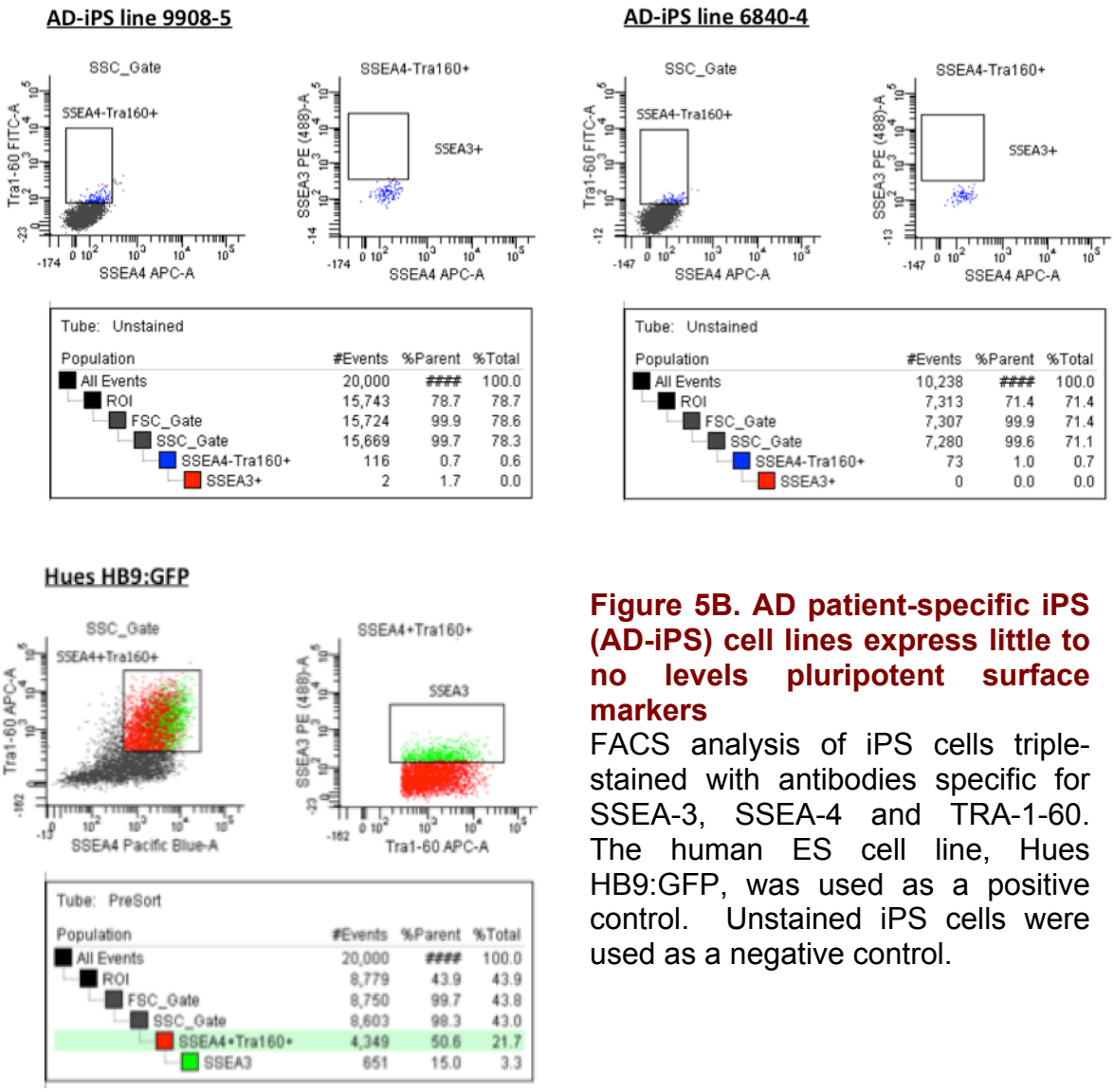

Figure 5B. AD patient-specific iPS (AD-iPS) cell lines express little to no levels pluripotent surface markers

FACS analysis of iPS cells triple-stained with antibodies specific for SSEA-3, SSEA-4 and TRA-1-60. The human ES cell line, Hues HB9:GFP, was used as a positive control. Unstained iPS cells were used as a negative control.

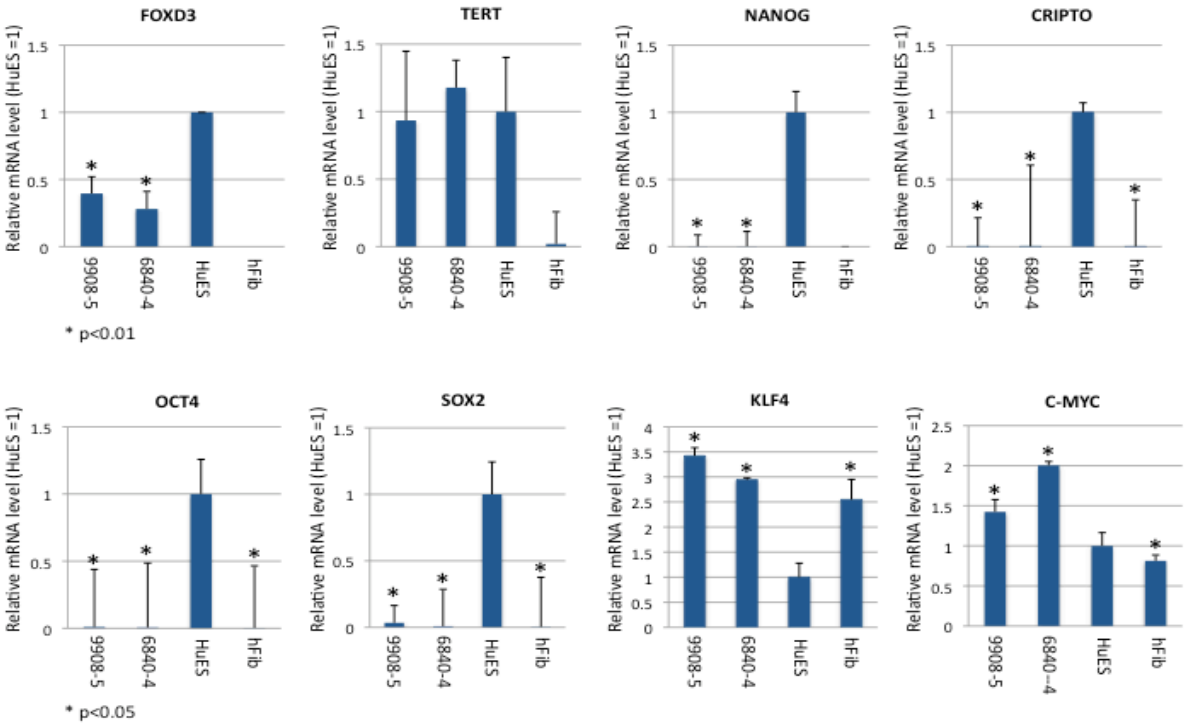

Figure 5C. AD patient-specific iPS (AD-iPS) cell lines expressed mostly low levels of pluripotency genes

Quantitative RT-PCR analysis for total mRNA levels of pluripotency genes associated with pluripotency, *FOXD3, TERT, NANOG, CRIPTO, OCT4, SOX2, KLF4 and C-MYC,* in AD-iPS cell lines 9908-5 and 6840-4. *TERT* transcript levels were comparable to human ES cells (HuES). FOXD3, NANOG, CRIPTO, OCT4 and SOX2 transcript levels were low to negligible. KLF4 and C-MYC total mRNA levels were about one- to two-fold higher than in HuES. Expression levels are normalized to *GAPDH*; *p<0.05 by ANOVA; n=3 for each line; error bars represent the standard error of the mean (SEM). HuES, Hues HB9:GFP cells; hFib, human fibroblasts

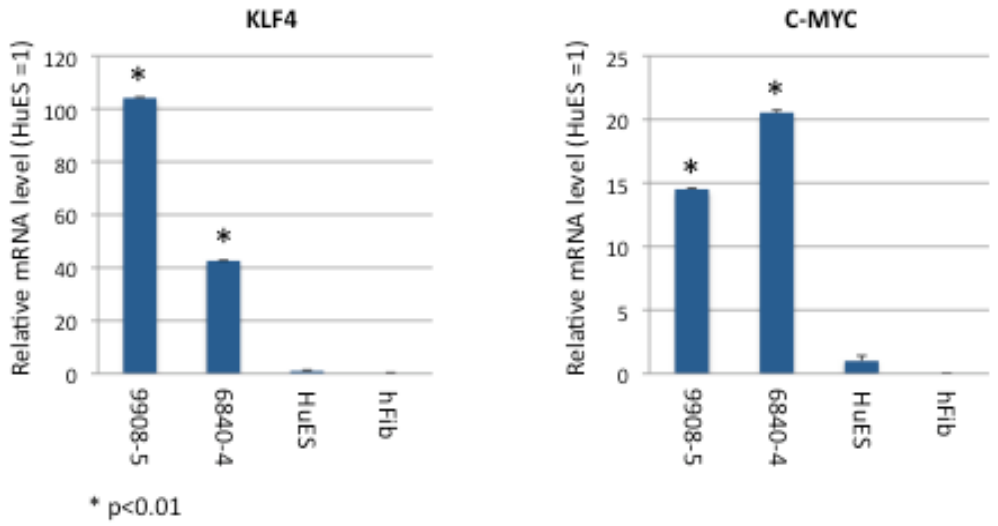

Figure 5D. AD patient-specific iPS (AD-iPS) cell lines expressed high levels of viral KLF4 and C-MYC transcripts

Quantitative RT-PCR analysis for viral mRNA levels of reprogramming factors *OCT4, SOX2, KLF4 and C-MYC,* in AD-iPS cell lines 9908-5 and 6840-4. Primers specific for virally encoded transcripts were used. Viral *KLF4* and *C-MYC* transcript levels were substantially higher than HuES. Expression of the viral *OCT4* and *SOX2* transgenes was not detectable (plot not shown). These results are consistent with analysis of total mRNA levels, which show high total levels of *KLF4* and *C-MYC* but extremely low total levels of *OCT4* and *SOX2* (Fig.5C). Expression levels are normalized to *GAPDH*; *p<0.01 by ANOVA; n = 3 for each line; error bars represent the standard error of the mean (SEM). HuES, Hues HB9:GFP cells; hFib, human fibroblasts

Chapter 3: Generating an iPS cell-based model of AD to understand cell-type specificity in AD

Introduction

The advent of induced pluripotent (iPS) cell technology has spurred great excitement in the generation of patient-specific disease models and the need for these bioengineered models in studying neurodegenerative diseases is irrefutable. Our aim was to utilize iPS cell technology to generate a patient-specific iPS cell-based model of Alzheimer's disease (AD). While animal models of AD have advanced our understanding of its pathophysiology, these models do not fully recapitulate aspects of the human disease. Furthermore, animal models and cellular models of AD (based on human cancer cell lines or human fibroblasts) do not recapitulate the human intraneuronal environment. A patient-specific cell-based model of AD offers a better representation of the intact neuronal environment in which the disease arises and as such, may be critical for fully elucidating the molecular mechanism of AD.

At the start of this undertaking, a few proof-of-concept studies had previously shown that neurodegenerative diseases can be modeled using iPS cell technology, including amyotrophic lateral sclerosis (ALS) (Dimos et al., 2008) and spinal muscular atrophy (SMA) (Ebert et al., 2009). However, an iPS-cell based model of AD had not been reported. We wanted to generate an AD patient-specific iPS (AD-iPS) cell-based model of AD that would recapitulate the molecular aspects of the disease in a human cellular context. Dominantly

inherited familial forms of AD (FAD) are caused by mutations in APP or in the two presenilin genes, presenilin 1 (PSEN1) and presenilin 2 (PSEN2), which encode part of the γ-secretase enzyme complex that cleaves APP to Aβ peptides. At the molecular level, these genetic mutations have been shown to affect APP processing and Aβ production, resulting in the preferential accumulation of Aβ42 peptides relative to the Aβ40 isoform (Shen and Kelleher, 2007; De Strooper and Annaert, 2010).

Furthermore, we wanted to utilize iPS cell technology to examine a key feature in AD: cell-type specificity in the manifestation of disease pathology (a critical phenomenon common among neurodegenerative diseases). Neurodegeneration in AD is largely limited to the medial temporal lobe of the cortex and the hippocampus; the major subtype of neurons affected are cortical glutamatergic neurons and cholinergic neurons (Khachaturian et al., 1985). The mechanism for this selective neuronal loss has been largely unexplored in AD - and indeed, among neurodegenerative diseases as a whole - due to the lack of molecular tools that would allow for the designing of proper experiments to answer this question. However, iPS technology may prove the contrary and potentially offers an excellent platform for studying this phenomenon, as it is possible to generate multiple neuron subtypes from disease-specific iPS cells and cross-analyze them for preferential neuronal targeting of disease phenotypes.

Experimental Design

The generation of a patient-specific iPS cell-based model of AD involved two sequential steps. The first step was to generate iPS cells from AD patient fibroblasts. Subsequently, these AD patient-derived iPS (AD-iPS) cells were differentiated into forebrain cortical glutamatergic neurons. Furthermore, for addressing the question of cell-type specificity in AD, we also differentiated AD-iPS cells into motor neurons in parallel. Our strategy was to compare AD-iPS cell-derived cortical neurons against AD-iPS cell-derived motor neurons, a neuron subtype that is not affected in AD. We decided to use motor neurons because these neurons are unaffected in AD and furthermore, a robust protocol exists for the differentiation of human embryonic stem (ES) cells into motor neurons (Boulting et al., 2011).

Our aim was to examine APP processing in the form of Aβ40 and Aβ42 production in AD-iPS cell-derived cortical neurons and to compare these findings against that in AD-iPS cell-derived motor neurons. Comparison of two neuron subtypes generated from the same AD-iPS cell line would allow for good internal control when examining differences in molecular and cellular phenotypes.

Results

Differentiating AD-iPS cells into glutamatergic forebrain neurons

Our first set of AD-iPS cells, B2-iPS and C8-iPS (see Chapter 2), were not able to differentiate into cortical neurons when subjected to a directed differentiation protocol for cortical neurons. We used a protocol that was adapted

from Eiraku et al., 2008, which we dubbed the EGF method. Briefly, iPS cells were suspended as embryoid bodies (EBs) in serum-free media. After 25-27 days in culture, EBs were dissociated and plated on poly-D-ornithine/laminin. B2-iPS, C8-iPS and control-iPS differentiation cultures contained cells that showed non-specific staining for a pan-neuronal marker, β-III-tubulin (TuJ1), and for mature glutamatergic neuron marker, vesicular glutamate transporter-1 (vGLUT1). Additionally, differentiated cells did not show characteristic neuronal cell bodies or processes (data not shown).

In differentiating our second set of AD-iPS cells, we focused on three iPS lines: 9908-5, which contains the PSEN N141I mutation, 6840-4, which contains the PSEN1 A246E mutation and 7871-2, a control line. Due to difficulty in generating neurons with our first set of AD-iPS cells, we decided to experiment with two cortical neuron differentiation protocols: our prior EGF method and the PALS-C method, which we developed by modifying a motor neuron differentiation protocol (Boulting et al., 2011). We also modified our prior EGF method by combining EB formation with active neuralization via dual SMAD inhibition with SB431542 and LDN193189 (Boulting et al., 2011). EBs were then treated with EGF and bFGF as before. In the PALS-C method, EBs were actively neuralized but not treated with EGF and bFGF.

We were able to generate forebrain/telencephalic progenitors from AD-iPS cell using both differentiation methods. Forebrain progenitor cells expressed high mRNA levels of the forebrain progenitor transcription factor, *FOXG1*, relative to a human fibroblast cell line, as determined by quantitative RT-PCR analysis. In

AD-iPS cell lines 9908-5 and 6840-4, *FOXG1* levels in progenitors derived from the EGF method was at least half-fold higher than that for the PALS-C method. In the control-iPS cell line, 7871-2, the difference in *FOXG1* levels for the two differentiation methods was not as pronounced (Figure 1A). iPS cell-derived forebrain progenitors also stained positive for a dorsal forebrain progenitor transcription factor, Pax6. However, the cells were indistinct and poorly-defined compared to telencephalic progenitors derived from human ES line, Hues HB9:GFP. Hues HB9:GFP cell-derived progenitor cells formed rosette-like structures whereas iPS cell-derived progenitors did not (Figure 1B).

We found this difference between the EGF and PALS-C methods to be carried to the mature neuron stage. Both protocols were able to generate neurons that stained positive for TuJ1 and vGLUT1. However, cells differentiated via the EGF method resulted in neurons with more mature branching morphology and strong, stereotypical punctate vGLUT1 immunostaining whereas neurons derived from the PALS-C method had less defined neuronal processes and weak vGLUT1 immunostaining (Figure 2). Neurons generated from the EGF method also stained positive for the neocortical glutamatergic neuron marker Tbr1, confirming their cortical glutamatergic nature (Figure 3).

The efficiency of neuron differentiation from iPS cells was very low relative to Hues HB9:GFP. In iPS cell lines, the yield of TuJ1-positive cells ranged from 0.015% to 0.06%, whereas the yield of TuJ1-positive cells in Hues HB9:GFP differentiation cultures was about 24%. In iPS cell cultures, 33% of Tuj1-positive

cells were also positive for vGLUT1. In HB9:GFP cell cultures 40% of Tuj1-positive cells were also positive for vGLUT1 (Figure 3). Given that at the progenitor stage, differentiated iPS cell cultures appeared unhealthy, it is not surprising that the neuronal yield was so low. It is possible that cells were trapped in the progenitor stage or underwent apoptosis as differentiation progressed towards the mature neuron stage.

Differentiating AD-iPS cells into motor neurons

We differentiated AD-iPS cell lines 9908-6, 6840-4, and control-iPS cell line, 7871-2 into motor neurons using a directed differentiation protocol (Boulting et al., 2011). Briefly, iPS cells were actively neuralized via dual SMAD inhibition with drugs SB431542 and LDN193189, and suspended as EBs. EBs were treated with retinoic acid (RA), and purmorphamine, an agonist for the sonic hedgehog (SHH) signaling pathway; RA and SHH are CNS regional specification factors that induce caudalization and ventralization, respectively. After 21-22 days in culture, EBs were dissociated into a single-cell suspension and plated on poly-D-ornithine/laminin. The resulting neurons stained positive for TuJ1, HB9, a motor neuron-specific marker (Wichterle et al., 2002), and Islet1, a transcription factor involved in motor neuron development (Wichterle et al., 2002; Li et al., 2005) (Figure 4).

Similar to cortical neuron differentiation, the efficiency of motor neuron differentiation of these iPS cell lines was very low, relative to Hues HB9:GFP. The yield of TuJ1-positive cells in iPS differentiation cultures ranged from 0.03%

to 0.07%, whereas the yield of TuJ1-positive cells in Hues HB9:GFP differentiation cultures was about 6%. In iPS cell cultures, 25% of Tuj1-positive cells were also positive for Islet1. In HB9:GFP cell cultures 40% of Tuj1-positive cells were also positive for Islet1 (Figure 4).

Discussion

Although we only succeeded in generating partially reprogrammed iPS cells, we nevertheless felt it prudent to proceed with neuronal differentiation because we had generated a large panel of partially reprogrammed iPS cell lines from both FAD and SAD patient fibroblasts. Indeed, due to their excellent morphology, we had high confidence in the pluripotency of our iPS cell lines and therefore conducted differentiation experiments in parallel with pluripotency validation experiments. As such, we only became aware of having incompletely reprogrammed iPS cell lines after differentiation experiments were well underway. Despite these findings, we resolved to continue our differentiation experiments because there was no evidence in the literature that partially reprogrammed iPS cells would not be able to differentiate into neurons. We reasoned that it was quite possible that our partially reprogrammed iPS cells were dedifferentiated enough for re-direction towards the neuronal lineage. Furthermore, because our end goal was to generate a patient-based model of AD, whether our original cells were true iPS cells was of little consequence if we could succeed in generating forebrain cortical glutamatergic neurons and motor neurons from them. Indeed, we were able to re-direct our partially

reprogrammed iPS cells toward the neuronal lineage and succeeded in generating both AD-iPS cell-derived forebrain cortical glutamatergic neurons and AD-iPS cell-derived motor neurons. However, differentiation efficiency was low, being less than 0.1% for both neuronal subtypes.

There is much technical challenge in the differentiation of iPS cell lines. Much variation exists among the differentiation efficiencies of iPS cell lines. While the overall differentiation efficiency was low among all iPS cell lines, the control-iPS cell line 7871-2 consistently yielded higher percentage of neurons, followed by AD-iPS line 6840-4 and last, AD-iPS line 9908-5. This disparity in differentiation efficiency has been reported in various other iPS cell studies (Hu et al., 2010; Taura et al., 2009; Tokumoto et al., 2010; Boulting et al., 2011).

Of specific interest, Boulting et al., 2011, reported a comprehensive study on a panel of 16 iPS cell lines, examining their pluripotency and ability to generate mature motor neurons. They found variation in the differentiation efficiencies among the panel of validated iPS cells lines. Furthermore, iPS cell lines which differentiated poorly into motor neurons could be coaxed into differentiation by active neuralization via dual SMAD inhibition using drugs SB431542 and LDN193189, the structural analog of dorsomorphin (Chambers et al., 2009; Zhou et al, 2010). SB431542 inhibits endogenous activin/lefty/TGF-β1 pathways via phosphorylation of ALK4, ALK5, and ALK7 receptors while LDN193189 inhibits BMP type I receptors ALK2 and ALK3. Endogenous BMP inhibitors, including noggin (Smith and Harland, 1992; Valenzuela et al., 1995),

chordin (Sasai et al., 1994) and follastatin (Hemmati-Brivanlou et al., 1994) are known to be critical neural inducing factors.

That the poorly differentiating iPS cell lines in the Boulting et al., study can be coaxed to into differentiation by active neuralization is curious. Indeed, we modified our differentiation protocols to include neuralizing drugs SB431542 and LDN193189 after discussions with members of Dr. Christopher Henderson's lab and Project A.L.S. The rationale for adding these drugs to the differentiation protocols was to shorten the amount of time for differentiation and increase neuronal yield in the differentiation of true iPS cells (i.e., at the time, we did not know we had partially reprogrammed iPS cells in our hands). However, it may be the case that active neuralization was the critical factor that allowed for the differentiation of our partially reprogrammed iPS cells into neurons. One could imagine a scenario where our partially reprogrammed cells were in a particular dedifferentiated state that when subjected to induction from strong neuralizing factors, their cell fate was pushed into the neural lineage.

Because reprogramming efficiencies were extremely low, we were unable to examine APP processing in these cultures, by assaying for secreted Aβ40 and Aβ42 using sandwich ELISA. As such, the validity of our AD-iPS cell based model for AD remains to be determined.

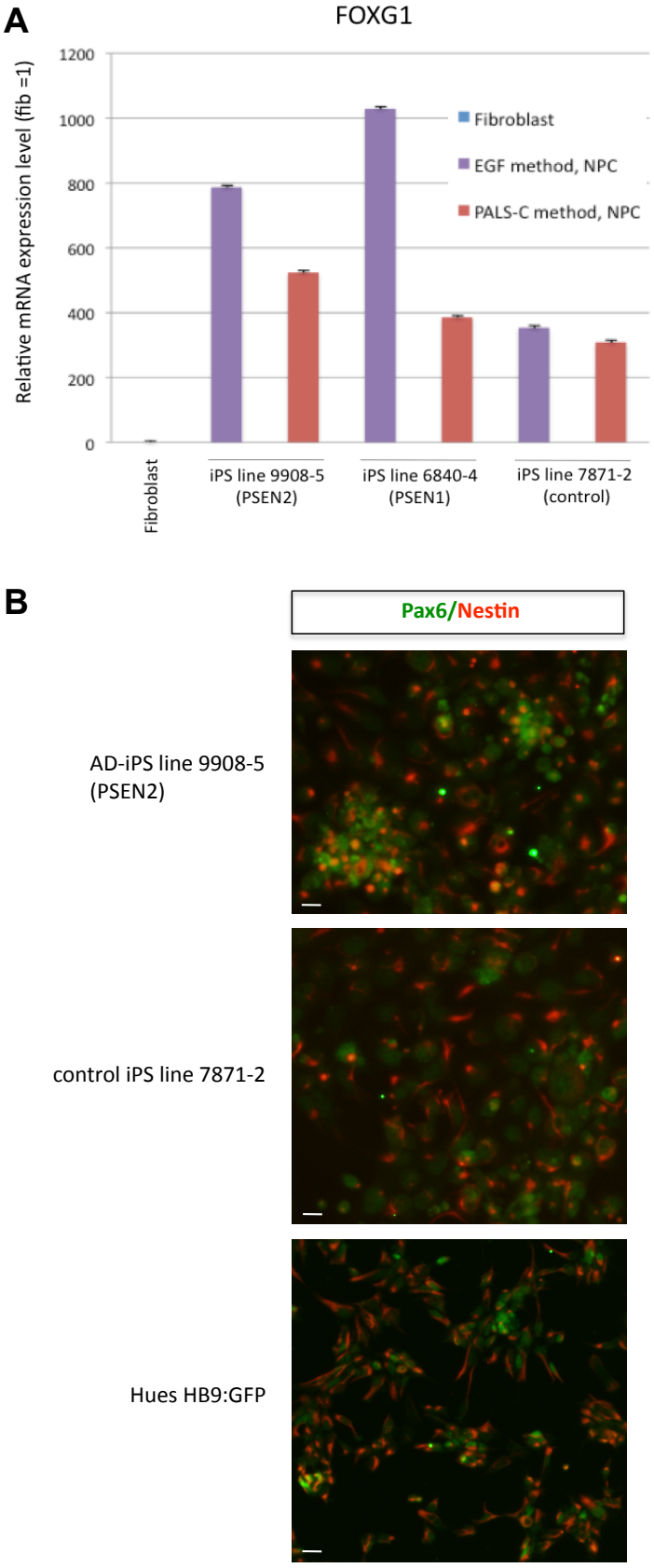

Figure 1. AD-iPS cells can differentiate into forebrain progenitor cells that express markers FOXG1 and PAX6

(A) Quantitative RT-PCR analysis for mRNA levels of forebrain progenitor transcription factor, *FOXG1*. AD-iPS cell lines, 9908-5, 6840-4 and 7871-2, were differentiated using the EGF method and PALS-C method (see methods chapter). *FOXG1* levels are substantially increased relative to human fibroblasts. *FOXG1* levels in progenitor cells derived using the EGF method are higher than that from the PALS-C method. Expression levels are normalized to *GAPDH*; error bars represent the standard error of the mean (SEM). NPC, neural progenitor cells

(B) Co-immunostain for dorsal forebrain progenitor marker, PAX6 and general neuronal progenitor marker, Nestin. iPS cell-derived progenitor cells (from AD-iPS cell lines 9908-5 and 7871-2 differentiated using the EGF method) express PAX6 but cells were indistinct/poorly-defined compared to human ES cell-derived progenitor cells (shown here from human ES line Hues HB9:GFP). See Figure 5 for Pax6 negative control stain.

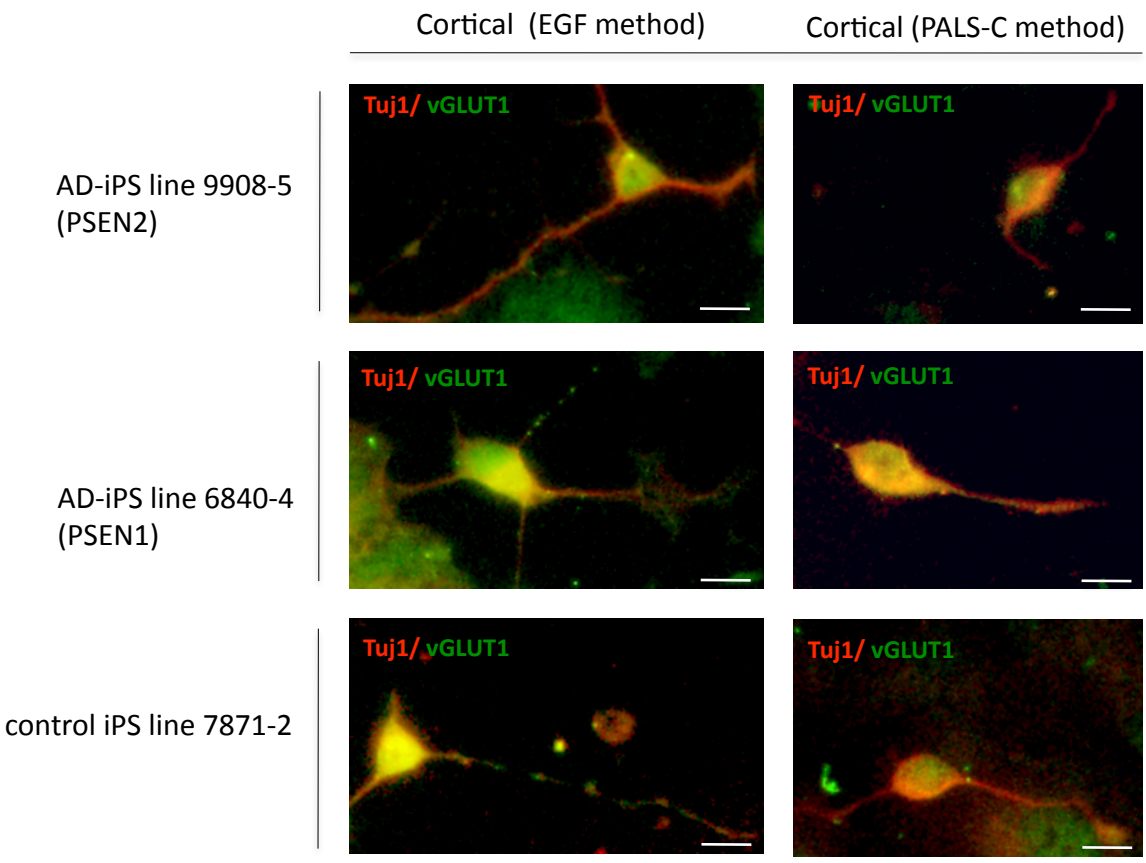

Figure 2. AD-iPS cells can differentiate into mature neurons that express TuJ1 and vGLUT1

iPS cell lines, 9908-5, 6840-4 and 7871-2 were differentiated to cortical neurons using the EGF method and PALS-C method (see methods chapter) and co-immunostained for antibodies specific to panneuronal marker, TuJ1, and mature gluatamatergic neuron marker, vGLUT1. Neurons derived from the EGF method had more mature branching morphology and strong, punctate immunostaining for vGLUT1. Neurons derived from the PALS-C method had less defined neuronal processes and weak VGLUT immunostaining. Scale bars, 10um.

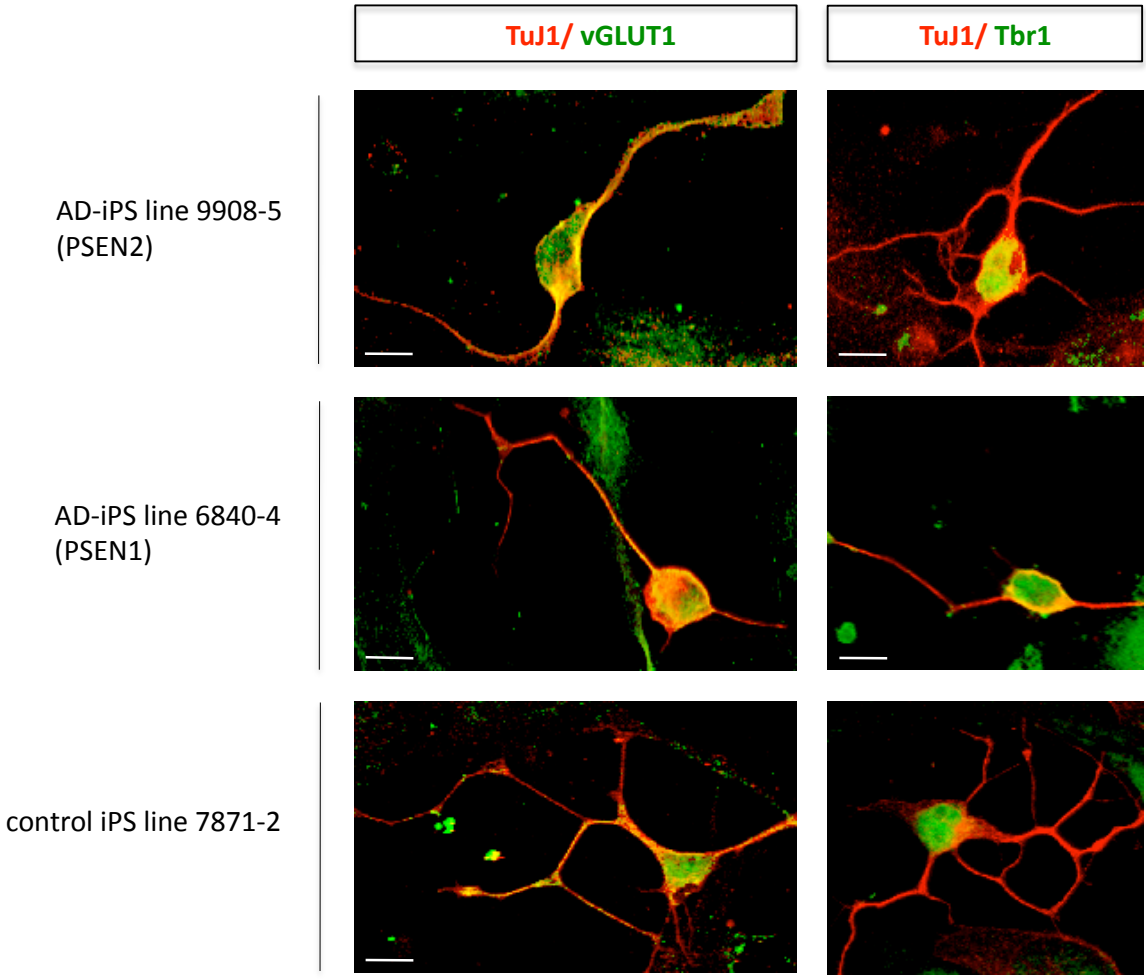

Cell line	TuJ1 (%)	Tbr1 (% of TuJ1)
Hues HB9:GFP	24.1	40
7871-2 (control)	~0.06	~33
6840-4 (PSEN2)	~0.03	~33
9908-5 (PSEN1)	~0.15	~33

Figure 3. AD-iPS cells can differentiate into glutamatergic forebrain neurons

iPS cell lines, 9908-5, 6840-4 and 7871-2, were differentiated to cortical neurons using the EGF method (see methods chapter) and co-immunostained for antibodies specific to TuJ1 (a panneuronal marker) and vGLUT1 (mature glutamatergic neuron marker) or Tbr1 (neocortical glutamatergic neuron marker). iPS cell-derived cortical glutamatergic neurons show co-expression of TuJ1 and Tbr1 and of TuJ1 and vGLUT1. The efficiency of cortical neuron differentiation from iPS cells is very low, compared to human ES cells (Hues HB9:GFP). Scale bars, 10um. (See Figure 6 for Tbr1 control stains).

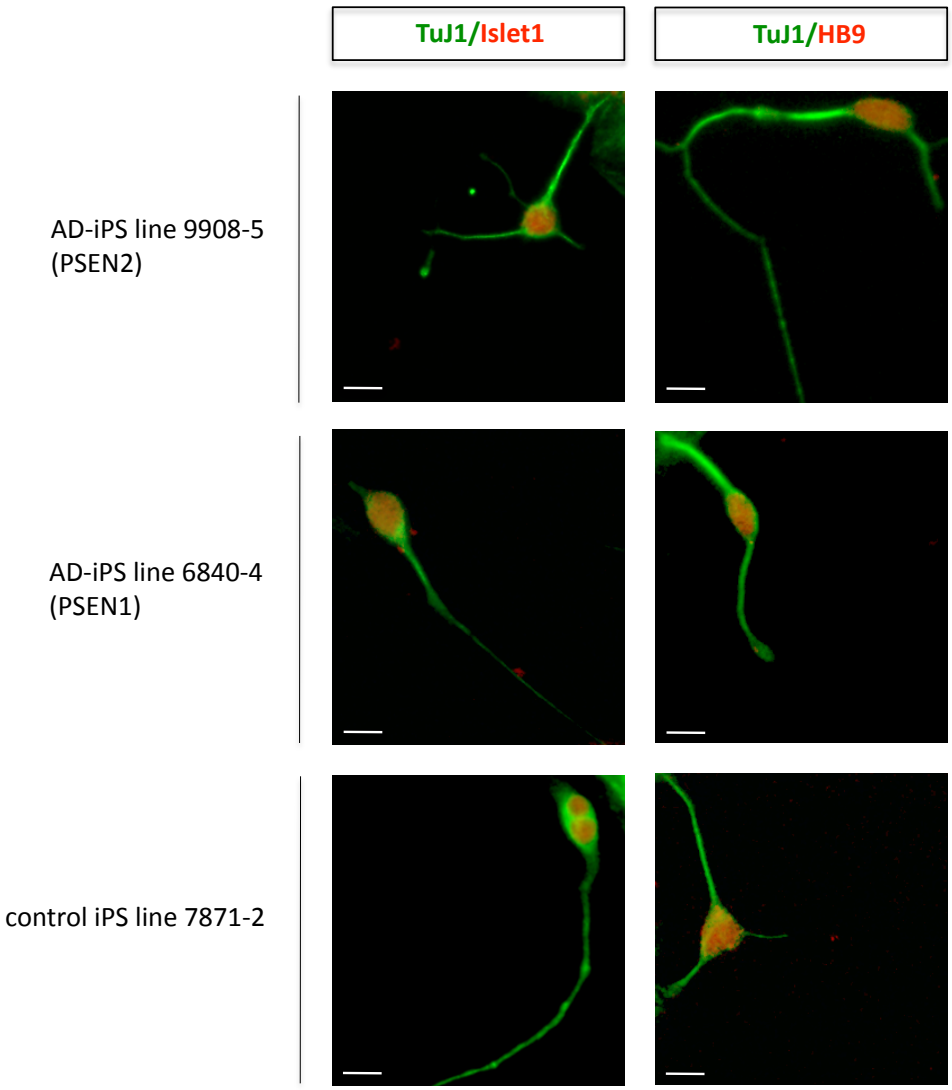

Cell line	GFP	TuJ1 (%)	Islet1 (% of TuJ1)
Hues HB9:GFP	positive	6	39.3
7871-2 (control)	negative	~0.07	~25
6840-4 (PSEN2)	negative	~0.04	~25
9908-5 (PSEN1)	negative	~0.03	~25

Figure 4. AD-iPS cells can differentiate into motor neurons
iPS cell lines, 9908-5, 6840-4 and 7871-2, were differentiated to motor neurons (see methods) and co-immunostained for antibodies specific to TuJ1 (a panneuronal marker), and HB9 (a motor neuron marker) or Islet1 (a transcription factor involved in motor neuron development). iPS cell-derived motor neurons show co-expression of TuJ1 and HB9 and of TuJ1 and Islet1. The efficiency of motor neuron differentiation from iPS cells is very low, compared to human ES cells (Hues HB9:GFP).
Scale bars, 10um.

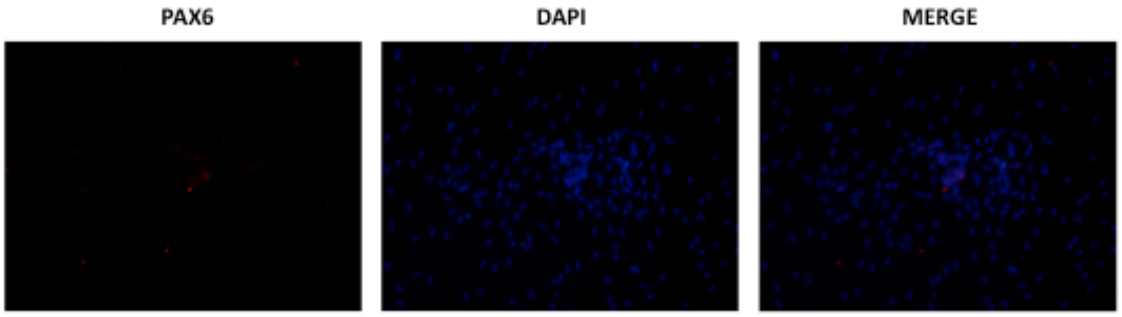

Figure 5. Negative control for PAX6 immunostain (Related to Figure 1)
Human fibroblasts were stained for an antibody specific to Pax6. DAPI is in blue. Negative Pax6 staining is seen here.

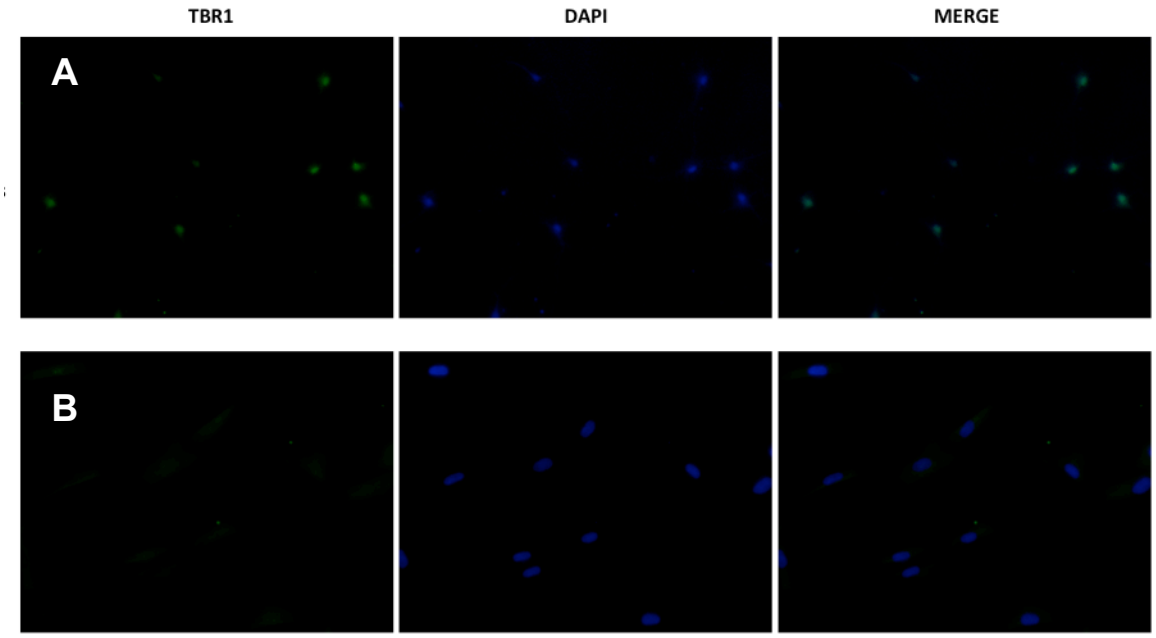

Figure 6. Postitive and negative controls for TBR1 immunostain (Related to Figure 3)

Primary mouse cortical neurons (top, panel A) and human fibroblasts (bottom, panel B) were stained for an antibody specifc to TBR1 (green). DAPI is in blue. Primary mouse cortical neuron stain positive for TBR1 whereas human fibroblasts do not.

Chapter 4: An in-vitro cell based model of AD using induced neuronal (iN) cell technology

Introduction

While pluripotent (iPS) cell technology offers an indirect approach to neurological disease modeling (generating patient-specific iPS cells and subsequent differentiation into neurons), iN cell technology allows for a direct approach via the direct conversion of somatic cells to neurons (Figure 1). Like iPS cell technology, iN cellular reprogramming technology has fueled excitement for human cell-based modeling of neurodegenerative diseases.

Because our effort to utilize iPS cell technology to generate a patient-specific cell-based model of AD was met with tremendous difficulties, we turned to iN cell technology as an alternative strategy to achieve our end. As previous studies had shown that neuronal lineage-specific transcription factors can directly convert mouse and human fibroblasts to cortical glutamatergic type neurons (Vierbuchen et al., 2010; Pang et al., 2011), we reasoned that AD patient fibroblast cells could be directly converted to forebrain cortical glutamatergic neurons. In doing so, we would generate a patient-specific cell-based model of AD.

As had been our goal with an iPS cell-based model of AD, we sought to generate an iN-cell based model of AD that would recapitulate molecular aspects of the disease in a human cellular context. Our aim was to utilize this iN cell-based AD model to examine APP processing and Aβ production.

Results [All experiments were performed in collaboration. I provided validated fibroblast cell lines (those that were able to generate partially reprogrammed iPS cells), generated iPS cell-derived neural progenitor cells, and performed controls for ELISAs using primary mouse cortical neurons. Much of the following is reproduced from Qiang et al., 2011.]

Reprogramming AD patient fibroblasts to glutamatergic forebrain neurons

In an initial attempt to generate human induced neuronal (hiN) cells, we introduced Brn2, Ascl1, and Myt1, three transcription factors that had been shown to be sufficient for reprogramming mouse fibroblast cells (Vierbuchen et al., 2010) into the human adult skin fibroblast line STC0022 (isolated from post-mortem dermal tissue) via lentiviral co-transduction. This experiment as not successful in converting of human fibroblasts to neuronal cells. Infected cultures were unhealthy and apoptotic cell death ensued within a few days of viral innoculation.

Subsequently, lentiviral co-transduction of a larger set of forebrain transcription regulators originally identified by Vierbuchen et al., Brn2, Ascl1, and Myt1l, Olig2 and Zic1, in the presence of neuronal survival factors brain-derived neurotrophic factor (BDNF), neurotrophin-3 (NT3), and glial-conditioned media (GCM), allowed for conversion of human adult fibroblasts to hiN cells displaying characteristic neuronal morphology (Figures 2A–2N).

Three weeks after lentiviral transduction, hiN cells were positive for neuronal markers, including Tuj1, MAP2, Tau1 and NeuN (Figures 2B–2G and

2J–2N). In contrast, fibroblasts transduced with control vectors never gave rise to neuronal cells (Figure 2H and 2I). More than 90% of MAP2-positive cells were positive for the neocortical glutamatergic neuron marker Tbr1 (Figure 2K), and these Tbr1-positive cells did not express the fibroblast marker, fibroblast-specific protein-1 (FSP1; Figure 2L). Approximately half of the MAP2-positive cells were positive for the mature glutamatergic neuron marker vesicular glutamate transporter-1 (vGLUT1) in a stereotypical punctate pattern (Figure 2M). Rare MAP2-positive cells (less than 1%) displayed the GABAergic neuron marker, glutamic acid decarboxylase-65 (GAD65; Figure 2N).

We applied our hiN cell conversion protocol to a panel of nine human skin fibroblast lines obtained from Coriell: three FAD patient fibroblast lines, three SAD patient fibroblast lines and three control fibroblast (Figure 3). The conversion efficiency of fibroblasts to MAP2-positive hiN cells across these lines ranged from 7.1% to 8.9% (as a percentage of input fibroblasts; n = 3 per group). After accounting for cell attrition during the 3-week culture, 28.4%–36.1% of the surviving cells were MAP2 positive (Figure 2O). Across these lines, 48.2%–60.9% of the MAP2-positive cells were also positive for vGLUT1 (Figure 2P).

Functional Neuronal Properties of hiN Cells

Electrophysiological characterization of hiN cells

We assayed the physiological properties of hiN cells via a series of electrophysiological studies conducted in collaboration with the lab of Dr. Herman Moreno. Patch-clamp recordings of cells at days 21–28 of culture indicated that

the majority of hiN cells displayed typical neuronal Na^+, K^+, and Ca^{2+} channel properties. Specifically, TTX-sensitive Na^+ currents were characterized by a typical current density-voltage relationship (Figures 4A and 4B). Outward K^+ currents, inhibited in the presence of intracellular cesium (Cs^+), were also detected (Figures 4C and 4D). Calcium channel function, measured using barium (Ba^{2+}) as the charge carrier, displayed typical neuronal characteristics (Figure 4E). Consistent with these channel properties, hiN cells were able to fire action potentials in response to depolarizing currents (Figure 4F). Furthermore, upon termination of hyperpolarizing pulses, hiN cells displayed a typical rebound spike (Figure 4F). The passive membrane properties of hiN cells were also consistent with an in vitro neuronal phenotype, with resting membrane potentials ranging from −67 mV to −32 mV (average −52 mV; n = 17), membrane time constant (τ) ranging from 1.00 to 0.30 ms, membrane resistance (R_m) ranging from 0.12 to 1.7 GΩ, and capacitance ranging from 22 to 70 pF. We further evaluated γ-aminobutyric acid (GABA)-ergic and glutamatergic ligand-gated ion channel activity in hiN cells. hiN cells responded to exogenous puff application of glutamate or GABA, displaying typical depolarizing and hyperpolarizing currents, respectively (Figures 4G–4J).

Integration of hiN cells into neuronal circuitry

Human iN cells can integrate into neuronal circuitry in vitro and in vivo. We did not observe spontaneous activity that is suggestive of neuronal connectivity in hiN cells using the standard culture conditions. We therefore

sought to develop alternative protocols that may provide the appropriate environmental cues for synaptic maturation. First, as glial cells can play a major role in the regulation of neuronal synaptic development and connectivity (Eroglu and Barres; 2010) hiN cells were co-cultured with murine glial cells (obtained from mice ubiquitously expressing red fluorescent protein) (Muzumdar et al., 2007). After two weeks of co-culture, whole-cell patch-clamp recordings of hiN cells (identified as nonfluorescent cells with a neuronal morphology) held at −70 mV revealed spontaneous membrane current changes that were sensitive to glutamatergic receptor inhibitors, NBQX and APV (Figures 5A-5C; n = 6 of 10 cells tested).

Furthermore, GFP-labeled hiN cells were transplanted in utero into embryonic day 13.5 mouse brain (Brustle et al., 1997). The transplanted cells migrated from the ventricles into various brain regions, as expected (Figures 5D and 5E). The identity of GFP-positive transplanted hiN cells was confirmed by immunostaining with an antibody specific for human NCAM (Figure 5F). Voltage-clamp recordings from GFP-positive hiN cells within acutely prepared brain slices from postnatal day 7 pups demonstrated spontaneous currents of various amplitudes and frequencies (Figure 5G). These events increased in frequency and amplitude upon blockade of $GABA_A$ receptors with picrotoxin (Figure 5H) and were suppressed with the glutamatergic receptor channel inhibitors NBQX and APV (Figure 5I). We confirmed the identity of the recorded cell by dual fluorescence imaging (Figures 6A and 6B). Subsequent to the recording, slices were immunostained to demonstrate expression of the human-specific

mitochondrial marker hMito within recorded cells (Figure 6C). Together, these findings support the idea that hiN cells are capable of neuronal connectivity.

hiN Cell Reprogramming is Directed

Consistent with the idea that the hiN cell phenotype can be achieved without neuronal progenitor intermediates, expression of the progenitor markers Sox2 and Pax6 was not apparent during hiN cell reprogramming (Figures 7A-7C and 7E–7G). Expression of Nestin, which is associated with neuronal progenitors but also functions more generally as a cytoskeleton regulator during morphological cell changes (Gilyarov et al., 2008) in a subpopulation of cells (<10%; Figures 7I-7K and 7M–7O). In contrast to hiN cell reprogramming, differentiation of human iPS cells to a neural progenitor state led to the robust accumulation of Sox2-positive, Pax6-positive, and Nestin-positive progenitors, as expected (Figures 7D, 7H, and 7L). RNA expression profiling by real-time quantitative RT-PCR similarly indicated that expression of neuronal progenitor markers such as FOXG1 and OTX2 was absent from hiN cell culture (Figure 7P).

Analysis of APP processing in AD-iN cells

We generated hiN cells from a panel of human skin fibroblasts derived from familial AD (FAD) patients with mutations in PSEN1 or PSEN2, sporadic AD (SAD) patients, or unaffected individuals (three lines per group). Given the likely heterogeneity of sporadic disease and the limited number of samples examined in our study, we focused on phenotypic examination of FAD lines. The

general neuronal properties of FAD fibroblast-derived hiN (FAD-iN) cells appeared similar to that of control fibroblast-derived hiN (UND-iN) cells, including neuronal reprogramming characteristics, such as efficiency of MAP2-positive hiN cell generation and the percentage of neurons that express vGLUT1 (Figures 2O and 2P). Quantitative RT-PCR analysis revealed that the level of expression of the mature neuron marker synaptophysin was comparable among the hiN cell cultures (Figure 8A), and cell density at three weeks was not significantly different across the hiN cell cultures (Figure 8B).

Increased Aβ42:Aβ40 ratio in FAD-iN cells relative to UND-iN cells and FAD fibroblasts

We evaluated the processing of amyloid precursor protein (APP) to the Aβ42 and Aβ40 fragments in the hiN cell cultures. A key pathological feature in FAD patient brain is an increased Aβ42:Aβ40 ratio (Hardy and Selkoe; 2002). Consistent with this phenomena, the Aβ42:Aβ40 ratio was dramatically increased in FAD-iN cell cultures relative to UND-iN cell cultures, as quantified in cell media by ELISA (Figure 9A; $p < 0.001$, ANOVA with post hoc Tukey HSD; $n = 3$ patient lines per FAD or UND group with 11–16 independent cultures per line). Similarly, on a pooled analysis of all FAD-iN versus all UND-iN cultures, the Aβ42:Aβ40 ratio is significantly increased in the FAD group ($p < 1 \times 10^{-9}$; ANOVA with post hoc Tukey HSD; $n > 38$ per group). The increased Aβ42:Aβ40 ratio is most evident in the AG07768 line (with mutation in PSEN1), but even in the absence of those AG07768 samples, the FAD group displayed an elevated Aβ42:Aβ40

ratio ($p < 1 \times 10^{-9}$; ANOVA with post hoc Tukey HSD, $n > 29$ per group). Critically, the Aβ42:Aβ40 ratio in FAD-iN cell cultures was also elevated relative to the originating FAD fibroblast cultures ($p < 1 \times 10^{-9}$; ANOVA with post hoc Tukey HSD; $n > 38$ per group). In contrast, the Aβ42:Aβ40 ratio in UND-iN cell cultures was not significantly elevated relative to the originating UND fibroblast cultures ($p > 0.05$; ANOVA with post hoc Tukey HSD; $n > 30$ per group).

Selective generation of Aβ42 in FAD-iN cells is not attributable to increased APP levels

More than just the Aβ42:Aβ40 ratio, FAD-iN cell conversion led to an increase in the total levels of Aβ (combined Aβ42 and Aβ40 polypeptides) relative to the originating FAD fibroblasts (Figure 9B; $p < 0.05$; ANOVA with post hoc Tukey HSD; $n = 3$ individual lines per group, with 11 to 16 independent wells for each line). This increase in total Aβ levels upon AD-iN cell conversion was not apparent in UND cultures. Using co-immunostaining with antibodies to Aβ42, Aβ40, and MAP2, we further observed that both isoforms of Aβ are selectively increased in the MAP2-positive neuronal cells, but not in the remaining fibroblastic cells, that compose the mixed hiN culture (Figures 9C-9F). Taken together, these data indicate that in the context of FAD PSEN-1 and -2 mutations, fibroblast conversion to induced neuronal cells appears to amplify the FAD-associated phenotype.

Levels of APP holoprotein (the Aβ42 and Aβ40 precursor) did not differ significantly between FAD-iN and UND-iN cell cultures, as quantified by ELISA

on cellular lysates (Figure 9G) and by quantitative RT-PCR on RNA transcripts (Figure 9H). However, an increase in APP holoprotein expression was detected in both FAD and UND cell cultures in comparison to their originating fibroblast cultures. Because FAD-iN and UND-iN cell cultures displayed similar levels of APP, it is unlikely that APP levels account for the selective generation of Aβ42 in FAD-iN cells.

Selective generation of Aβ42 in FAD-iN cells is not caused by increased BACE1 activity

Cleavage of APP by BACE1 β-secretase activity is thought to be a rate-limiting step in the production of Aβ and precedes cleavage by γ-secretase (Thinakaran and Koo, 2008). As such, we quantified the BACE1 cleavage product of APP, soluble extracellular sAPPβ, in hiN cell cultures. The levels of sAPPβ were elevated in both FAD-iN and UND-iN cell cultures, relative to their respective fibroblasts. However, levels of sAPPβ were comparable between FAD-iN and UND-iN cell cultures (Figure 10A). Additionally, BACE1 transcript levels, as determined by quantitative RT-PCR, did not appear altered in all hiN cell cultures relative to fibroblasts, regardless of disease status (Figure 10B). Thus, the elevated level of Aβ42 in FAD-iN is not caused by increased BACE1 activity.

Discussion

Recent cellular reprogramming methods are of great utility for human cell-based disease modeling. We sought to generate a patient-specific model of AD via iPS cell reprogramming. However, this strategy was labor intensive and wrought with technical challenge. As such we turned to iN cell reprogramming strategy as alternative approach to achieve our end. Unlike iPS cell reprogramming, iN cell reprogramming offered a direct method for generating forebrain cortical glutamatergic neurons. Here we have shown proof-of-principle for the utility of iN cell reprogramming technology for human cell-based neuronal disease modeling and in particular, for modeling AD.

Our analysis of FAD patient-derived hiN cell cultures revealed that this iN cell-based model of AD recapitulated the key molecular features of AD. hiN cells from PSEN mutant FAD patient fibroblasts display an increased Aβ42:Aβ40 ratio relative to UND hiN cells, consistent with patient brain pathology and with the well-characterized role of PSENs as essential components of the γ-secretase complex (Hardy and Selkoe, 2002). Surprisingly, the impact of FAD PSEN mutations on the Aβ42:Aβ40 ratio was amplified upon hiN cell conversion from fibroblasts. This suggests a model in which PSEN FAD mutants may alter APP processing at multiple levels: through modified γ-secretase activity, as well as with altered cellular context.

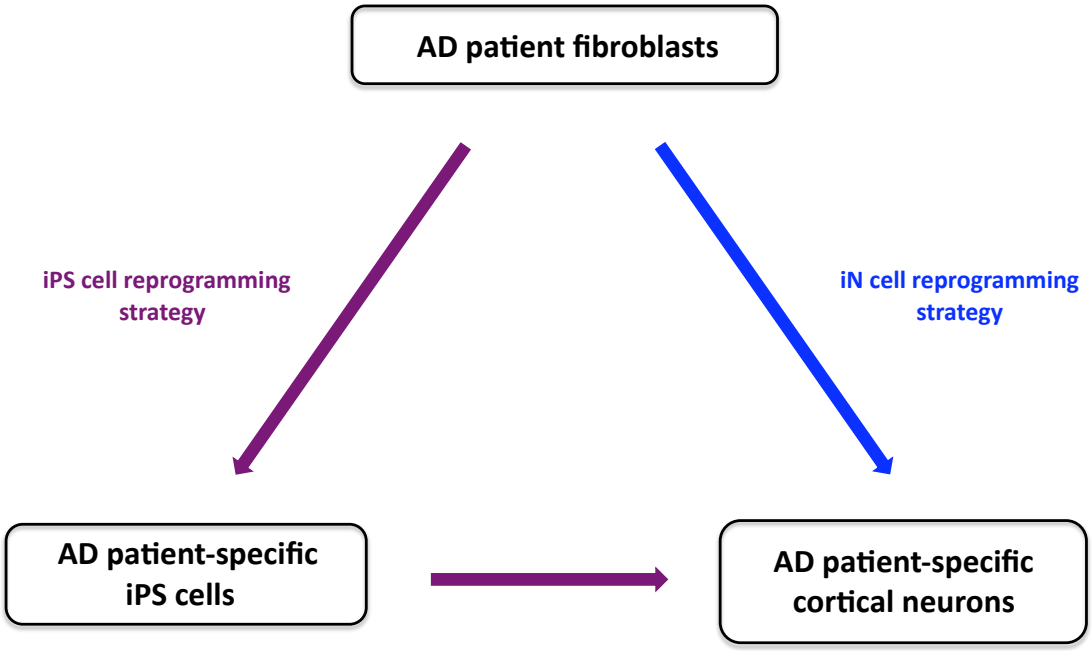

Figure 1. Modeling AD using iPS vs. iN cell reprogramming technology
iPS cell technology offers an indirect approach to neurological disease-modeling that involves a two-step process: first generating patient-specific iPS cells and subsequently differentiating iPS cells into neurons. iN cell technology allows for a direct approach to neurological disease-modeling via the direct conversion of somatic cells to neurons.

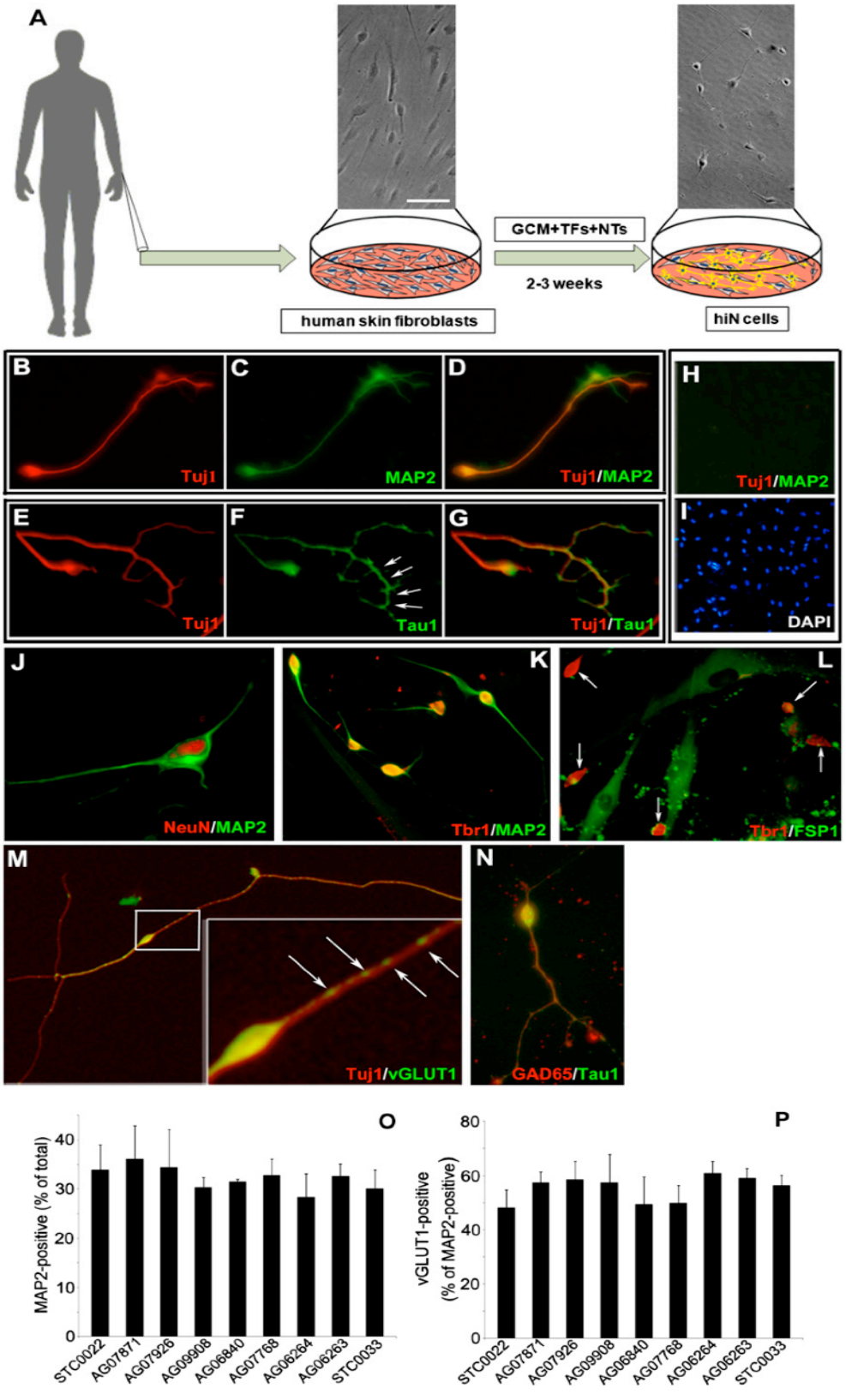
A
human skin fibroblasts
GCM+TFs+NTs
2-3 weeks
hiN cells
B
Tuj1
C
MAP2
D
Tuj1/MAP2
H
Tuj1/MAP2
E
Tuj1
F
Tau1
G
Tuj1/Tau1
I
DAPI
J
NeuN/MAP2
K
Tbr1/MAP2
L
Tbr1/FSP1
M
Tuj1/vGLUT1
N
GAD65/Tau1
O
MAP2-positive (% of total)
0
10
20
30
40
STC0022
AG07871
AG07926
AG09908
AG06840
AG07768
AG06264
AG06263
STC0033
P
vGLUT1-positive (% of MAP2-positive)
0
20
40
60
80

Figure 2

Figure 2. hiN Cells Display a Forebrain Glutamatergic Neuron Phenotype
(A) Schematic of the conversion method. Top panels show phase contrast images of human skin fibroblast (left) or hiN cell (right) cultures. TFs, lentiviral vectors encoding transcription regulators Ascl1, Brn2, Myt1l, Olig2, and Zic1; NTs, neurotrophins BDNF and NT3; GCM, glial-conditioned medium.
(B–G) Neuronal marker analysis of hiN cell cultures. Human skin fibroblasts (line STC0022) were transduced with transcription regulators, cultured for 3 weeks as in (A), and subsequently immunostained with antibodies specific to Tuj1 (B and E), MAP2 (C), or Tau-1 (F). (D) Merged image of (B) and (C). (G) Merged image of (E) and (F). Arrows in (F) indicate the typical distal enrichment pattern of Tau1 antibody immunostaining.
(H and I) Absence of neuronal markers in lentiviral vector-only transduced fibroblast cultures. Human skin fibroblasts (line STC0022) transduced with control lentiviral vector only were analyzed for expression of Tuj1 and MAP2. Cultures were counterstained with the nuclear marker DAPI. Neuronal marker expression was not detected.
(J) Costaining of hiN culture with the neuronal nuclear marker NeuN and MAP2 is shown.
(K and L) Forebrain marker expression in hiN cells. The majority of hiN cells expressed the neocortical glutamatergic neuron nuclear marker Tbr1 along with MAP2. In contrast, Tbr1-positive hiN cells were not stained by the fibroblast marker fibroblast-specific protein-1. Arrows in (L) demarcate Tbr1-positive nuclei.
(M) A majority of Tuj-1-positive hiN cells expressed the glutamatergic neuron marker vGLUT1. Inset shows magnified view of the boxed region; arrows indicate the typical vGLUT1-positive punctate pattern.
(N) Only rare (<1%) hiN Tau-1-positive cells also stained positively for GAD65.
(O and P) Quantification of MAP2- and vGLUT1-positive cells in hiN cell cultures derived from a panel of nine human fibroblast lines. (O) Black bars indicate the percent of total cells that are MAP2-positive cells with extended processes (at least 3-fold greater than soma diameter, as in F). (P) Black bars indicate the percent of MAP2-positive cells that stain for the glutamatergic neuron marker vGLUT1 as in (M). n = 3 wells for each group; data are presented as mean ± SEM.Scale bars: (J) and inset of (M), 10 μm; (B–G), (K–L), and (N), 20 μm; (A), (H), (I), and (M), 40 μm

	Culture	Origin
UND	STC0022	65yo F
	AG07871	49yo F
	AG07926	N/A[a] F
FAD	AG09908	81yo F PSEN2 (N141I)
	AG06840	56yo M PSEN1(A246E)
	AG07768	31yo F PSEN1(A246E)
SAD	AG06264	62yo F
	AG06263	67yo F
	STC0033	81yo M

[a]Culture was derived from spouse of an AD patient, precise age data unavailable.

Figure 3. Summary of individual hiN cell cultures and corresponding skin fibroblasts of origin. Related to Figure 1. All skin fibroblast lines were derived from de-identified, banked tissue samples. STC0022 and STC0033 were obtained from the Columbia University Taub Institute New York Brain Bank. Other cultures were obtained from Coriell Institute (Camden, NJ, USA). Diagnosis is based on clinical diagnosis from Coriell or the New York Brain Bank.

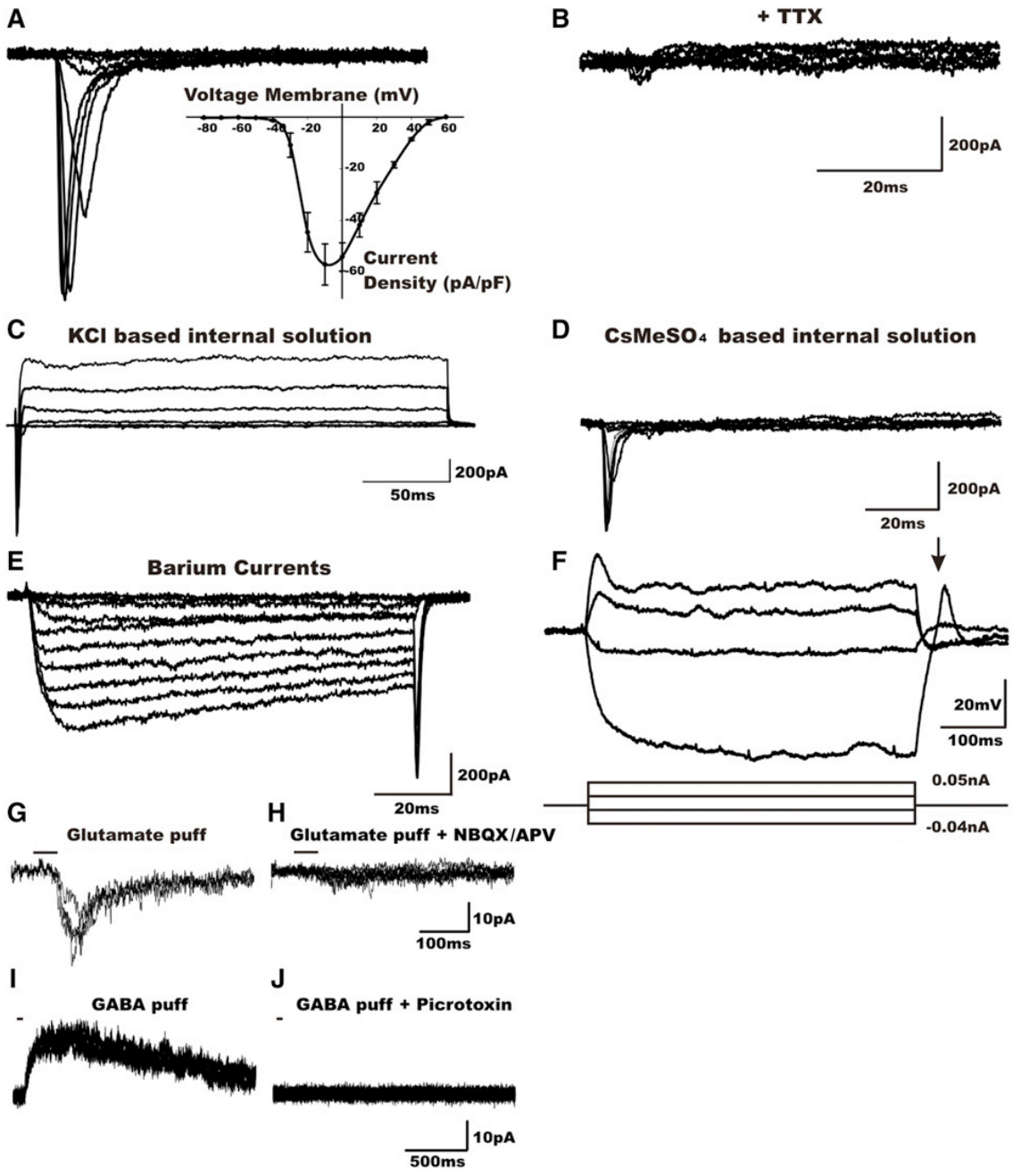
A
Voltage Membrane (mV)
-80 -60 -40 -20 20 40 60
-20
-40
-60
Current
Density (pA/pF)
B
+ TTX
200pA
20ms
C
KCl based internal solution
200pA
50ms
D
CsMeSO4 based internal solution
200pA
20ms
E
Barium Currents
200pA
20ms
F
20mV
100ms
0.05nA
-0.04nA
G
Glutamate puff
H
Glutamate puff + NBQX/APV
10pA
100ms
I
GABA puff
J
GABA puff + Picrotoxin
10pA
500ms

Figure 4

Figure 4. Electrophysiological Characterization and Evoked Calcium Transients of Cultured hiN Cells

(A) An example voltage-clamp recording from an hiN cell. Stepping the membrane voltage from −80 mV to more depolarized potentials (−70 to +60 mV in 10 mV increments) resulted in fast inward currents in 18 of 22 cell analyzed. Shown are example traces between −40 to 0 mV. Inset illustrates the pooled current density-voltage relationship (error bars represent the SEM).

(B) The fast inward currents were sensitive to bath application of the Na^+ channel blocker tetrodotoxin (TTX, 600 nM).

(C) Outward K^+ currents were obtained (in 14 of the 16 hiN cells recorded) with a KCl-based pipette solution upon depolarizing steps as described above.

(D) Minimal or no outward K^+ currents were observed in cells recorded with a Cs^+-based pipette solution, as expected, but note the presence of the inward sodium currents.

(E) Macroscopic whole-cell voltage-dependent Ca^{2+} channel activity of hiN cells was identified using Ba^{2+} as the charge carrier. Currents were elicited in response to depolarizing steps from −70 mV in 10 mV steps (in 3 of the 4 hiN cells analyzed).

(F) In current-clamp mode, hiN cells exhibited a rebound action potential (arrow) at the end of hyperpolarizing current injections and action potentials upon depolarizing current injection. Bottom panel is a time schematic of the current injection protocol.

(G) Glutamate-mediated postsynaptic currents (PSCs) were elicited by focal application of 1 mM glutamate puffs for 50 ms in cells voltage clamped at −70 mV; shown are three traces elicited once every 3 min.

(H) Induced PSCs were sensitive to the AMPA channel blocker NBQX (20 μM) and the NMDA blocker APV (50 μM).

(I) Focal application of GABA (50 ms puff, 1 mM) to cells voltage clamped at +20 mV and dialyzed with a low Cl^- solution elicited current responses; shown are three traces evoked every 3 min.

(J) GABA-mediated currents were sensitive to the $GABA_A$ antagonist picrotoxin (50 μM). Puff applications of neurotransmitter are indicated by a solid line above tracings.

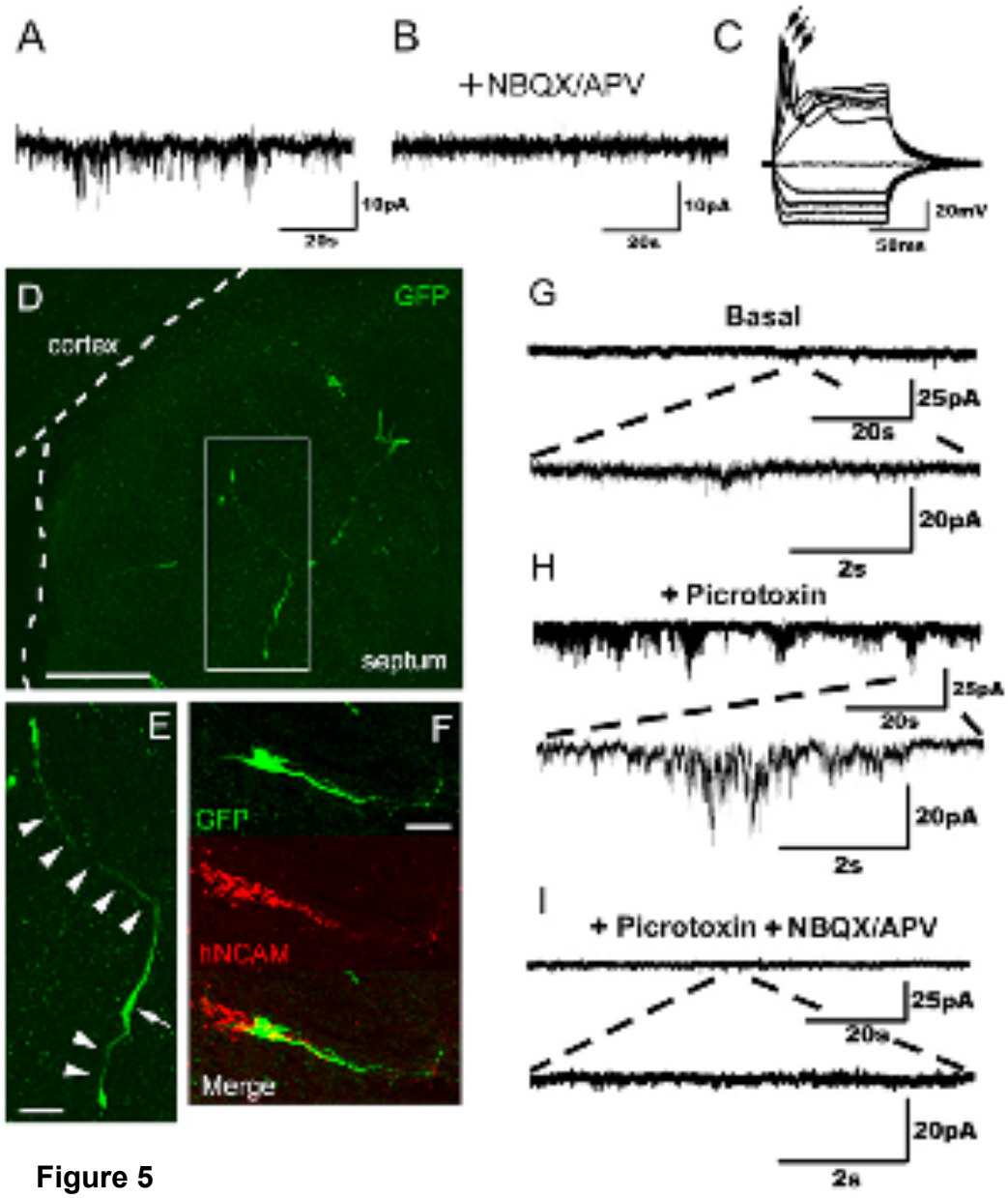
A
B
+NBQX/APV
C
10pA
20s
10pA
20s
20mV
50ms
D
GFP
cortex
septum
E
F
GFP
hNCAM
Merge
G
Basal
25pA
20s
20pA
2s
H
+ Picrotoxin
25pA
20s
20pA
2s
I
+ Picrotoxin + NBQX/APV
25pA
20s
20pA
2s

Figure 5

Figure 5. Evidence of hiN Cell Functional Integration

(A) Representative spontaneous postsynaptic currents recorded from an hiN cell present in a murine glial monolayer coculture. The cell was held at −70 mV. Events of various amplitudes (5–20 pA) are seen.

(B) Spontaneous postsynaptic currents as observed in (A) were abolished by bath application of NBQX/APV.

(C) Upon depolarizing current injections in current-clamp mode, action potentials were induced. Individual traces represent independent recorded events; action potentials (indicated by arrows) were seen in five of the nine tracings.

(D and E) Confocal fluorescent images of brain slices prepared from postnatal day 3 animals that had been grafted in utero with hiN cells. Transplanted hiN cells migrated extensively and extended neurite processes. An arrowhead indicates cell soma; arrows point to apparent processes. Scale bars: (D) 100 μm, (E) 20 μm.

(F) Confocal reconstruction of a transplanted GFP-positive hiN cell stained with a human-specific NCAM antibody. GFP, green; hNCAM, red. Scale bar, 50 μm.(

G) Voltage-clamp recording of an hiN cell (Vh = −70 mV) integrated into the piriform cortex of the host brain, demonstrating spontaneous events of low frequency and amplitude.

(H) The frequency and amplitude of the spontaneous excitatory postsynaptic currents (sEPSCs, as in G) increased upon blockade of $GABA_A$ receptors with 50 μM picrotoxin.

(I) sEPSCs were drastically reduced by blocking glutamatergic synaptic transmission with 20 μM NBQX and 50 μM APV.

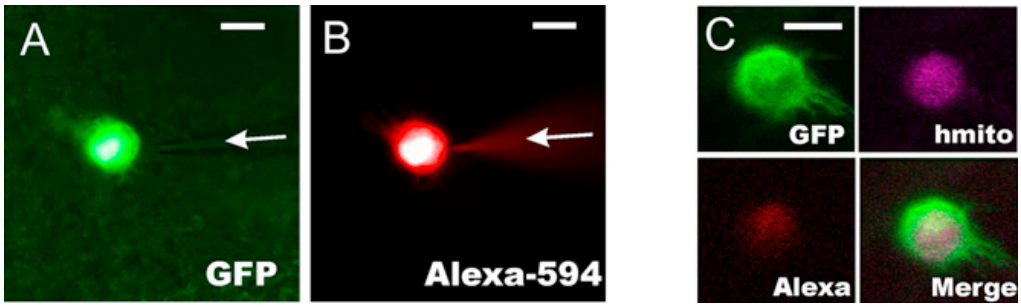

Figure 6. Identification of Transplanted hiN Cells in Vivo, Related to Figure 5

(A) GFP-labeled hiN cells were visualized by fluorescent microscopy within acutely prepared brain slices of P7 to P20 mice after in utero transplantation. A red fluorescent dye, Alexa-598, was included in the patch recording pipette buffer for facile identification of recorded cells. Fluorescense images are shown using an excitation wavelength of 470 nm (see corresponding cell recording in Figures 5G to 5J). Arrows point to recording pipette.

(B)The red fluorescent dye Alexa-594 was present within the holding pipette solution to allow visual identification of the patched cell. Five munites after whole cell access, the cell in (A) was re-imaged for red fluorescence (using an excitation wavellength of 590 nM). Arrows point to recording pipette.

(C) Subsequent to electrophysiological recording from the acutely prepared brain slice (as in Figures 5G to 5J), the slice was processed by paraformaldehyde fixation followed by immunostaining with an antibody for the human-specific mitochondrial antigen (hmito). Multicolor confocal fluorescence imaging confirmed that the GFP-positive, Alexa-598-positive neuron in (A) and (B) stained positively with the hmito antibody (n=3).

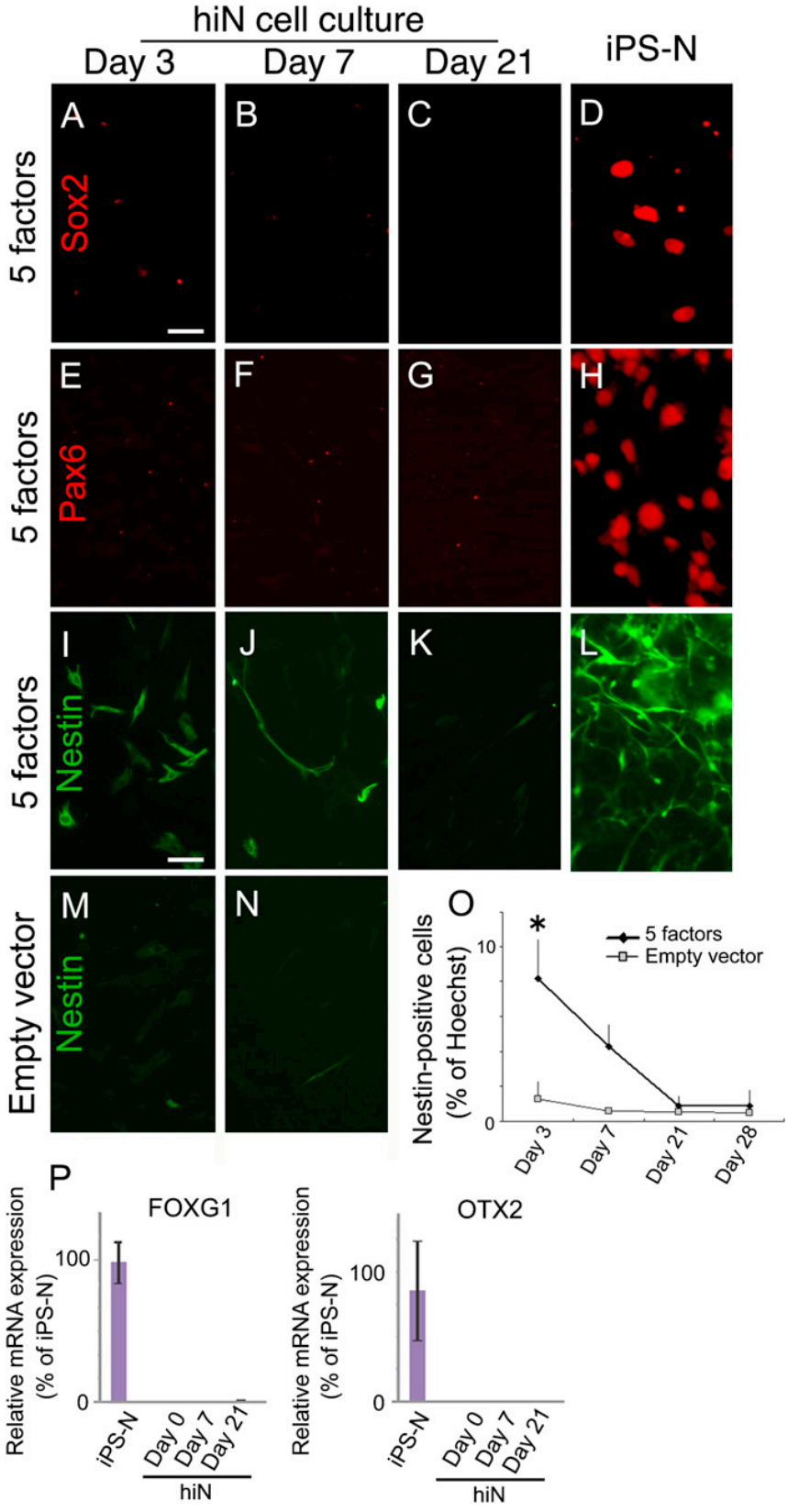
hiN cell culture
Day 3
Day 7
Day 21
iPS-N
5 factors
Sox2
Pax6
Nestin
Empty vector
A
B
C
D
E
F
G
H
I
J
K
L
M
N
O
Nestin-positive cells (% of Hoechst)
5 factors
Empty vector
Day 3
Day 7
Day 21
Day 28
P
FOXG1
OTX2
Relative mRNA expression (% of iPS-N)
iPS-N
Day 0
Day 7
Day 21
hiN

Figure 7

Figure 7. hiN Cell Reprogramming Is Directed

(A–H) Progenitor markers are not detected in hiN cell cultures. Sox2 (A–C) and Pax6 (E–G) expression were not detected during hiN cell reprogramming at 3, 7, and 21 days after transduction. In contrast, human iPSC cultures differentiated toward a neuroblast stage (IPS-N; D and H) displayed prominent intranuclear expression of the factors. Scale bar, 20 μm.

(I–N) Nestin is transiently expressed in a subset of cells within hiN cell cultures (I–K), albeit less robustly than in iPS-N cells (L). Staining was not apparent in empty vector-transduced cells (M and N).

(O) Temporal profile of Nestin-positive cells in hiN cell cultures or empty vector-transduced skin fibroblasts. n = 3 at each time point. $^{*}p < 0.05$ by ANOVA with Bonferroni correction. Results represent the mean ± SEM.

(P) Quantitative real-time RT-PCR analysis of neural progenitor marker gene expression in hiN cell cultures at 0, 7, or 21 days after transduction as indicated or in iPSC-N cells. Expression levels are normalized to *GAPDH*; error bars represent the standard error of the mean (SEM); n > 9 per group

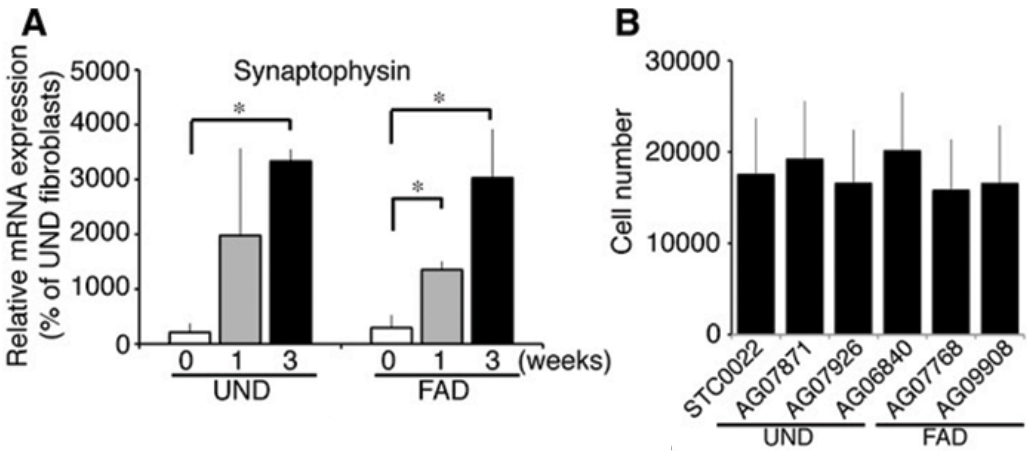

Figure 8. FAD fibroblast-derived hiN (FAD-iN) and control fibroblast-derived hiN (UND-iN) exhibit similar general neuronal properties

(A) Time course gene expression for *synaptophysin* in UND and FAD hiN cell cultures. Samples were collected at 0, 1, and 3 weeks after gene transduction with the 5 hiN cell conversion factors, as indicated. Analyses were by quantitative RT-PCR. Expression was comparable in the UND and FAD cultures. All data were normalized to *GAPDH* expression. $p<0.05$; n=9. Results represent th mean ± SEM.

(B) Quantification of average cell number per well in hiN cell cultures at 3 weeks, using Hoechst nuclear staining. Results represent mean ± SEM.

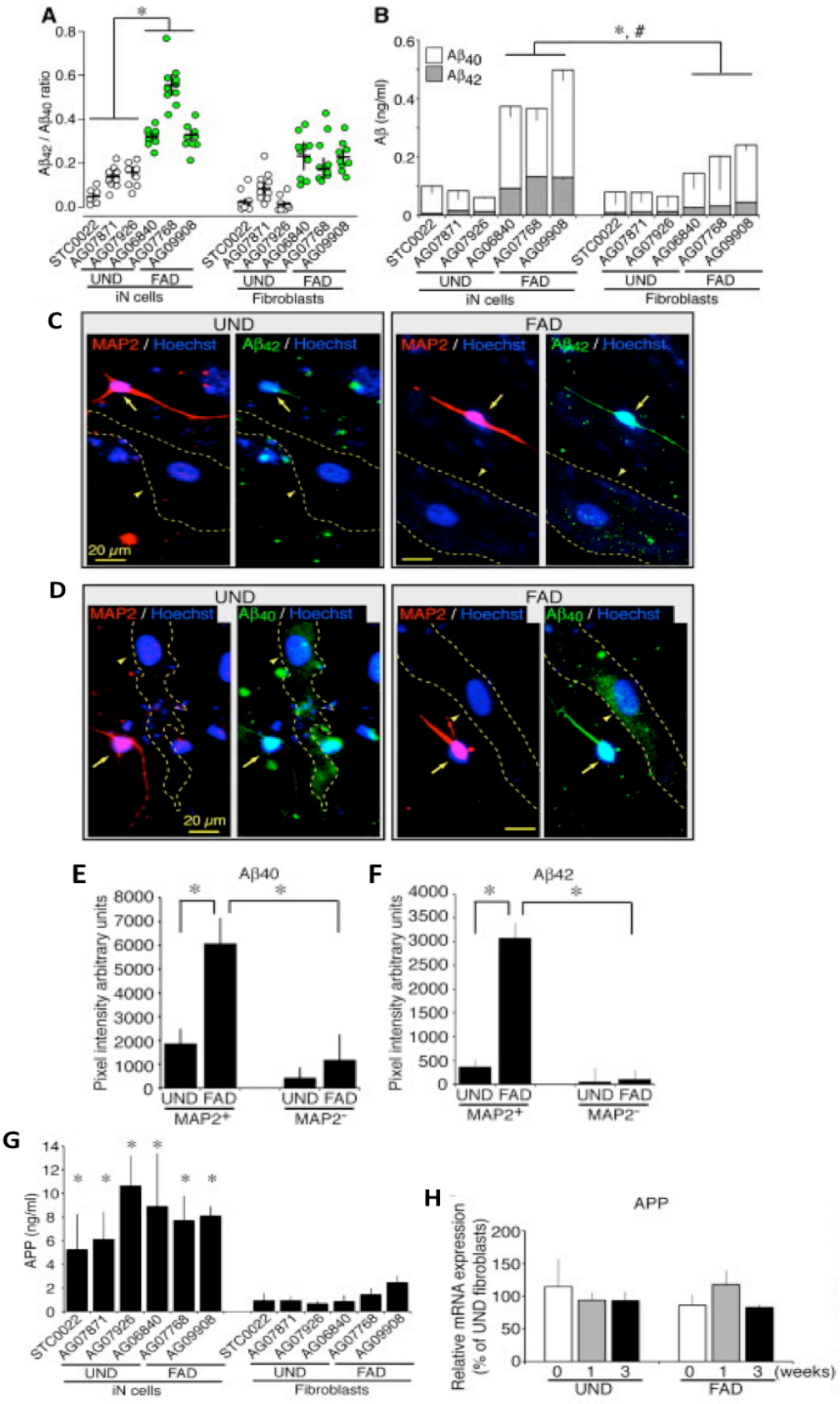
A
Aβ42 / Aβ40 ratio
STC0022
AG07871
AG07926
AG06840
AG07768
AG09908
UND
FAD
iN cells
Fibroblasts
B
Aβ40
Aβ42
Aβ (ng/ml)
*, #
C
UND
FAD
MAP2 / Hoechst
Aβ42 / Hoechst
20 μm
D
Aβ40 / Hoechst
E
Aβ40
Pixel intensity arbitrary units
MAP2+
MAP2-
F
Aβ42
G
APP (ng/ml)
H
APP
Relative mRNA expression
(% of UND fibroblasts)
0 1 3 (weeks)

Figure 9

Figure 9. Modified APP Processing in FAD hiN Cell Cultures

(A) The Aβ42:Aβ40 ratio is selectively increased in FAD hiN cell cultures relative to UND hiN cell cultures or fibroblasts. Media from hiN cell cultures (at 3 weeks post-transduction, empty circles) or fibroblast cultures (green circles), as indicated, was assayed for secreted Aβ40 and Aβ42 by sandwich ELISA. Results represent the mean ± SEM. n = 3 individual lines per group, with 11 to 16 independent wells for each line. $^{*}p < 0.05$ by ANOVA with post hoc Tukey HSD test.

(B) Total absolute extracellular Aβ levels ($Aβ_{40}$ [white bars] + $Aβ_{42}$ [gray bars]) are presented for cultures as in (A). Total Aβ was increased by neuronal hiN cell conversion in the context of FAD patient cultures. In contrast, UND fibroblast cultures were not significantly different from UND hiN cell cultures. n = 3 individual lines per group, with 11 to 16 independent wells for each line. $^{*}p < 0.05$. Results represent the mean ± SEM.

(C-D) MAP2-positive neuronal cells within the hiN cultures are enriched for the Aβ42 and Aβ40 fragment, compared to fibroblastic MAP2-negative cells. FAD and UND hiN cell cultures were co-immunostained with antibodies to MAP2 along with Aβ42 (C) or Aβ40 (D); nuclei are identified by Hoechst staining. MAP2-negative fibroblastic cells (demarcated with dotted lines) display low levels of Aβ42 and Aβ40 relative to the MAP2-positive cells, as quantified in (E and F).

(E-F) Aβ42 (F; from C above) and Aβ40 (E; from D above) immunostaining fluorescence was quantified within MAP2-positive ('neuron-like') and MAP2-negative ('fibroblastic') cells in terms of total Aβ42 (F) or Aβ40 (E) pixel intensity per cell using Image J software (NIH). Immunostaining fluorescence pixel intensities were quantified for each of the 6 hiN cell cultures (3 FAD and 3UND, as per Figure 3); data presented are aggregated into FAD and UND groups. Results represent as the mean ± SEM (n = 35-50 cells per well per MAP2-positive or MAP2-negative group, with 3-4 independent wells per line). $^{*}p < 0.05$.

(G) Quantification of total intracellular APP holoprotein using sandwich ELISA. APP is enriched in hiN cell cultures relative to fibroblast precursors ($^{*}p < 0.05$ for all comparisons), but UND and FAD genotypes do not differ significantly. Results represent the means ± SEM (n = 6–9 wells per group). $^{*}p < 0.05$.

(H) Time course gene expression for *APP* in UND and FAD hiN cultures. Samples were collected at 0, 1, and 3 weeks after gene transduction with the 5 hiN cell conversion factors, as indicated. Analyses were by quantitative RT-PCR. Expression was comparable in the UND and FAD cultures. All data were normalized to *GAPDH* expression. n = 9. Results represent the mean ± SEM.

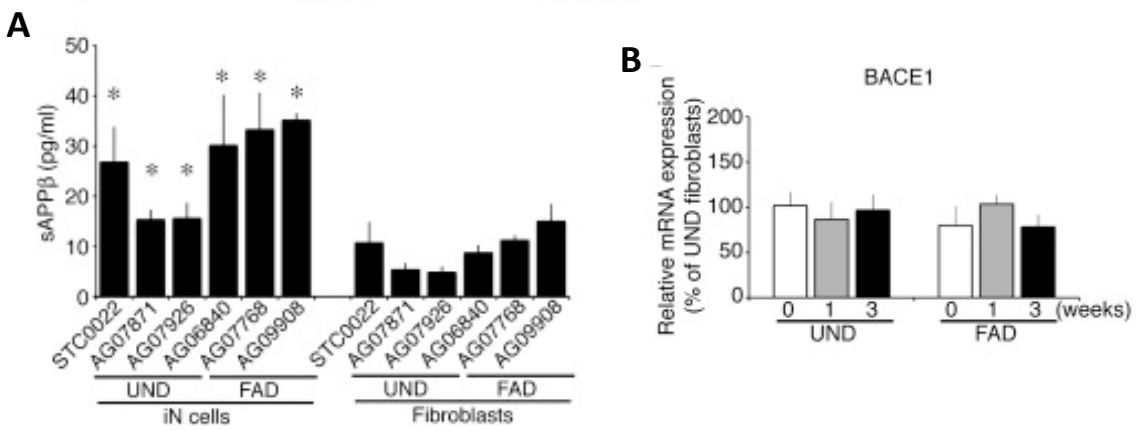

Figure 10. Modified APP Processing in FAD hiN Cell Cultures: Anaylsis of BACE1 Activity

(A) Accumulation of sAPPβ in the media of UND and FAD cultures, as determined by sandwich ELISA. Results represent the means ± SEM; n = 4–5 wells per individual line.

(B)Time course gene expression profiles for *BACE1* in UND and FAD hiN cultures. Samples were collected at 0, 1, and 3 weeks after gene transduction with 5 hiN cell conversion factors, as indicated. Analyses were by quantitative RT-PCR. Expression was comparable in the UND and FAD cultures. All data were normalized to *GAPDH* expression. n = 9. Results represent the mean ± SEM.

Chapter 5. Summary and Conclusions

Two cellular reprogramming technologies have emerged that demonstrate that cell fate can be converted by ectopic expression of defined transcription factors: induced pluripotent stem (iPS) cell technology and induced neuronal (iN) cell technology. These recent advances in cell reprogramming strategies have great potential utility for patient-specific disease modeling and for applications in regenerative medicine. Here we have demonstrated the potential of both iPS and iN cellular reprogramming technologies for modeling Alzheimer's disease (AD). These bioengineered human cell-based models of AD provide unique and invaluable tools for elucidating the mechanism of AD pathogenesis.

The generation of an iPS cell-based model of AD involved a two-step approach, in which AD-patient specific iPS cells were first derived via direct reprogramming of AD patient skin fibroblasts by transcription factors, Oct4, Sox2, Klf4 and c-Myc, and then subsequently differentiated into forebrain cortical glutamatergic neurons. One caveat in our results is that we were unable to generate true iPS cells that expressed the panel of pluripotency markers necessary for the validation of stemness. Rather, our AD-iPS cells were partially reprogrammed and only expressed a few pluripotency markers, namely, Oct4, Nanog and Tert. That we were able to generate both motor and cortical neurons from these partially reprogrammed iPS cells is curious. One explanation for this result may be our use of neuralizing drugs that mediate dual SMAD inhibition - SB431542 and LDN193189, the structural analog of dorsomorphin (Chambers et

al., 2009; Zhou et al, 2010) - in our differentiation cultures. Indeed, in a recent study, Boulting et al., have shown that iPS cell lines which differentiated poorly into motor neurons could be coaxed into differentiation by active neuralization via drugs SB431542 and LDN193189. It may be the case that active neuralization was the critical factor that allowed for the differentiation of our partially reprogrammed iPS cells into neurons. One could imagine a scenario where our partially reprogrammed cells were in a particular dedifferentiated state that when subjected to induction from strong neuralizing factors, their cell fate was pushed into the neural lineage. Because reprogramming efficiencies were extremely low, we were unable to examine APP processing in these cultures, by assaying for secreted Aβ40 and Aβ42 using sandwich ELISA. As such, the validity of our AD-iPS cell based model for AD remains to be determined.

While we originally sought to generate a patient-specific model of AD via iPS cell reprogramming, this strategy proved to be labor intensive and wrought with technical challenge. As such we turned to iN cell reprogramming strategy as alternative approach to achieve our end. Unlike iPS cell reprogramming, iN cell reprogramming offered a direct method for generating forebrain cortical glutamatergic neurons. We generated an iN-cell based model of AD by directly reprogramming AD patient fibroblast cells to cortical glutamatergic neurons via lentiviral expression of lineage-specific conversion factors, Brn2, Ascl1, and Myt1l, Olig2 and Zic1 (Vierbuchen et al., 2010). As previous studies had shown that neuronal lineage-specific transcription factors can directly convert mouse and human fibroblasts to cortical glutamatergic type neurons (Vierbuchen et al.,

2009; Pang et al., 2011), we reasoned that AD patient fibroblast cells could be directly converted to forebrain cortical glutamatergic neurons.

In generating our AD-iN cell-based model, we have shown proof-of-principle for the utility of iN cell reprogramming technology for human cell-based neuronal disease modeling and in particular, for modeling AD. Our analysis of FAD patient-derived hiN cell cultures revealed that our model recapitulated key molecular features of AD. hiN cells from PSEN mutant FAD patient fibroblasts display an increased Aβ42:Aβ40 ratio relative to control hiN cells, consistent with patient brain pathology and with the role of PSENs as essential components of the γ-secretase complex (Hardy and Selkoe, 2002). Furthermore, the effect of FAD PSEN mutations on the Aβ42:Aβ40 ratio was amplified upon hiN cell conversion from fibroblasts. This suggests a model in which PSEN FAD mutants may alter APP processing at multiple levels: through modified γ-secretase activity, as well as with altered cellular context.

Bioengineered human cell-based models of AD provide unique and invaluable tools for elucidating the mechanism of AD pathogenesis. Patient-specific models of AD offer the opportunity to study the disease in a human cellular context. Current models of AD, including transgenic animal models do not fully recapitulate the AD phenotype. While transgenic models of AD have been important tools for understanding the pathophysiological mechanism underlying AD, they remain limited in their scope. Although FAD is linked to mutations in APP and PSEN, mutant mice harboring FAD mutations show limited representation of the disease profile. APP mice exhibit only some features of

AD, including amyloid plaque formation, synaptic degeneration and memory decline. Furthermore, despite accounting for the overwhelming majority of FAD cases, PSEN mutant mice show only accumulation of Aβ42. While the 3xTg-AD mouse model recapitulates many aspects of AD, including NFT pathology, amyloid plaque formation, synaptic deficits and memory decline, MAPT mutations are not linked to FAD. Furthermore, that this aggressive genetic approach was necessary to recapitulate salient features of AD speaks to the complexity of modeling AD in mice and more importantly, the limitation of the mouse system for modeling this human disease (that involves higher cognitive function and occurs late in life).

Previous cellular models for AD have been based on available tissue, such as human cancer cell lines and patient fibroblast cell lines, but these models cannot recapitulate the unique neuronal environment in which disease pathology occur. In this regard, primary neuronal cultures from animal models have been used in studies but this approach also has its limitations since these models do not fully recapitulate clinical disease phenotypes and are therefore limited in their representation of disease pathophysiology. Indeed, various AD animal models have been generated because no one model fully recapitulates the human disease. Compounding this problem is that the same FAD mutation modeled in mice with different genetic backgrounds results in different phenotypes. As such, while cellular and animal models have allowed for tremendous strides in elucidating the pathogenic mechanisms of AD, our understanding of the molecular mechanisms of this disease remains incomplete.

In contrast, to mouse models, patient-specific models recapitulate the disease within the genetic background of patients. These models offer the unprecedented opportunity for examining disease pathophysiology within the human neuronal context and moreover, a patient-specific context.

Lastly, cell reprogramming-based models of AD may be of great utility for modeling sporadic AD. While FAD mutations have provided a genetic signature to model AD, it remains that FAD represents less than 1% of all AD cases. The majority of AD cases are sporadic, with no known genetic links, although studies have identified susceptibility genes, including *ApoE.* As such, cell reprogramming strategies may be uniquely positioned to enable the modeling of SAD. Sporadic AD patient-based models may provide answers that can help fill the gaps in our knowledge of the disease mechanism of AD. However, while these models are important, much difficulty nevertheless lies ahead in dissecting the mechanisms of sporadic AD using these models.

Chapter 6. Methods

Cell Culture

Primary fibroblast lines were obtained from Coriell Cell Repository. Fibroblasts were cultured in fibroblast medium (DMEM supplemented with 10% FBS (Invitrogen-Gibco), 1 mM glutamine (Invitrogen). Human ES cells and iPS cells were maintained on a feeder layer of mitotically inactivated MEFs plated at 25,000 cells/cm^2 (GlobalStem) in human ES cell medium (DMEM/F12 with GlutaMAX supplemented with 20% knockout serum replacement, 1% nonessential amino acids, 0.055 mM b-mercaptoethanol (all Invitrogen-Gibco), and 20 ng/ml bFGF (Peprotech). Cells were routinely passaged every 5 to 7 days with dispase (1 mg/ml) at a dilution of 1:10 to 1:20.

Lentiviral Infection and iPS Cell Derivation

The protocol used to generate human iPS cells was adapted from established protocols (Takahashi et al., 2007; Yu et al., 2007; Park et al., 2008b). VSVg-coated lentiviral supernatant was generated in 293 FT cells by co-transfection of a polycistronic lentiviral vector encoding Oct4, Klf4, Sox2 and c-Myc (Sommer et al., 2010) with psPAX2 and pMD2.G (Addgene) into 293 FT cells. Culture medium was changed 12 hr post-transfection, and virus-containing supernatant was collected 60–72 hr post-transfection. Viral supernatant was filtered through a 0.45 μm filter. Fibroblasts were seeded at 1 x 10^4 cells/cm^2 one day before infection. Four consecutive infections were performed every 12 hours over a

period of 48 hr in the presence of 8 μg/ml of polybrene. Culture medium was changed 12 hours after the last infection. Six days after transduction, fibroblasts were passaged using trypsin and re-plated at different densities between 5×10^4 and 5×10^5 cells/cm^2 on MEF feeder layers and cultured in fibroblast medium (see above). Culture medium was replaced by human ES cell medium (see above) the following day. After 2-3 weeks, human iPS cell colonies were picked manually based on morphology and manually passaged at least 5 times until a stable line was established. For the first set of iPS cell lines, 4 separate VSVg-coated lentiviruses were produced for each of 4 reprogramming factors. Viral supernatant was concentrated and pooled for a stock virus. Fibroblasts were infected only once.

Reverse Transcription of Total RNA and Quantitative RT-PCR

RNA was isolated from fibroblasts, neural progenitor cells, hESCs, and iPSCs using Trizol extraction (hES cells and iPS cells were mechanically separated from feeder cells). Reverse transcription was performed on 1μg of total RNA using oligo dT priming and the SuperScript III First-Strand Synthesis System for RT-PCR (Invitrogen) according to manufacturer's instructions. Real-time PCR was performed using ABI Prism 7900HT (Applied Biosystems) with Power SYBR Green PCR Master Mix (Invitrogen). Gene expression levels were quantified by the ΔΔCt method.

Primers for the analysis of total gene expressions were:

*OCT4-F: 'ATGCACAACGAGAGGATTTTGA3'

*OCT4-R: CTTTGTGTTCCCAATTCCTTCC

SOX2-F: TAAATACCGGCCCCGGCGGA

SOX2-R: GCTCGCCATGCTATTGCCGC

KLF4-F: GGTCTCTTCGTGCACCCACTTG

KLF4-R: GCTCAGCACTTCCTCAAGACCC

*CMYC-F: AGCAGAGGAGCAAAAGCTCATT

*CMYC-R: CCAAAGTCCAATTTGAGGCAGT

*FOXD3-F: AAGCCCAAGAACAGCCTAGTGA

*FOXD3-R: GGGTCCAGGGTCCAGTAGTTG

*TERT-F: AGCATTCCTGCTCAAGCTGACT

*TERT-R: ACTCACTCAGGCCTCAGACTCC

*NANOG-F: CCAAATTCTCCTGCCAGTGAC

*NANOG-R: CACGTGGTTTCCAAACAAGAAA

*CRIPTO-F: TACCTGGCCTTCAGAGATGACA

*CRIPTO-R: CCAGCATTTACACAGGGAACAC

FOXG1-F: 5’AGAAGAACGGCAAGTACGAGA3’

FOXG1-R: 5’TGTTGAGGGACAGATTGTGGC3’

Primers for viral gene expression were:

OCT-F2A-F: 5’TATGGGAGCCCTCACTTCAC3’

OCT-F2A-R: 5’CGCCAACTTGAGAAGGTCA3’

IRES-SOX-F: 5’GGGACGTGGTTTTCCTTTG3’

IRES-SOX-R: 5’GGGCTGTTTTTCTGGTTGC3’

KLF4-IRES-F: 5’GACCACCTCGCCTTACACAT3’

KLF4-IRES-R: 5'CCCTCACATTGCCAAAAGAC3'

CMYC-WPRE-F: 5'CAGCTACGGAACTCTTGTGCGT3'

CMYC-WPRE-R: 5'GCCATACGGGAAGCAATAGCATGA3'

Gene expression was normalized using GAPDH primers:

GAPDH-F: 5'GTGAGGGTCTCTCTCTTCCT3'

GAPDH-R: 5'GGTCTCCTCTGACTTCAACA3'

*From Dimos et al., 2008

FACS Analysis of iPS Cells

iPS cells were detached using TrypLE Express (Invitrogen). After gentle trituration, cells were filtered through cell strainer caps (40 mm mesh) to obtain a single cell suspension. Cell were then pelleted by centrifugation at 1000 rpm and resuspended in staining buffer (PBS, 0.5% bovine serum albumin [BSA], 2 mM EDTA and 20 mM Glucose). Cell suspensions were incubated with antibodies from BD Biosciences: SSEA-3 PE (1:100, 560237), SSEA-4 AlexaFluor647 (1:100, 560219) and Tra-1-60 AlexaFluor488 (1:100, 560173) for 30 min protected from light at 37 deg C. The stained cells were washed twice with 1ml staining buffer and again pelleted by centrifugation at 1000 rpm. The pellet was resuspended in 400 ml staining buffer. Cells were analyzed using FACS Aria IIu (BD Bioscience, CA). SSEA-4^{+}Tra-1-60^{+} populations were first analyzed by forward and side scatter properties (FSC, SSC) then analysis gates were set based on fluorescence intensity and negative control. FACS of iPS cell cultures

in the absence of antibody staining (negative control) defined the unstained population threshold parameters.

Cortical Neuron Differentiation

EGF method

The EGF method was developed by modifying cortical neuron differentiation protocol in Eiraku et al., 2008. Cell colonies were triturated to aggregates of about 50 cells in size and seeded in low-adherence dishes at about 300,000 cells/ml in hES medium (without bFGF). For the first 3 days, cells were treated with 20 μM Y-27632. From days 1-9, cells were treated with SB431542 (10 μM, Tocris) and LDN193189 (0.2 μM, Stemgent) to neuralize the cultures. On day 12, hES medium was replaced with DMEM/F12 with GlutaMAX supplemented with 1x N2 (Invitrogen), 1% nonessential amino acids and 10 ng/ml bFGF (Peprotech). On day 25-27, embryoid bodies were dissociated with 0.05% trypsin (Invitrogen), and plated onto poly-D-lysine/laminin-coated 24-well plates at a density of about 125,000-250,000 cells per well. The culture medium was changed to Neurobasal supplemented with 1x B27, 50 ng/ml BDNF (Peprotech) and 50ng/ml NT3 (Peprotech). Cultures were fixed after 3-4 days.

PALS-C method

The PALS-C method was developed by modifying the motor neuron differentiation (see below) protocol to omit patterning factors specific for motor

neurons, namely RA and SAG, caudalizing and ventralizing factors, respectively. Additionally, CNTF was not used.

Motor neuron differentiation

Motor neuron differentiation was performed as described in Boulting et al., 2011. iPS cells were treated with dispase (1mg/ml) and mechanically separated from feeder cells. Cell colonies were triturated to aggregates of about 50 cells in size and seeded in low-adherence dishes at about 300,000 cells/ml in hES medium supplemented with 20 ng/ml of bFGF and 20 μM Y-27632 for the first 3 days. From days 1-9, cells were treated with SB431542 (10 μM, Tocris) and LDN193189 (0.2 μM, Stemgent) to neuralize the cultures. At day 4, hES medium was replaced with a neural induction medium (NIM; DMEM/F12 with GlutaMAX supplemented with 1x N2 supplement (Invitrogen), 1% nonessential amino acids, 2 μg/ml heparin, and 20 ng/ml bFGF. Starting from day 5, 1μM retinoic acid (RA; Sigma), 10 ng/ml BDNF (Peprotech), 0.4 μg/ml ascorbic acid (Sigma) were added to the cultures. Starting from day 7, 1 μM smoothened agonist 1.3 (SAG; Calbiochem) was added to cultures. On day 21, embryoid bodies were dissociated with 0.05% trypsin (Invitrogen), and plated onto poly-D-lysine/laminin-coated 24-well plates at a density of about 125,000-250,000 cells per well. The base medium of NIM was changed to Neurobasal (Invitrogen). All factors were maintained and additionally, 25 μM β-mercaptoethanol (Millipore), 25 μM glutamic acid (Sigma), 1x B27 (Invitrogen) and 10ng/ml each of BDNF, GDNF and CNTF (Peprotech) were added. Cultures were fixed after 2-3 days.

Plasmid Construction for hiN

cDNA of the five reprogramming factors used here–Ascl1, Brn2, Myt1l, Oligo2 and Zic1–were obtained from Addgene. Inserts were PCR cloned into the lentiviral vector construct pLenti6.3/V5-Dest (Invitrogen) by LR clonase reaction using standard Gateway Technology cloning techniques (MacLeod et al., 2006). To generate a polycistronic vector for expression of Ascl1, Brn2, and Zic1, we used a modified pHAGE2-EF1a vector (Sommer et al., 2009). A DNA fragments consisting of cDNAs for murine Ascl1 and Brn2, separated by an intervening sequence encoding the F2A peptide, was generated by overlapping polymerase chain reactions using AccuPrime Taq DNA Polymerase (Invitrogen) as per the manufacturer's instructions. PCRs were carried out using the primer pairs Ascl1 5' XbaI/Ascl1-F2A 3' and F2A-Brn2 5'/ Brn2 3' Sal1 (see below), and with the lentiviral single gene vectors above as substrate. Aliquots of the two purified amplicons were then mixed in a 1:1 ratio and used in a second PCR round with the primers Ascl1 50 XbaI and Brn2 30 Sal1. The resulting fragment (Ascl1-F2A-Brn2) was gel-purified and inserted by directional cloning into Xba1 and Sal1-digested pHAGE2-EF1a-Oct4F2AKlf4- IRES-Sox2E2AcMyc upstream of an internal ribosome entry site (IRES) element. Next, a Zic1 cDNA fragment was obtained by PCR with primers pairs Zic1 50 NdeI and Zic1 30 ClaI. This fragment was then inserted between the NdeI and ClaI sites, downstream of the IRES element, of the pHAGE2-Ascl1F2ABrn2 vector. The final construct structure was confirmed by sequencing.

Ascl15'XbaI: CACCGTCTAGAACCATGGAGAGCTCTGGCAAGATGGAGAGTG

Ascl1-F2A3': FCTTGAGAAGGTCAAAATTCAAAGTCTGTTTCACGCCACTT
CCGTTGAACCAGTTGGTAAAGTCCAGCAGCTC
F2A-Brn2 5': AAACAGACTTTGAATTTTGACCTTCTCAAGTTGGCGGGAGA
CGTGGAGTCCAACCCAGGGCCCATGGCGACCGCAGCGTCTAACCACTA
Brn2 3'Sal1: TTTGTCGACTCACTGGACGGGCGTCTGCACC
Zic1 5'NdeI: TGCCATATGATGCTCCTGGACGCCGGA
Zic1 3'ClaI: GGTTTATCGATTTAAACGTACCATTCGTTAAAATTGGAAGAG
AGCGCGCTGT

hiN Cell Induction and Transfection

Fibroblasts were plated at 20,000 cells/well in 24-well plates one day before infection and maintained in standard fibroblast media (Dulbecco's minimal essential medium [DMEM] with 10% fetal bovine serum). Culture plates and dishes were treated with Poly-L- Ornithine (Sigma) and Laminin (Invitrogen) before the application of the cells as per the manufacturer's instructions. Fibroblasts were transduced with replication-incompetent, VSVg-coated lentiviral particles encoding Ascl1, Brn2, Myt1l, Oligo2 and Zic1, in fibroblast media containing polybrene (8 mg/ml). Each lentiviral type was added at a multiplicity of infection 2:1. Two day after transduction, the media was replaced with glial-conditioned N2 media (GCM; N2 media is DMEM/F12 with N2 supplement; Invitrogen) containing 20 ng/ml BDNF and 20 ng/ml NT3 (Peprotech). For glial conditioned media, primary cultures of type 1 astroglia were prepared from the cortices of P1 rat pups using standard techniques (Kaech and Banker, 2006),

and these were subsequently cultured in N2 media for 4 days (Kaech and Banker, 2006); media was harvested and filtered through a 45-micron filter (Corning) and used immediately. For the first 4 days in N2 media, dorsomorphin (1 mM; Stemgent) was applied to the culture. Media was changed every 2-3 days for the duration of the culture period.

Immunocytochemistry and Immunohistochemistry

Cells were fixed in 4% paraformaldehyde for 10 min at room temperature, followed by rinsing 3 times with phosphate-buffered saline (PBS). Cells were then permeabilized with 0.1% Triton X-100 in 1XPBS for 10 min at room temperature. After again rinsing 3 times with PBS, cells were incubated with blocking buffer containing 10% goat serum and 10 mg/ml BSA at room temperature for 1 hr. All primary antibodies were diluted in PBS. Cells were incubated with primary antibodies as listed at 4 deg C for 12-16 hr, followed by the corresponding secondary antibody solutions in 37 deg C for 1 hr. Cells were rinsed with 1XPBS three times followed by mounting of coverslips with anti-fade solution (Invitrogen). Primary antibodies used were (dilutions listed in parentheses): OCT4 (1:500 Santa Cruz); SSEA-4 (1:100, DSHB); TRA1-60 (1:500, Chemicon); TRA1-81 (1:500, Chemicon); Nanog (1:500 R&D); Islet1/2 (1:100, DSHB); HB9 (1:100 DSHB); mouse anti-Tuj1 (Covance, 1:1000); rabbit anti-Tuj1(Covance, 1:2000); rabbit anti-MAP2 (Sigma,1:400); mouse anti-MAP2 (Sigma, 1:500); mouse anti- Tau (Tau1, Millipore, 1:500); mouse anti-NeuN (Millipore, 1:200); rabbit anti-vGLUT1 (Synaptic System, 1:100); rabbit anti-

GAD65 (Millipore, 1:500); chicken anti-Tbr1 (Millipore, 1:500); mouse anti-human neurofilament (Sigma, 1:500); rabbit anti-Pax6 (Millipore, 1:500); mouse anti-Nestin (Millipore, 1:500); mouse anti-Ascl1 (BD PharMingen, 1:10). Also used were: mouse anti-APP (22C11, Milli-pore, 1:500), rabbit anti-APP (KDI, Millipore, 1:500), rabbit anti-BACE1 (Covance, 1: 500; this was further purified by protein G sepharose chromatography kit from GE healthcare), mouse anti-BACE1 (3D5, gifts from Robert Vassar), rabbit anti-EEA1 (Millipore, 1:500), mouse anti-M6PR (Abcam, 1:500), rabbit anti-LAMP2 (Sigma, 1:400). Dylight 488-, Dylight 549- and Dylight 649-conjugated secondary antibodies were purchased from Jackson Immunoresearch. Alexa-488, Alexa-633-conjugated secondary antibodies were obtained from Invitrogen. Alkaline phosphatase activity was detected in live cultures using the alkaline phosphatase substrate kit (Vector) according to manufacture's instructions.

For immunohistochemical analysis of acutely prepared brain sections, the following primary anti- bodies were used: rabbit anti-GFP antibody (Invitrogen, 1:200), mouse anti-human NCAM (Santa Cruz Biotechnology, 1:50), mouse anti-human mitochondria (hMito, MTC02; Abcam, 1:200). Imaging was performed by laser-scanning confocal microscopy with a 63x /1.4 objective (LSM510, Carl Zeiss) or by epifluorescence microscope (Olympus 1X71; Japan). hiN cell counts and fluorescence intensities were quantified by taking 10 to 35 images of randomly selected views per well. Subsequently, images were analyzed for cell counts and fluorescent intensity using Image J 1.42q software (National Institute of Health, USA). Values are presented as mean ± SEM.

FACS Sorting and RNA Extraction for hiN

hiN cell cultures (106 cells) were detached using TrypLE Express (Invitrogen, CA). After gentle trituration, cells were filtered through cell strainer caps (40 mm mesh) to obtain a single cell suspension. Cell were then pelleted by centrifugation at 1000 rpm and resuspended in 50 ml staining buffer (PBS, 0.5% bovine serum albumin [BSA], 2 mM EDTA and 20 mM Glucose). 50 ml antibody solution was prepared at 2X concentration (2 ml mouse anti human NCAM antibody labeled with a V450 fluorophore [BD Bioscience, CA, 1:50] in 50 ml staining buffer). The antibody solution was mixed with the cell suspension in a 1.5ml eppendorf tube and incubated for 15 min at room temperature. The stained cells were washed twice with 1ml staining buffer and again pelleted by centrifugation at 1000 rpm. The pellet was resuspended in 400 ml staining buffer in a FACS tube (BD Bioscience, CA) and placed on ice. Cells were analyzed using a FACS Aria IIu (BD Bioscience, CA). Gating was based on fluorescence intensity of the NCAM-V450 chromophore (at 450 nm) as well as autofluorescence (at 660 nm). FACS of hiN cell cultures in the absence of the NCAM-V450 antibody (negative control; see S2I) defined the unstained population threshold parameters. Subsequently, NCAM-V450 antibody stained hiN cells were gated based on these parameters. Cells were sorted directly into RNA lysis solution (Ambion, TX) by BD FACS Aria IIu (BD Bioscience, CA).

In Utero Transplantation

In order to mark transplanted hiN cells, human skin fibroblasts (STC0022) were

transduced with a GFP-encoding lentiviral vector 10 days prior to hiN cell induction. After three passages to remove contaminating virus, the fibroblasts were transduced with lentiviral vectors encoding Ascl1, Brn2, Myt1l, Oligo2 and Zic1 as described above. 7 to 10 days after hiN cells induction, hiN cells were trypsinized and triturated to single-cell suspensions in the presence of 0.1% DNase (QIAGEN). Timed-pregnant C57BL/6N mice at day 13.5 of gestation were anesthetized with oxygen containing 2% isoflurane administered through an inhalation mask, and 2-5 x10^5 cells were injected into the telencephalic vesicle of each embryo as described (Brustle et al., 1997; Wernig et al., 2008). Transplanted mice were spontaneously delivered and analyzed 1 to 2 weeks after surgery as indicated. Following deep isoflurane anesthesia, mice were decapitated, and the brains were rapidly removed and put in 4% paraformaldehyde for two days for fixation. For immunohistochemistry, 50 mm sections were cut with a vibrating blade microtome.

Electrophysiology and Calcium Imaging

Recordings in cultured cells were performed from hiN cells at 3-4 weeks after viral infection. Tight-seal whole cell recordings (WCR) were performed with borosilicate glass pipettes (resistance 5-8 MU). Recordings were made with an Axopatch 200B amplifier (Axon Instruments), and signals were sampled and filtered at 10 Khz and 5 Khz, respectively; whole cell capacitance was cancelled and S2 Cell 146, 359–371, August 5, 2011 ª2011 Elsevier Inc.series resistance compensated 60%–80% using standard techniques. The extracellular solution

contained: 140 mM NaCl, 5 mM KCl, 1.5 mM CaCl2, 1 mM MgCl2, 10 mM HEPES and 10 mM glucose, pH 7.4 adjusted with NaOH. To study Na+ currents, the intracellular solution used was 135 mM CsMeSO4, 4.1 mM MgCl2, 10 mM HEPES, 10 mM EGTA, 0.4 mM Na-GTP, 3.6 mM Na-ATP (pH 7.4 adjusted with CsOH). To study barium currents the bath solution contained: 132 mM tetraethylammonium (TEA)-Cl, 10 mM BaCl2, 10 mM HEPES, and 10mM glucose (pH 7.4 adjusted with CsOH). To elicit K+ currents, to view spontaneous voltage clamp events, and in the context of glutamate puff and current-clamp recordings, the pipette solution had K+ replacing Cs+ as the main cation. GABA puff experiments were performed with a lower Cl- intracellular solution, approximating physiological levels, as follows: 150 mM Cs-gluconate, 4.6 mM MgCl2, 0.1 mM CaCl2, 1 mM EGTA, 10 mM HEPES-Cs, 0.4 mM Na-GTP, and 4 mM Na-ATP. GABA responses were also elicited using a solution with a Cl- concentration close to the extracellular solution (data not shown). Its composition was: 150 mM CsCl, 4.6 mM MgCl2, 0.1 mM CaCl2, 1 mM EGTA, 10 mM HEPES-Cs, 0.4 mM Na-GTP, and 4 mM Na-ATP, pH 7.4. Liquid junction potentials were measured and subtracted for generation of current density-voltage plots and to measure passive membrane properties. Voltage dependent currents were recorded both with and without a P/4 protocol (Bezanilla and Armstrong, 1977). Recordings from transplanted cells were performed in acutely prepared horizontal and vertical brain slices through the entire cerebrum (180 mm thick) as described in detail (Llano and Bezanilla, 1980). For glial co-culture studies: murine astroglial cells were obtained from mice ubiquitously expressing

red fluorescent protein (Muzumdar et al., 2007). Glial cells were prepared as previously described (Kaech and Banker, 2006) and added into hiN cultures prepared as above, 2 to 2.5 weeks after viral cocktail transduction. 20,000-25,000 glial cells added/well of a 24-well plate. Recordings from co-cultures were performed on cells with a neuronal that lack red fluorescence, 1-2 weeks after initiation of co-culturing.

For recordings from acutely prepared brain slices after in utero transplantation: animals were sacrificed at postnatal days as indicated. Brain slices were prepared using standard techniques. Recordings were performed at 20-23 C in GFP-expressing cells identified by fluorescence microscopy. In the recording chamber, slices were perfused (1.5 ml/min) with a saline solution containing 125 mM NaCl, 2.5 mM KCl, 1.25 mM NaH2PO4, 26 mM NaHCO3, 2 mM CaCl2, 1 mM MgCl2 and 10 mM glucose equilibrated with a 95% O2-5% CO2 mixture. The pipette solution was the same as that used to elicit K+ currents above, with the addition of Alexa-598 (Invitrogen) as per the manufacturer's instructions, to allow for visualization of the recorded cells.

Sandwich ELISAs

APP ELISA was performed using a human APP ELISA kit (Invitrogen, Camarillo, CA), according to the manufacturer's instruction. Absorbance was read on a VersaMax ELISA Microplate Reader (Molecular Devices, Inc. Sunnyvale, CA) at 450 nm. The amount of APP was normalized to the total cell protein (determined with the DC Protein Assay Reagent kit; Bio-Rad, Hercules, CA). sAPPb and Ab

ELISA were performed on supernatant media from hiN cell cultures at 21 days after viral transduction using BetaMark sAPP Beta ELISA kit (Covance, Princeton, NJ), according to the manufacturer's instruction. The chemiluminescence was read on a microplate luminometer (SPECTRAFluoR Plus, TECAN, Mannedorf Switzerland). Ab quantification was performed by ELISA as described previously (Cirrito et al., 2003). Media was conditioned for 48 hr prior to harvesting. Samples were analyzed for Ab40 or Ab42 using specific sandwich ELISAs. Briefly, Ab40, and Ab42 were captured using monoclonal antibodies targeted against amino acids 35-40 (HJ2.0), or 33-42 (HJ7.4) of Ab, respectively. The antibodies HJ2.0, HJ5.1 and HJ7.4 were gifts from David M. Holtzman. For Ab40 and Ab42 assays, a biotinylated central domain monoclonal antibody (HJ5.1) followed by streptavidin-poly-HRP-40 was used for detection (Sigma). All assays were developed using Super Slow ELISA TMB (Sigma) and read on a VersaMax ELISA Microplate Reader (Molecular Devices, Inc. Sunnyvale, CA) at 650 nm. ELISA signals were reported as the mean ± SEM of three replica wells in ng of Ab per ml supernatant, based on standard curves using synthetic Ab40 and Ab42 peptides (rPeptide; Bogart, GA) Samples was optimized to detect Ab40 and Ab42 in the ranges of 1-3,000 ng/ml and 0.03–30 ng/ml, respectively (Figures S5F and S5G). The amount of sAPPb and Ab was normalized to the cell number per well as indicated.

References

Aasen, T., A. Raya, et al. (2008). "Efficient and rapid generation of induced pluripotent stem cells from human keratinocytes." Nat Biotechnol 26(11): 1276-1284.

Alzheimer, A., R. A. Stelzmann, et al. (1995). "An English translation of Alzheimer's 1907 paper, "Uber eine eigenartige Erkankung der Hirnrinde"." Clin Anat 8(6): 429-431.

Aoi, T., K. Yae, et al. (2008). "Generation of pluripotent stem cells from adult mouse liver and stomach cells." Science 321(5889): 699-702.

Baguisi, A., E. Behboodi, et al. (1999). "Production of goats by somatic cell nuclear transfer." Nat Biotechnol 17(5): 456-461.

Banito, A., S. T. Rashid, et al. (2009). "Senescence impairs successful reprogramming to pluripotent stem cells." Genes Dev 23(18): 2134-2139.

Bell, K. F. and A. Claudio Cuello (2006). "Altered synaptic function in Alzheimer's disease." Eur J Pharmacol 545(1): 11-21.

Bernstein, B. E., A. Meissner, et al. (2007). "The mammalian epigenome." Cell 128(4): 669-681.

Bertram, L. and R. E. Tanzi (2005). "The genetic epidemiology of neurodegenerative disease." J Clin Invest 115(6): 1449-1457.

Bertram, L. and R. E. Tanzi (2008). "Thirty years of Alzheimer's disease genetics: the implications of systematic meta-analyses." Nat Rev Neurosci 9(10): 768-778.

Billings, L. M., S. Oddo, et al. (2005). "Intraneuronal Abeta causes the onset of early Alzheimer's disease-related cognitive deficits in transgenic mice." Neuron 45(5): 675-688.

Blelloch, R., Z. Wang, et al. (2006). "Reprogramming efficiency following somatic cell nuclear transfer is influenced by the differentiation and methylation state of the donor nucleus." Stem Cells 24(9): 2007-2013.

Boland, M. J., J. L. Hazen, et al. (2009). "Adult mice generated from induced pluripotent stem cells." Nature 461(7260): 91-94.

Borchelt, D. R., T. Ratovitski, et al. (1997). "Accelerated amyloid deposition in the brains of transgenic mice coexpressing mutant presenilin 1 and amyloid precursor proteins." Neuron 19(4): 939-945.

Boulting, G. L., E. Kiskinis, et al. (2011). "A functionally characterized test set of human induced pluripotent stem cells." Nat Biotechnol 29(3): 279-286.

Boyer, L. A., T. I. Lee, et al. (2005). "Core transcriptional regulatory circuitry in human embryonic stem cells." Cell 122(6): 947-956.

Braak, H. and E. Braak (1991). "Neuropathological stageing of Alzheimer-related changes." Acta Neuropathol 82(4): 239-259.

Brambrink, T., R. Foreman, et al. (2008). "Sequential expression of pluripotency markers during direct reprogramming of mouse somatic cells." Cell Stem Cell 2(2): 151-159.

Briggs, R. and T. J. King (1952). "Transplantation of Living Nuclei From Blastula Cells into Enucleated Frogs' Eggs." Proc Natl Acad Sci U S A 38(5): 455-463.

Brookmeyer, R., S. Gray, et al. (1998). "Projections of Alzheimer's disease in the United States and the public health impact of delaying disease onset." Am J Public Health 88(9): 1337-1342.

Brustle, O., A. C. Spiro, et al. (1997). "In vitro-generated neural precursors participate in mammalian brain development." Proc Natl Acad Sci U S A 94(26): 14809-14814.

Buttini, M., E. Masliah, et al. (2005). "Beta-amyloid immunotherapy prevents synaptic degeneration in a mouse model of Alzheimer's disease." J Neurosci 25(40): 9096-9101.

Byrne, J. A., D. A. Pedersen, et al. (2007). "Producing primate embryonic stem cells by somatic cell nuclear transfer." Nature 450(7169): 497-502.

Caiazzo, M., M. T. Dell'Anno, et al. (2011). "Direct generation of functional dopaminergic neurons from mouse and human fibroblasts." Nature 476(7359): 224-227.

Calhoun, M. E., P. Burgermeister, et al. (1999). "Neuronal overexpression of mutant amyloid precursor protein results in prominent deposition of cerebrovascular amyloid." Proc Natl Acad Sci U S A 96(24): 14088-14093.

Calhoun, M. E., K. H. Wiederhold, et al. (1998). "Neuron loss in APP transgenic mice." Nature 395(6704): 755-756.

Calon, F., G. P. Lim, et al. (2004). "Docosahexaenoic acid protects from dendritic pathology in an Alzheimer's disease mouse model." Neuron 43(5): 633-645.

Carey, B. W., S. Markoulaki, et al. (2009). "Reprogramming of murine and human somatic cells using a single polycistronic vector." Proc Natl Acad Sci U S A 106(1): 157-162.

Chambers, S. M., C. A. Fasano, et al. (2009). "Highly efficient neural conversion of human ES and iPS cells by dual inhibition of SMAD signaling." Nat Biotechnol 27(3): 275-280.

Chan, E. M., S. Ratanasirintrawoot, et al. (2009). "Live cell imaging distinguishes bona fide human iPS cells from partially reprogrammed cells." Nat Biotechnol 27(11): 1033-1037.

Chen, G., K. S. Chen, et al. (2000). "A learning deficit related to age and beta-amyloid plaques in a mouse model of Alzheimer's disease." Nature 408(6815): 975-979.

Chishti, M. A., D. S. Yang, et al. (2001). "Early-onset amyloid deposition and cognitive deficits in transgenic mice expressing a double mutant form of amyloid precursor protein 695." J Biol Chem 276(24): 21562-21570.

Coovert, D. D., T. T. Le, et al. (1997). "The survival motor neuron protein in spinal muscular atrophy." Hum Mol Genet 6(8): 1205-1214.

Cowan, C. A., J. Atienza, et al. (2005). "Nuclear reprogramming of somatic cells after fusion with human embryonic stem cells." Science 309(5739): 1369-1373.

Cowan, C. A., I. Klimanskaya, et al. (2004). "Derivation of embryonic stem-cell lines from human blastocysts." N Engl J Med 350(13): 1353-1356.

Crouch, P. J., S. M. Harding, et al. (2008). "Mechanisms of A beta mediated neurodegeneration in Alzheimer's disease." Int J Biochem Cell Biol 40(2): 181-198.

Cruts, M., C. M. van Duijn, et al. (1998). "Estimation of the genetic contribution of presenilin-1 and -2 mutations in a population-based study of presenile Alzheimer disease." Hum Mol Genet 7(1): 43-51.

Daffner, K. R. (2010). "Promoting successful cognitive aging: a comprehensive review." J Alzheimers Dis 19(4): 1101-1122.

Davis, R. L., H. Weintraub, et al. (1987). "Expression of a single transfected cDNA converts fibroblasts to myoblasts." Cell 51(6): 987-1000.

De Strooper, B. and W. Annaert (2010). "Novel research horizons for presenilins and gamma-secretases in cell biology and disease." Annu Rev Cell Dev Biol 26: 235-260.

Delacourte, A., N. Sergeant, et al. (2002). "Nonoverlapping but synergetic tau and APP pathologies in sporadic Alzheimer's disease." Neurology 59(3): 398-407.

Dimos, J. T., K. T. Rodolfa, et al. (2008). "Induced pluripotent stem cells generated from patients with ALS can be differentiated into motor neurons." Science 321(5893): 1218-1221.

Do, J. T., D. W. Han, et al. (2006). "Reprogramming somatic gene activity by fusion with pluripotent cells." Stem Cell Rev 2(4): 257-264.

Dodart, J. C., K. R. Bales, et al. (2002). "Immunization reverses memory deficits without reducing brain Abeta burden in Alzheimer's disease model." Nat Neurosci 5(5): 452-457.

Duff, K., C. Eckman, et al. (1996). "Increased amyloid-beta42(43) in brains of mice expressing mutant presenilin 1." Nature 383(6602): 710-713.

Duyao, M., C. Ambrose, et al. (1993). "Trinucleotide repeat length instability and age of onset in Huntington's disease." Nat Genet 4(4): 387-392.

Ebert, A. D., J. Yu, et al. (2009). "Induced pluripotent stem cells from a spinal muscular atrophy patient." Nature 457(7227): 277-280.

Edbauer, D., E. Winkler, et al. (2003). "Reconstitution of gamma-secretase activity." Nat Cell Biol 5(5): 486-488.

Eggan, K., K. Baldwin, et al. (2004). "Mice cloned from olfactory sensory neurons." Nature 428(6978): 44-49.

Eiraku, M., K. Watanabe, et al. (2008). "Self-organized formation of polarized cortical tissues from ESCs and its active manipulation by extrinsic signals." Cell Stem Cell 3(5): 519-532.

Eminli, S., A. Foudi, et al. (2009). "Differentiation stage determines potential of hematopoietic cells for reprogramming into induced pluripotent stem cells." Nat Genet 41(9): 968-976.

Eminli, S., R. Jaenisch, et al. (2006). "Strategies to induce nuclear reprogramming." Ernst Schering Found Symp Proc(5): 83-98.

Eminli, S., J. Utikal, et al. (2008). "Reprogramming of neural progenitor cells into induced pluripotent stem cells in the absence of exogenous Sox2 expression." Stem Cells 26(10): 2467-2474.

Eroglu, C. and B. A. Barres (2010). "Regulation of synaptic connectivity by glia." Nature 468(7321): 223-231.

Feng, R., S. C. Desbordes, et al. (2008). "PU.1 and C/EBPalpha/beta convert fibroblasts into macrophage-like cells." Proc Natl Acad Sci U S A 105(16): 6057-6062.

Games, D., D. Adams, et al. (1995). "Alzheimer-type neuropathology in transgenic mice overexpressing V717F beta-amyloid precursor protein." Nature 373(6514): 523-527.

Gilyarov, A. V. (2008). "Nestin in central nervous system cells." Neurosci Behav Physiol 38(2): 165-169.

Glenner, G. G. and C. W. Wong (1984). "Alzheimer's disease: initial report of the purification and characterization of a novel cerebrovascular amyloid protein." Biochem Biophys Res Commun 120(3): 885-890.

Goate, A., M. C. Chartier-Harlin, et al. (1991). "Segregation of a missense mutation in the amyloid precursor protein gene with familial Alzheimer's disease." Nature 349(6311): 704-706.

Goedert, M., C. M. Wischik, et al. (1988). "Cloning and sequencing of the cDNA encoding a core protein of the paired helical filament of Alzheimer disease: identification as the microtubule-associated protein tau." Proc Natl Acad Sci U S A 85(11): 4051-4055.

Gordon, M. N., D. L. King, et al. (2001). "Correlation between cognitive deficits and Abeta deposits in transgenic APP+PS1 mice." Neurobiol Aging 22(3): 377-385.

Gotz, J., F. Chen, et al. (2001). "Formation of neurofibrillary tangles in P301l tau transgenic mice induced by Abeta 42 fibrils." Science 293(5534): 1491-1495.

Gruhne, B., R. Sompallae, et al. (2009). "The Epstein-Barr virus nuclear antigen-1 promotes genomic instability via induction of reactive oxygen species." Proc Natl Acad Sci U S A 106(7): 2313-2318.

Grundke-Iqbal, I., K. Iqbal, et al. (1986). "Microtubule-associated protein tau. A component of Alzheimer paired helical filaments." J Biol Chem 261(13): 6084-6089.

Gu, G., J. Yuan, et al. (2007). "Prostate cancer cells with stem cell characteristics reconstitute the original human tumor in vivo." Cancer Res 67(10): 4807-4815.

Gurdon, J. B. (1962). "The developmental capacity of nuclei taken from intestinal epithelium cells of feeding tadpoles." J Embryol Exp Morphol 10: 622-640.

Gurdon, J. B. (2006). "From nuclear transfer to nuclear reprogramming: the reversal of cell differentiation." Annu Rev Cell Dev Biol 22: 1-22.

Gurdon, J. B. and J. A. Byrne (2003). "The first half-century of nuclear transplantation." Proc Natl Acad Sci U S A 100(14): 8048-8052.

Gurdon, J. B. and V. Uehlinger (1966). ""Fertile" intestine nuclei." Nature 210(5042): 1240-1241.

Haass, C., C. A. Lemere, et al. (1995). "The Swedish mutation causes early-onset Alzheimer's disease by beta-secretase cleavage within the secretory pathway." Nat Med 1(12): 1291-1296.

Haass, C. and D. J. Selkoe (1998). "Alzheimer's disease. A technical KO of amyloid-beta peptide." Nature 391(6665): 339-340.

Hacein-Bey-Abina, S., C. Von Kalle, et al. (2003). "LMO2-associated clonal T cell proliferation in two patients after gene therapy for SCID-X1." Science 302(5644): 415-419.

Hanna, J., K. Saha, et al. (2009). "Direct cell reprogramming is a stochastic process amenable to acceleration." Nature 462(7273): 595-601.

Hardy, J. (1997). "Amyloid, the presenilins and Alzheimer's disease." Trends Neurosci 20(4): 154-159.

Hardy, J. and D. J. Selkoe (2002). "The amyloid hypothesis of Alzheimer's disease: progress and problems on the road to therapeutics." Science 297(5580): 353-356.

Hargus, G., O. Cooper, et al. (2010). "Differentiated Parkinson patient-derived induced pluripotent stem cells grow in the adult rodent brain and reduce motor asymmetry in Parkinsonian rats." Proc Natl Acad Sci U S A 107(36): 15921-15926.

Harold, D., R. Abraham, et al. (2009). "Genome-wide association study identifies variants at CLU and PICALM associated with Alzheimer's disease." Nat Genet 41(10): 1088-1093.

Hawley, R. G. (2008). "Does retroviral insertional mutagenesis play a role in the generation of induced pluripotent stem cells?" Mol Ther 16(8): 1354-1355.

Hebbes, T. R., A. W. Thorne, et al. (1988). "A direct link between core histone acetylation and transcriptionally active chromatin." EMBO J 7(5): 1395-1402.

Hedlund, E., J. Pruszak, et al. (2007). "Selection of embryonic stem cell-derived enhanced green fluorescent protein-positive dopamine neurons using the tyrosine hydroxylase promoter is confounded by reporter gene expression in immature cell populations." Stem Cells 25(5): 1126-1135.

Hemmati-Brivanlou, A., O. G. Kelly, et al. (1994). "Follistatin, an antagonist of activin, is expressed in the Spemann organizer and displays direct neuralizing activity." Cell 77(2): 283-295.

Hochedlinger, K. and R. Jaenisch (2002). "Monoclonal mice generated by nuclear transfer from mature B and T donor cells." Nature 415(6875): 1035-1038.

Hochedlinger, K. and R. Jaenisch (2006). "Nuclear reprogramming and pluripotency." Nature 441(7097): 1061-1067.

Hochedlinger, K., Y. Yamada, et al. (2005). "Ectopic expression of Oct-4 blocks progenitor-cell differentiation and causes dysplasia in epithelial tissues." Cell 121(3): 465-477.

Holcomb, L., M. N. Gordon, et al. (1998). "Accelerated Alzheimer-type phenotype in transgenic mice carrying both mutant amyloid precursor protein and presenilin 1 transgenes." Nat Med 4(1): 97-100.

Hong, H., K. Takahashi, et al. (2009). "Suppression of induced pluripotent stem cell generation by the p53-p21 pathway." Nature 460(7259): 1132-1135.

Howe, S. J., M. R. Mansour, et al. (2008). "Insertional mutagenesis combined with acquired somatic mutations causes leukemogenesis following gene therapy of SCID-X1 patients." J Clin Invest 118(9): 3143-3150.

Hsiao, K., P. Chapman, et al. (1996). "Correlative memory deficits, Abeta elevation, and amyloid plaques in transgenic mice." Science 274(5284): 99-102.

Hu, B. Y., J. P. Weick, et al. (2010). "Neural differentiation of human induced pluripotent stem cells follows developmental principles but with variable potency." Proc Natl Acad Sci U S A 107(9): 4335-4340.

Huang, P., Z. He, et al. (2011). "Induction of functional hepatocyte-like cells from mouse fibroblasts by defined factors." Nature 475(7356): 386-389.

Huangfu, D., R. Maehr, et al. (2008a). "Induction of pluripotent stem cells by defined factors is greatly improved by small-molecule compounds." Nat Biotechnol 26(7): 795-797.

Huangfu, D., K. Osafune, et al. (2008b). "Induction of pluripotent stem cells from primary human fibroblasts with only Oct4 and Sox2." Nat Biotechnol 26(11): 1269-1275.

Hutton, M., C. L. Lendon, et al. (1998). "Association of missense and 5'-splice-site mutations in tau with the inherited dementia FTDP-17." Nature 393(6686): 702-705.

Hyun, I., K. Hochedlinger, et al. (2007). "New advances in iPS cell research do not obviate the need for human embryonic stem cells." Cell Stem Cell 1(4): 367-368.

Ieda, M., J. D. Fu, et al. (2010). "Direct reprogramming of fibroblasts into functional cardiomyocytes by defined factors." Cell 142(3): 375-386.

Iqbal, K., E. Braak, et al. (1991). "A silver impregnation method for labeling both Alzheimer paired helical filaments and their polypeptides separated by sodium dodecyl sulfate-polyacrylamide gel electrophoresis." Neurobiol Aging 12(4): 357-361.

Irizarry, M. C., M. McNamara, et al. (1997a). "APPSw transgenic mice develop age-related A beta deposits and neuropil abnormalities, but no neuronal loss in CA1." J Neuropathol Exp Neurol 56(9): 965-973.

Irizarry, M. C., F. Soriano, et al. (1997b). "Abeta deposition is associated with neuropil changes, but not with overt neuronal loss in the human amyloid precursor protein V717F (PDAPP) transgenic mouse." J Neurosci 17(18): 7053-7059.

Jaenisch, R. and A. Bird (2003). "Epigenetic regulation of gene expression: how the genome integrates intrinsic and environmental signals." Nat Genet 33 Suppl: 245-254.

Jaenisch, R. and R. Young (2008). "Stem cells, the molecular circuitry of pluripotency and nuclear reprogramming." Cell 132(4): 567-582.

Janus, C., J. Pearson, et al. (2000). "A beta peptide immunization reduces behavioural impairment and plaques in a model of Alzheimer's disease." Nature 408(6815): 979-982.

Janus, C., A. L. Phinney, et al. (2001). "New developments in animal models of Alzheimer's disease." Curr Neurol Neurosci Rep 1(5): 451-457.

Jayadev, S., J. B. Leverenz, et al. (2010). "Alzheimer's disease phenotypes and genotypes associated with mutations in presenilin 2." Brain 133(Pt 4): 1143-1154.

Jellinger, K., H. Braak, et al. (1991). "Alzheimer lesions in the entorhinal region and isocortex in Parkinson's and Alzheimer's diseases." Ann N Y Acad Sci 640: 203-209.

Judson, R. L., J. E. Babiarz, et al. (2009). "Embryonic stem cell-specific microRNAs promote induced pluripotency." Nat Biotechnol 27(5): 459-461.

Jun, G., A. C. Naj, et al. (2010). "Meta-analysis confirms CR1, CLU, and PICALM as alzheimer disease risk loci and reveals interactions with APOE genotypes." Arch Neurol 67(12): 1473-1484.

Kaji, K., K. Norrby, et al. (2009). "Virus-free induction of pluripotency and subsequent excision of reprogramming factors." Nature 458(7239): 771-775.

Kang, J., H. G. Lemaire, et al. (1987). "The precursor of Alzheimer's disease amyloid A4 protein resembles a cell-surface receptor." Nature 325(6106): 733-736.

Kang, L., J. Wang, et al. (2009). "iPS cells can support full-term development of tetraploid blastocyst-complemented embryos." Cell Stem Cell 5(2): 135-138.

Kato, Y., T. Tani, et al. (1998). "Eight calves cloned from somatic cells of a single adult." Science 282(5396): 2095-2098.

Kawamura, T., J. Suzuki, et al. (2009). "Linking the p53 tumour suppressor pathway to somatic cell reprogramming." Nature 460(7259): 1140-1144.

Khachaturian, Z. S. (1985). "Diagnosis of Alzheimer's disease." Arch Neurol 42(11): 1097-1105.

Kim, J., J. Chu, et al. (2008). "An extended transcriptional network for pluripotency of embryonic stem cells." Cell 132(6): 1049-1061.

Kim, D., C. H. Kim, et al. (2009). "Generation of human induced pluripotent stem cells by direct delivery of reprogramming proteins." Cell Stem Cell 4(6): 472-476.

Kim, J., S. C. Su, et al. (2011). "Functional integration of dopaminergic neurons directly converted from mouse fibroblasts." Cell Stem Cell 9(5): 413-419.

Kishigami, S., E. Mizutani, et al. (2006). "Significant improvement of mouse cloning technique by treatment with trichostatin A after somatic nuclear transfer." Biochem Biophys Res Commun 340(1): 183-189.

Kondo, M., D. C. Scherer, et al. (2000). "Cell-fate conversion of lymphoid-committed progenitors by instructive actions of cytokines." Nature 407(6802): 383-386.

Kornilova, A. Y., J. Kim, et al. (2006). "Deducing the transmembrane domain organization of presenilin-1 in gamma-secretase by cysteine disulfide cross-linking." Biochemistry 45(24): 7598-7604.

Kotilinek, L. A., B. Bacskai, et al. (2002). "Reversible memory loss in a mouse transgenic model of Alzheimer's disease." J Neurosci 22(15): 6331-6335.

LaFerla, F. M., K. N. Green, et al. (2007). "Intracellular amyloid-beta in Alzheimer's disease." Nat Rev Neurosci 8(7): 499-509.

LaFerla, F. M. and S. Oddo (2005). "Alzheimer's disease: Abeta, tau and synaptic dysfunction." Trends Mol Med 11(4): 170-176.

Laiosa, C. V., M. Stadtfeld, et al. (2006). "Reprogramming of committed T cell progenitors to macrophages and dendritic cells by C/EBP alpha and PU.1 transcription factors." Immunity 25(5): 731-744.

Lambert, J. C., S. Heath, et al. (2009). "Genome-wide association study identifies variants at CLU and CR1 associated with Alzheimer's disease." Nat Genet 41(10): 1094-1099.

Lefebvre, S., L. Burglen, et al. (1995). "Identification and characterization of a spinal muscular atrophy-determining gene." Cell 80(1): 155-165.

Levy-Lahad, E., W. Wasco, et al. (1995). "Candidate gene for the chromosome 1 familial Alzheimer's disease locus." Science 269(5226): 973-977.

Lewis, J., D. W. Dickson, et al. (2001). "Enhanced neurofibrillary degeneration in transgenic mice expressing mutant tau and APP." Science 293(5534): 1487-1491.

Lewitzky, M. and S. Yamanaka (2007). "Reprogramming somatic cells towards pluripotency by defined factors." Curr Opin Biotechnol 18(5): 467-473.

Li, W., H. Zhou, et al. (2009). "Generation of human-induced pluripotent stem cells in the absence of exogenous Sox2." Stem Cells 27(12): 2992-3000.

Li, X. J., Z. W. Du, et al. (2005). "Specification of motoneurons from human embryonic stem cells." Nat Biotechnol 23(2): 215-221.

Li, Z., J. Dullmann, et al. (2002). "Murine leukemia induced by retroviral gene marking." Science 296(5567): 497.

Lichtenthaler, S. F., N. Ida, et al. (1997). "Mutations in the transmembrane domain of APP altering gamma-secretase specificity." Biochemistry 36(49): 15396-15403.

Liu, H., F. Zhu, et al. (2008). "Generation of induced pluripotent stem cells from adult rhesus monkey fibroblasts." Cell Stem Cell 3(6): 587-590.

Loh, Y. H., S. Agarwal, et al. (2009). "Generation of induced pluripotent stem cells from human blood." Blood 113(22): 5476-5479.

Lowry, W. E., L. Richter, et al. (2008). "Generation of human induced pluripotent stem cells from dermal fibroblasts." Proc Natl Acad Sci U S A 105(8): 2883-2888.

Maherali, N., R. Sridharan, et al. (2007). "Directly reprogrammed fibroblasts show global epigenetic remodeling and widespread tissue contribution." Cell Stem Cell 1(1): 55-70.

Marion, R. M., K. Strati, et al. (2009). "A p53-mediated DNA damage response limits reprogramming to ensure iPS cell genomic integrity." Nature 460(7259): 1149-1153.

Markoulaki, S., J. Hanna, et al. (2009). "Transgenic mice with defined combinations of drug-inducible reprogramming factors." Nat Biotechnol 27(2): 169-171.

Marro, S., Z. P. Pang, et al. (2011). "Direct lineage conversion of terminally differentiated hepatocytes to functional neurons." Cell Stem Cell 9(4): 374-382.

Marson, A., S. S. Levine, et al. (2008). "Connecting microRNA genes to the core transcriptional regulatory circuitry of embryonic stem cells." Cell 134(3): 521-533.

Masters, C. L., G. Simms, et al. (1985). "Amyloid plaque core protein in Alzheimer disease and Down syndrome." Proc Natl Acad Sci U S A 82(12): 4245-4249.

Meissner, A., T. S. Mikkelsen, et al. (2008). "Genome-scale DNA methylation maps of pluripotent and differentiated cells." Nature 454(7205): 766-770.

Meissner, A., M. Wernig, et al. (2007). "Direct reprogramming of genetically unmodified fibroblasts into pluripotent stem cells." Nat Biotechnol 25(10): 1177-1181.

Miller, R. A. and F. H. Ruddle (1976). "Pluripotent teratocarcinoma-thymus somatic cell hybrids." Cell 9(1): 45-55.

Miura, K., Y. Okada, et al. (2009). "Variation in the safety of induced pluripotent stem cell lines." Nat Biotechnol 27(8): 743-745.

Morgan, D., D. M. Diamond, et al. (2000). "A beta peptide vaccination prevents memory loss in an animal model of Alzheimer's disease." Nature 408(6815): 982-985.

Mucke, L., E. Masliah, et al. (2000). "High-level neuronal expression of abeta 1-42 in wild-type human amyloid protein precursor transgenic mice: synaptotoxicity without plaque formation." J Neurosci 20(11): 4050-4058.

Mullan, M., F. Crawford, et al. (1992). "A pathogenic mutation for probable Alzheimer's disease in the APP gene at the N-terminus of beta-amyloid." Nat Genet 1(5): 345-347.

Muller, U., N. Cristina, et al. (1994). "Behavioral and anatomical deficits in mice homozygous for a modified beta-amyloid precursor protein gene." Cell 79(5): 755-765.

Murrell, J., M. Farlow, et al. (1991). "A mutation in the amyloid precursor protein associated with hereditary Alzheimer's disease." Science 254(5028): 97-99.

Muzumdar, M. D., B. Tasic, et al. (2007). "A global double-fluorescent Cre reporter mouse." Genesis 45(9): 593-605.

Nakagawa, M., M. Koyanagi, et al. (2008). "Generation of induced pluripotent stem cells without Myc from mouse and human fibroblasts." Nat Biotechnol 26(1): 101-106.

Narazaki, G., H. Uosaki, et al. (2008). "Directed and systematic differentiation of cardiovascular cells from mouse induced pluripotent stem cells." Circulation 118(5): 498-506.

Navarro, S., N. W. Meza, et al. (2006). "Hematopoietic dysfunction in a mouse model for Fanconi anemia group D1." Mol Ther 14(4): 525-535.

Nelson, T. J. and A. Terzic (2009). "Induced pluripotent stem cells: reprogrammed without a trace." Regen Med 4(3): 333-335.

Nguyen, H. N., B. Byers, et al. (2011). "LRRK2 mutant iPSC-derived DA neurons demonstrate increased susceptibility to oxidative stress." Cell Stem Cell 8(3): 267-280.

Nilsberth, C., A. Westlind-Danielsson, et al. (2001). "The 'Arctic' APP mutation (E693G) causes Alzheimer's disease by enhanced Abeta protofibril formation." Nat Neurosci 4(9): 887-893.

Noggle, S., H. L. Fung, et al. (2011). "Human oocytes reprogram somatic cells to a pluripotent state." Nature 478(7367): 70-75.

Oddo, S., A. Caccamo, et al. (2003). "Triple-transgenic model of Alzheimer's disease with plaques and tangles: intracellular Abeta and synaptic dysfunction." Neuron 39(3): 409-421.

Okita, K., T. Ichisaka, et al. (2007). "Generation of germline-competent induced pluripotent stem cells." Nature 448(7151): 313-317.

Okita, K., M. Nakagawa, et al. (2008). "Generation of mouse induced pluripotent stem cells without viral vectors." Science 322(5903): 949-953.

Olson, L. E., J. T. Richtsmeier, et al. (2004). "A chromosome 21 critical region does not cause specific Down syndrome phenotypes." Science 306(5696): 687-690.

Orkin, S. H. and L. I. Zon (2008). "Hematopoiesis: an evolving paradigm for stem cell biology." Cell 132(4): 631-644.

Pang, Z. P., N. Yang, et al. (2011). "Induction of human neuronal cells by defined transcription factors." Nature 476(7359): 220-223.

Park, I. H., N. Arora, et al. (2008a). "Disease-specific induced pluripotent stem cells." Cell 134(5): 877-886.

Park, I. H., R. Zhao, et al. (2008b). "Reprogramming of human somatic cells to pluripotency with defined factors." Nature 451(7175): 141-146.

Pasinelli, P. and R. H. Brown (2006). "Molecular biology of amyotrophic lateral sclerosis: insights from genetics." Nat Rev Neurosci 7(9): 710-723.

Pfisterer, U., A. Kirkeby, et al. (2011). "Direct conversion of human fibroblasts to dopaminergic neurons." Proc Natl Acad Sci U S A 108(25): 10343-10348.

Pickering, S. J., S. L. Minger, et al. (2005). "Generation of a human embryonic stem cell line encoding the cystic fibrosis mutation deltaF508, using preimplantation genetic diagnosis." Reprod Biomed Online 10(3): 390-397.

Poorkaj, P., T. D. Bird, et al. (1998). "Tau is a candidate gene for chromosome 17 frontotemporal dementia." Ann Neurol 43(6): 815-825.

Qiang, L., R. Fujita, et al. (2011). "Directed conversion of Alzheimer's disease patient skin fibroblasts into functional neurons." Cell 146(3): 359-371.

Ramsden, M., L. Kotilinek, et al. (2005). "Age-dependent neurofibrillary tangle formation, neuron loss, and memory impairment in a mouse model of human tauopathy (P301L)." J Neurosci 25(46): 10637-10647.

Reik, W., W. Dean, et al. (2001). "Epigenetic reprogramming in mammalian development." Science 293(5532): 1089-1093.

Rideout, W. M., 3rd, K. Eggan, et al. (2001). "Nuclear cloning and epigenetic reprogramming of the genome." Science 293(5532): 1093-1098.

Roberson, E. D., K. Scearce-Levie, et al. (2007). "Reducing endogenous tau ameliorates amyloid beta-induced deficits in an Alzheimer's disease mouse model." Science 316(5825): 750-754.

Rogaev, E. I., R. Sherrington, et al. (1995). "Familial Alzheimer's disease in kindreds with missense mutations in a gene on chromosome 1 related to the Alzheimer's disease type 3 gene." Nature 376(6543): 775-778.

Sasai, Y., B. Lu, et al. (1994). "Xenopus chordin: a novel dorsalizing factor activated by organizer-specific homeobox genes." Cell 79(5): 779-790.

Schultz, R. M., W. Davis, Jr., et al. (1999). "Reprogramming of gene expression during preimplantation development." J Exp Zool 285(3): 276-282.

Seibler, P., J. Graziotto, et al. (2011). "Mitochondrial Parkin recruitment is impaired in neurons derived from mutant PINK1 induced pluripotent stem cells." J Neurosci 31(16): 5970-5976.

Sekiya, S. and A. Suzuki (2011). "Direct conversion of mouse fibroblasts to hepatocyte-like cells by defined factors." Nature 475(7356): 390-393.

Selkoe, D. J. (1991). "The molecular pathology of Alzheimer's disease." Neuron 6(4): 487-498.

Selkoe, D. J. (2002). "Alzheimer's disease is a synaptic failure." Science 298(5594): 789-791.

Selkoe, D. J. and D. Schenk (2003). "Alzheimer's disease: molecular understanding predicts amyloid-based therapeutics." Annu Rev Pharmacol Toxicol 43: 545-584.

Shen, J. and R. J. Kelleher, 3rd (2007). "The presenilin hypothesis of Alzheimer's disease: evidence for a loss-of-function pathogenic mechanism." Proc Natl Acad Sci U S A 104(2): 403-409.

Sherrington, R., E. I. Rogaev, et al. (1995). "Cloning of a gene bearing missense mutations in early-onset familial Alzheimer's disease." Nature 375(6534): 754-760.

Shi, Y., C. Desponts, et al. (2008). "Induction of pluripotent stem cells from mouse embryonic fibroblasts by Oct4 and Klf4 with small-molecule compounds." Cell Stem Cell 3(5): 568-574.

Shi, Y., J. T. Do, et al. (2008). "A combined chemical and genetic approach for the generation of induced pluripotent stem cells." Cell Stem Cell 2(6): 525-528.

Smith, W. C. and R. M. Harland (1992). "Expression cloning of noggin, a new dorsalizing factor localized to the Spemann organizer in Xenopus embryos." Cell 70(5): 829-840.

Soldner, F., D. Hockemeyer, et al. (2009). "Parkinson's disease patient-derived induced pluripotent stem cells free of viral reprogramming factors." Cell 136(5): 964-977.

Sommer, C. A., A. G. Sommer, et al. (2010). "Excision of reprogramming transgenes improves the differentiation potential of iPS cells generated with a single excisable vector." Stem Cells 28(1): 64-74.

Sommer, C. A., M. Stadtfeld, et al. (2009). "Induced pluripotent stem cell generation using a single lentiviral stem cell cassette." Stem Cells 27(3): 543-549.

Son, E. Y., J. K. Ichida, et al. (2011). "Conversion of mouse and human fibroblasts into functional spinal motor neurons." Cell Stem Cell 9(3): 205-218.

Sparman, M., V. Dighe, et al. (2009). "Epigenetic reprogramming by somatic cell nuclear transfer in primates." Stem Cells 27(6): 1255-1264.

Spires, T. L., M. Meyer-Luehmann, et al. (2005). "Dendritic spine abnormalities in amyloid precursor protein transgenic mice demonstrated by gene transfer and intravital multiphoton microscopy." J Neurosci 25(31): 7278-7287.

Stadtfeld, M., N. Maherali, et al. (2008a). "Defining molecular cornerstones during fibroblast to iPS cell reprogramming in mouse." Cell Stem Cell 2(3): 230-240.

Stadtfeld, M., M. Nagaya, et al. (2008b). "Induced pluripotent stem cells generated without viral integration." Science 322(5903): 945-949.

Sturchler-Pierrat, C., D. Abramowski, et al. (1997). "Two amyloid precursor protein transgenic mouse models with Alzheimer disease-like pathology." Proc Natl Acad Sci U S A 94(24): 13287-13292.

Sun, N., N. J. Panetta, et al. (2009). "Feeder-free derivation of induced pluripotent stem cells from adult human adipose stem cells." Proc Natl Acad Sci U S A 106(37): 15720-15725.

Suzuki, N., T. T. Cheung, et al. (1994). "An increased percentage of long amyloid beta protein secreted by familial amyloid beta protein precursor (beta APP717) mutants." Science 264(5163): 1336-1340.

Szabo, E., S. Rampalli, et al. (2010). "Direct conversion of human fibroblasts to multilineage blood progenitors." Nature 468(7323): 521-526.

Tada, M., Y. Takahama, et al. (2001). "Nuclear reprogramming of somatic cells by in vitro hybridization with ES cells." Curr Biol 11(19): 1553-1558.

Takahashi, K., K. Tanabe, et al. (2007). "Induction of pluripotent stem cells from adult human fibroblasts by defined factors." Cell 131(5): 861-872.

Takahashi, K. and S. Yamanaka (2006). "Induction of pluripotent stem cells from mouse embryonic and adult fibroblast cultures by defined factors." Cell 126(4): 663-676.

Takeuchi, A., M. C. Irizarry, et al. (2000). "Age-related amyloid beta deposition in transgenic mice overexpressing both Alzheimer mutant presenilin 1 and amyloid beta precursor protein Swedish mutant is not associated with global neuronal loss." Am J Pathol 157(1): 331-339.

Taura, D., M. Noguchi, et al. (2009). "Adipogenic differentiation of human induced pluripotent stem cells: comparison with that of human embryonic stem cells." FEBS Lett 583(6): 1029-1033.

Terry, R. D., E. Masliah, et al. (1991). "Physical basis of cognitive alterations in Alzheimer's disease: synapse loss is the major correlate of cognitive impairment." Ann Neurol 30(4): 572-580.

The Huntington's Disease Collaborative Research Group. (1993). "A novel gene containing a trinucleotide repeat that is expanded and unstable on Huntington's disease chromosomes. The Huntington's Disease Collaborative Research Group." Cell 72(6): 971-983.

Thinakaran, G. and E. H. Koo (2008). "Amyloid precursor protein trafficking, processing, and function." J Biol Chem 283(44): 29615-29619.

Thomson, J. A., J. Itskovitz-Eldor, et al. (1998). "Embryonic stem cell lines derived from human blastocysts." Science 282(5391): 1145-1147.

Tokumoto, Y., S. Ogawa, et al. (2010). "Comparison of efficiency of terminal differentiation of oligodendrocytes from induced pluripotent stem cells versus embryonic stem cells in vitro." J Biosci Bioeng 109(6): 622-628.

Tokuzawa, Y., E. Kaiho, et al. (2003). "Fbx15 is a novel target of Oct3/4 but is dispensable for embryonic stem cell self-renewal and mouse development." Mol Cell Biol 23(8): 2699-2708.

Tsai, J., J. Grutzendler, et al. (2004). "Fibrillar amyloid deposition leads to local synaptic abnormalities and breakage of neuronal branches." Nat Neurosci 7(11): 1181-1183.

Utikal, J., J. M. Polo, et al. (2009). "Immortalization eliminates a roadblock during cellular reprogramming into iPS cells." Nature 460(7259): 1145-1148.

Valenzuela, D. M., A. N. Economides, et al. (1995). "Identification of mammalian noggin and its expression in the adult nervous system." J Neurosci 15(9): 6077-6084.

Van Broeckhoven, C., H. Backhovens, et al. (1992). "Mapping of a gene predisposing to early-onset Alzheimer's disease to chromosome 14q24.3." Nat Genet 2(4): 335-339.

Varas, F., M. Stadtfeld, et al. (2009). "Fibroblast-derived induced pluripotent stem cells show no common retroviral vector insertions." Stem Cells 27(2): 300-306.

Vassar, R., B. D. Bennett, et al. (1999). "Beta-secretase cleavage of Alzheimer's amyloid precursor protein by the transmembrane aspartic protease BACE." Science 286(5440): 735-741.

Vierbuchen, T., A. Ostermeier, et al. (2010). "Direct conversion of fibroblasts to functional neurons by defined factors." Nature 463(7284): 1035-1041.

Wakayama, T., A. C. Perry, et al. (1998). "Full-term development of mice from enucleated oocytes injected with cumulus cell nuclei." Nature 394(6691): 369-374.

Walsh, J. S., H. G. Welch, et al. (1990). "Survival of outpatients with Alzheimer-type dementia." Ann Intern Med 113(6): 429-434.

Watanabe, K., D. Kamiya, et al. (2005). "Directed differentiation of telencephalic precursors from embryonic stem cells." Nat Neurosci 8(3): 288-296.

Weintraub, H., S. J. Tapscott, et al. (1989). "Activation of muscle-specific genes in pigment, nerve, fat, liver, and fibroblast cell lines by forced expression of MyoD." Proc Natl Acad Sci U S A 86(14): 5434-5438.

Wernig, M., C. J. Lengner, et al. (2008). "A drug-inducible transgenic system for direct reprogramming of multiple somatic cell types." Nat Biotechnol 26(8): 916-924.

Wernig, M., A. Meissner, et al. (2008). "c-Myc is dispensable for direct reprogramming of mouse fibroblasts." Cell Stem Cell 2(1): 10-12.

Wernig, M., A. Meissner, et al. (2007). "In vitro reprogramming of fibroblasts into a pluripotent ES-cell-like state." Nature 448(7151): 318-324.

Wernig, M., J. P. Zhao, et al. (2008). "Neurons derived from reprogrammed fibroblasts functionally integrate into the fetal brain and improve symptoms of rats with Parkinson's disease." Proc Natl Acad Sci U S A 105(15): 5856-5861.

Westerman, M. A., D. Cooper-Blacketer, et al. (2002). "The relationship between Abeta and memory in the Tg2576 mouse model of Alzheimer's disease." J Neurosci 22(5): 1858-1867.

Wichterle, H., I. Lieberam, et al. (2002). "Directed differentiation of embryonic stem cells into motor neurons." Cell 110(3): 385-397.

Wilmut, I., N. Beaujean, et al. (2002). "Somatic cell nuclear transfer." Nature 419(6907): 583-586.

Wilmut, I., A. E. Schnieke, et al. (1997). "Viable offspring derived from fetal and adult mammalian cells." Nature 385(6619): 810-813.

Wolfe, M. S. (2006). "The gamma-secretase complex: membrane-embedded proteolytic ensemble." Biochemistry 45(26): 7931-7939.

Wolffe, A. P. and M. A. Matzke (1999). "Epigenetics: regulation through repression." Science 286(5439): 481-486.

Woltjen, K., I. P. Michael, et al. (2009). "piggyBac transposition reprograms fibroblasts to induced pluripotent stem cells." Nature 458(7239): 766-770.

Wu, X., Y. Li, et al. (2003). "Transcription start regions in the human genome are favored targets for MLV integration." Science 300(5626): 1749-1751.

Xie, H., M. Ye, et al. (2004). "Stepwise reprogramming of B cells into macrophages." Cell 117(5): 663-676.

Yamanaka, S. (2007). "Strategies and new developments in the generation of patient-specific pluripotent stem cells." Cell Stem Cell 1(1): 39-49.

Yamanaka, S., J. Li, et al. (2008). "Pluripotency of embryonic stem cells." Cell Tissue Res 331(1): 5-22.

Yang, N., Y. H. Ng, et al. (2011). "Induced neuronal cells: how to make and define a neuron." Cell Stem Cell 9(6): 517-525.

Yagi, T., D. Ito, et al. (2011). "Modeling familial Alzheimer's disease with induced pluripotent stem cells." Hum Mol Genet 20(23): 4530-4539.

Yu, J., K. Hu, et al. (2009). "Human induced pluripotent stem cells free of vector and transgene sequences." Science 324(5928): 797-801.

Yu, J., M. A. Vodyanik, et al. (2006). "Human embryonic stem cells reprogram myeloid precursors following cell-cell fusion." Stem Cells 24(1): 168-176.

Yu, J., M. A. Vodyanik, et al. (2007). "Induced pluripotent stem cell lines derived from human somatic cells." Science 318(5858): 1917-1920.

Zhang, N., M. C. An, et al. (2010). "Characterization of Human Huntington's Disease Cell Model from Induced Pluripotent Stem Cells." PLoS Curr 2: RRN1193.

Zhao, L., Q. L. Ma, et al. (2006). "Role of p21-activated kinase pathway defects in the cognitive deficits of Alzheimer disease." Nat Neurosci 9(2): 234-242.

Zhao, X. Y., W. Li, et al. (2009). "iPS cells produce viable mice through tetraploid complementation." Nature 461(7260): 86-90.

Zheng, H., M. Jiang, et al. (1995). "beta-Amyloid precursor protein-deficient mice show reactive gliosis and decreased locomotor activity." Cell 81(4): 525-531.

Zhou, H., S. Wu, et al. (2009). "Generation of induced pluripotent stem cells using recombinant proteins." Cell Stem Cell 4(5): 381-384.

Zhou, J., P. Su, et al. (2010). "High-efficiency induction of neural conversion in human ESCs and human induced pluripotent stem cells with a single chemical inhibitor of transforming growth factor beta superfamily receptors." Stem Cells 28(10): 1741-1750.

Zhou, Q., J. Brown, et al. (2008). "In vivo reprogramming of adult pancreatic exocrine cells to beta-cells." Nature 455(7213): 627-632.

Zhou, W. and C. R. Freed (2009). "Adenoviral gene delivery can reprogram human fibroblasts to induced pluripotent stem cells." Stem Cells 27(11): 2667-2674.